GEL SPUN POLYACRYLONITRILE BASED CARBON FIBERS CONTAINING LIGNIN AND CARBON NANOTUBES

A Dissertation
Presented to
The Academic Faculty

by

Hsiang-Hao Clive Liu

In Partial Fulfillment
of the Requirements for the Degree
Doctor of Philosophy in the
School of Materials Science and Engineering

Georgia Institute of Technology
May 2017

GEL SPUN POLYACRYLONITRILE BASED CARBON FIBERS CONTAINING LIGNIN AND CARBON NANOTUBES

Approved by:

Dr. Satish Kumar, Advisor
School of Materials Science and Engineering
Georgia Institute of Technology

Dr. Fred Cook
School of Materials Science and Engineering
Georgia Institute of Technology

Dr. Meisha Shofner
School of Materials Science and Engineering
Georgia Institute of Technology

Dr. Yulin Deng
School of Chemical and Biomolecular Engineering
Georgia Institute of Technology

Dr. Donggang Yao
School of Materials Science and Engineering
Georgia Institute of Technology

Date Approved: December 6, 2016

To Su-Hua, my beloved grandmother.

ACKNOWLEDGEMENTS

First and foremost, I would like to express my deepest gratitude to my advisor, Dr. Satish Kumar, for providing all the invaluable guidance and support throughout the years beyond the extent of this study, and for always encouraging me to seek advancements in self constitution. I would also like to thank my committee members, Dr. Fred Cook, Dr. Yulin Deng, Dr. Meisha Shofner, and Dr. Donggang Yao for their service, guidance, and their critical contribution of time, expertise, and encouragement. I am grateful to the support from the Renewable Bioproducts Institute and the Air Force Office of Scientific Research for funding this study.

Many thanks to all the past and current group members: Dr. Bradley Newcomb, for his help on Raman spectroscopy, XRD analysis, and various valuable discussions; Mr. Amir Ahmad Bakhtiary Davijani for his assistance on experiments and all the scientific discussions; Mr. Huibin Chang, Mr. Po-Hsiang Wang, and Mr. Jeffrey Luo always kindly sharing their strengths in assisting various experiments; Dr. Han Gi Chae, Dr. Yaodong Liu, Dr. Prabhakar Gulgunje, and Dr. Kishor Gupta, Dr. Sushanta Ghoshal, Dr. M.G. Kamath, and Mr. Kevin Lyons for their contributed insights. Special thanks to Dr. An-Ting Chien, for the assistance on the initial fiber spinning trials and all the attentive mentorship in various professional and personal aspects. I would also like to acknowledge Dr. Xudong Fang, and Chia-Chi Tuan for their contributions on collaborative experiments.

Finally, I would like to thank my family for their unceasing support, encouragement, love, and understanding; and I am undoubtfully grateful and indebted to Winnie, for everything.

TABLE OF CONTENTS

LIST OF TABLES

LIST OF FIGURES

Page

SUMMARY

Forestry bioproduct lignin has been long proposed as an ideal material for carbon fiber precursor due to its abundance, renewability, high carbon yield and cost-effectiveness as the biorefinery by-product. However, little success of lignin-based commercial carbon fibers has been reported due to the barriers such as its varying chemical structure, complex thermal stabilization process, poor miscibility with other polymers, all of which that result in unmanageable processing, and limited mechanical performance. In this research, using gel spinning technology, various types of lignin and polyacrylonitrile (PAN) are processed to form blend fibers in single-component geometry, and sheath/core bi-component fibers. The effects of lignin on solution properties and processing are characterized by rheology. The structure, thermal properties, mechanical performance, and morphology of the gel-spun fibers and the resultant carbon fibers are reported and discussed herein.

Chapter 1, as the overview, introduces the background, the fabrication, and the advancement of PAN and lignin-based carbon fibers, as well as the carbon nanotube (CNT) incorporated carbon fibers. Chapter 2 presents the rheology study of PAN with various lignin content in solutions to characterize the interactions of PAN and lignin and to investigate the potential boundary conditions for lignin incorporation. Chapter 3 reports the effects of softwood lignin (SWL) on gel-spun PAN fiber properties along with thermal stabilization kinetics of fibers, and shows the incorporation of 25 wt% SWL to reduce reaction activation energy and to increase the reaction rates of cyclization, oxidation, and crosslinking reactions. Chapter 4 discusses the processing, structure and the properties of PAN, PAN/annual plant lignin (APL), PAN/APL/CNT fibers, and the resultant carbon fibers. PAN fiber, pore-free PAN/APL, and PAN/APL/CNT fibers (with 30 wt% lignin

incorporation) are processed without phase separation and successfully fabricated into carbon fibers. Raman spectroscopy indicates that, at increasing carbonization temperature, PAN carbon fiber undergoes a reordering process and forms a more refined graphitic structure, and the lignin containing carbon fiber undergoes reordering of polyaromatic carbon stacks. The incorporation of CNT is shown to promote both reordering processes.

Chapter 5 reports the PAN sheath, PAN/APL core bi-component fibers, and the derived carbon fibers. The bi-component fiber morphology and maximum draw ratios change with the ratio between the overall fiber diameter to core component diameter (i.e., the size of the core component in the fiber cross section). In addition to the successful fabrication of the pore-free PAN sheath and PAN/APL core bi-component carbon fiber, porous bi-component carbon fiber with approximate 24.2% cross section porosity can be fabricated by changing core component size in fiber cross section. The porous bi-component carbon fiber serves as an approach for low-density carbon fiber manufacturing. With an effective lignin incorporation of ~31 wt%, pore-free PAN/APL bi-component carbon fiber (carbonized at 1,200 °C), exhibits a tensile strength and a tensile modulus of around 2.1 GPa and 260 GPa, respectively. When carbonized at 1,300 °C, the tensile modulus of the carbon fibers increases to 274 GPa. PAN fiber carbonized at 1,200 °C and 1,300 °C exhibits a tensile strength of 2.47 GPa and 2.08 GPa, respectively, and a tensile modulus of 280 GPa and 288 GPa, respectively. Conclusions of the study along with the recommendations for future works are summarized in Chapter 6.

CHAPTER 1
INTRODUCTION

1.1 OVERVIEW

Carbon fibers, owing to the remarkable specific strength and modulus, have been utilized as a versatile reinforcing material in aerospace and automotive industries, sporting goods, special industrial applications, and even in constructions in the past decades.[14] By definition, carbon fibers are comprised of high (≥ 90 wt. %) carbon content which can be converted from precursor materials such as cellulose, lignin, and petroleum derived polyacrylonitrile (PAN), pitch, or some polyolefins with appropriate modifications. Currently, carbon fibers are predominantly manufactured from PAN precursors, and with a small fraction derived from pitch precursors. In general, PAN-based carbon fibers exhibit a tensile strength ranging from 3 to 7 GPa and tensile modulus from 230 GPa to as high as 590 GPa, with optional graphitization.[20] Pitch-based carbon fibers are more known for the high tensile modulus (up to ~ 960 GPa), while exhibiting a relatively low tensile strength (< 3.5 GPa) than PAN-based carbon fibers. In addition to the excellent mechanical performance, carbon fibers can be employed to impart functionality because of their good thermal and electrical conductivities. Typically, PAN-based carbon fibers exhibit electrical conductivity and thermal conductivity around ~ 10^4 to 10^5 S/m, and ~10^1 W/mK, respectively. By comparison, electrical conductivity and thermal conductivity of pitch-based carbon fibers are generally better than PAN-based carbon fiber, in the range of ~10^5 – 10^6 S/m, and ~10^2 – 10^3 W/mK, respectively. This is attributed to the more well-

developed sheet-like graphitic structures of pitch-based carbon fibers along the fiber axis compared to PAN-based carbon fibers. (Figure **1.1**).

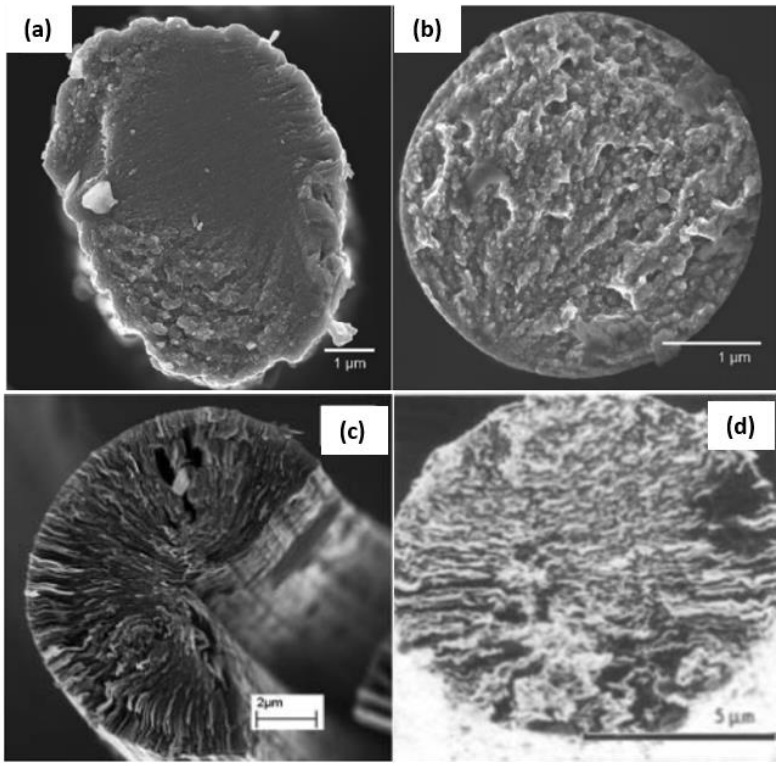

Figure 1.1. Scanning electron micrographs showing the transverse microsctructures of PAN-based carbon fibers (a) T300, (b) IM7,[15] and pitch-based carbon fibers, (c) Thornel K-1100,[17, 24-25] and (d) P-100 fractures. [17]

Currently, carbon fibers derived from cellulose, lignin, polyolefins are not prevalent commercially. Yet the continuing efforts and momentum of low cost carbon fiber development have called for increasing attention globally. A mechanical performance comparison of PAN and pitch commercial carbon fibers, along with the state-of-the-art lignin and polyolefin-based carbon fibers is shown in Figure **1.2**. (Details of the carbon fiber manufacturers and the corresponding properties are listed in Table A.1. and Table A.2. in APPENDIX A)

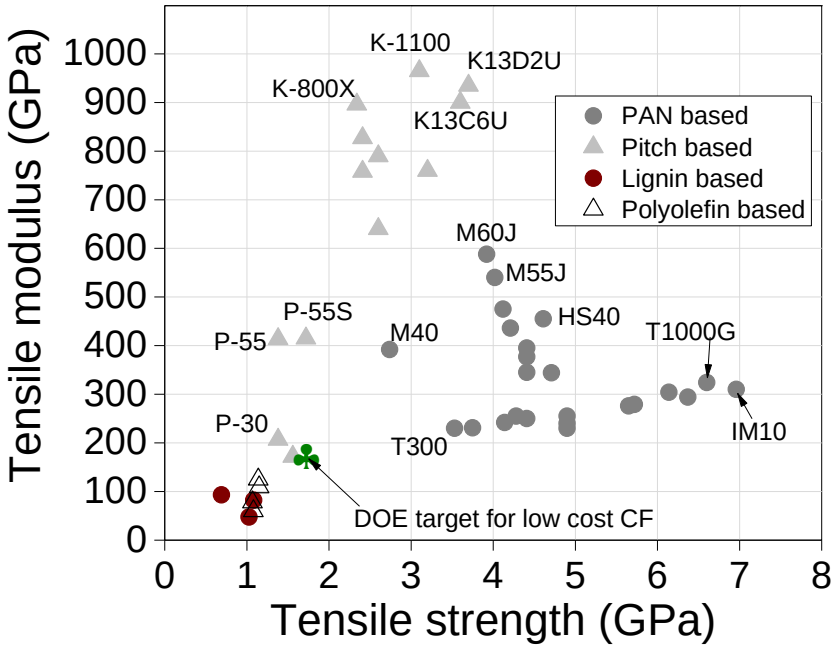

Figure 1.2. Comparison of mechanical performance of PAN and pitch commercial carbon fibers, and lignin and polyolefin-based carbon fibers.

1.2 CARBON FIBERS

1.2.1 Polyacrylonitrile-Based Carbon Fibers

Polyacrylonitrile, initially developed by DuPont as textile fibers in 1950s, has been a predominant precursor of carbon fibers due to high carbon yields, good tensile and compressive properties. Homopolymer PAN is polymerized via monomer acrylonitrile (AN) that contains highly polar nitrile groups, which can induce strong intermolecular interactions between polymer chains that hinders molecular orientations and alignment during fiber manufacturing. To fabricate polymeric fibers, conventional fiber spinning methods are solvent-free melt spinning, solution-based spinning including dry-jet-wet spinning, and dry spinning. Owing to the fact that homopolymer PAN can undergo thermal

decomposition before reaching polymer melting point, melt spinning of homopolymer PAN is difficult without the aid of plasticizers or incorporation of co-monomers.[28] Common co-monomers of PAN, with typical content of 2 to 15 %, are methyl acrylate, vinyl acetate, methyl methacrylate, methacrylic acid, acrylic acid, and itaconic acid. While methyl acrylate and vinyl acetate were used as co-monomers with PAN in order to ensure better coagulation process and spinnability, incorporation of co-monomer can also improve molecular orientations in both precursor and carbon fibers to enhance resultant fiber mechanical performance.[25] In addition, acrylic and itaconic acids as co-monomers with PAN can facilitate cyclization reaction during thermal stabilization step towards carbon fiber. While textile grade PAN fibers are typically manufactured with molecular weights ranging from 70,000 to 200,000 g/mol, PAN fibers for carbon fiber precursors are conventionally fabricated with higher molecular weights up to millions g/mol due to the desired positive impacts on mechanical properties.[31-32]

In early 1960s, the first reported carbonized and graphitized PAN fiber only showed tensile strength and modulus of 0.75 GPa and 112 GPa, respectively.[33] Through the continuous development over the past decades, state-of-art aerospace grade PAN-based carbon fiber IM7 exhibits tensile strength of 5.5 GPa and tensile modulus of 276 GPa. To date, high strength commercial PAN-based carbon fibers (IM10 and T1100G) were reported to achieve tensile strength ranging from 6.6 GPa to 6.9 GPa and tensile modulus between 310 and 324 GPa,[35-37] rendering less than 10% of the theoretical strength and approximately 30% of theoretical modulus of carbon-carbon bonds.

1.2.1.1 Stabilization scheme of PAN-based fibers

Stabilization is a critical and complicated process during carbon fiber conversion. Conventional temperature range of stabilization process is between 200 °C and 300°C, with precursor fibers under tension in oxidative environment. In general, PAN precursor fibers are considered to undergo reactions include cyclization, oxidation, dehydrogenation, and intermolecular crosslinking during the stabilization process in few hours. Figure 1.3. shows the model reaction paths of PAN during carbon fiber conversion.

Among the thermal stabilization reactions, cyclization reaction refers to how linear PAN molecular nitrile groups are converted to from stable, cyclic, ladder structures. During cyclization, exothermic heat is observed and PAN fiber undergoes progressive color change from slight yellow to gold, brown and then black. This is attributed to the transformation from the C≡N nitrile group to the conjugated carbon nitrogen double bond structure, –C=N–.[42] Although cyclization can be induced thermally under inert environment, oxygen-containing groups evolves in PAN ladder structure can improve stability toward higher temperature carbonization step. Therefore, typical cyclization step in carbon fiber industry are initiated with the presence of oxygen.

During stabilization process of PAN, dehydrogenation can occur simultaneously with cyclization. It is accompanied by introducing unsaturated bonds and oxygen into polymer chains to form conjugated C=C bonds in the polymer backbone and stabilize carbon chains. During dehydrogenation, nitrile groups are left unreacted and water is eliminated with the formation of C=C bonds. When PAN fibers are stabilized in oxidative environment, oxygen uptake reactions occur and incorporate oxygen into ladder polymer backbone. While some studies suggest that oxidation requires cyclized ladder structure as

prerequisites,[41] some reported that oxygen uptake reactions can take place at any stage of heat treatment to accelerate cyclization initiation and promote crosslinking among polymer chains. In general, optimal oxygen uptake for improved carbon yield and carbon fiber mechanical properties is about 8% to 10%.[49-51] Intermolecular azomethine crosslinking reaction originates from protons abstracted from a polymer chain by the nitrile nitrogen in the neighboring chain. While cyclization can be intramolecular or intermolecular, studies have proposed the propagation of crosslinking when cyclization skips from one chain to another chain.

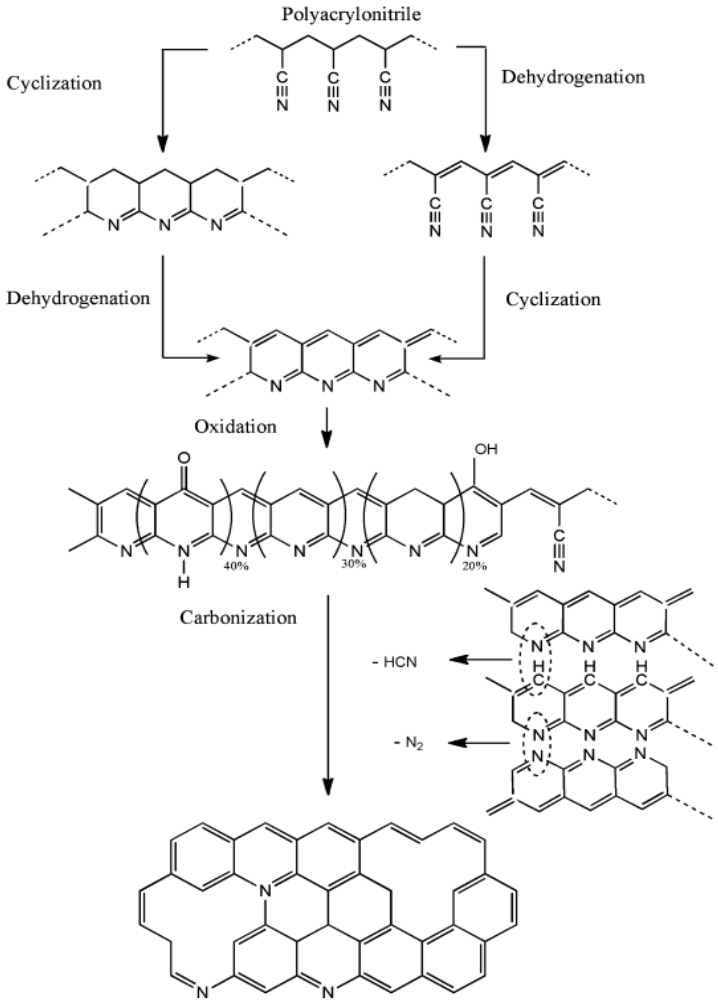

Figure 1.3. Chemical reaction during stabilization and carbonization of PAN fiber production.[6]

1.2.1.2 Carbonization and Graphitization of PAN-based Fibers

After the thermal stabilization stage, the non-meltable and flame-resistant stabilized fibers are heated in inert environment typically from 1,000 ˚C to 1,700 ˚C in order to convert to carbon fibers.[52] During this stage, the ladder polymer structure first undergoes crosslinking in low temperature and subsequently goes through condensation reactions to result in turbostratic carbon forms when carbonized around 1,600 ˚C. This carbon phase is comprised of well-oriented, three-dimensional carbon-type crosslinks between graphite-like layers which attribute to improved tensile strength of carbon fibers. The process with further heating up to 3,000 ˚C is called graphitization. Although graphitized fibers normally show higher moduli due to more ordered structure, tensile strength of graphitized fibers are generally compromised.

1.2.2 Lignin-based Carbon Fibers

1.2.2.1 Lignin Background and Structure

Lignin, often referred as the second most abundant natural biopolymer to cellulose on earth,[54] is a polymer of phenylpropane units that accounts for 10% to 30% of wood.[53,55] Within plants, lignin provides essential functions such as internal transport of water and nutrients, imparting rigidity to cell wall, and acting as a permanent bonding agent between cell walls to create impact, bending and compression resistant structures. Although first recognized in 1838 as an "encrusting materials" that embeds cellulose in woods, the term "lignin" was not introduced until 1865 as a name derived from Latin word of wood, *lignum*.[53, 55-57] However, the concept and the chemical structure of lignin have been left in nebulous state ever since its discovery. In general, lignin is considered as an amorphous, three-dimensional polyaromatic heteropolymer that comprises of phenylpropane

monomers that linked in various ways through enzymatic dehydrogenation followed by radical coupling. The main three monomers, or monolignols, are p-coumaryl, coniferyl, and sinapyl alcohols that are different in the number and positions of the methoxyl groups on the aromatic rings. In the lignin structure, the monolignols undergo combinatorial radial coupling process and are thus present in forms of p-hydroxylphenol, guaiacyl, and syringyl units, shown as Figure 1.4. Although lignins from all species of plants consist more or less of all three units, grass or annual plant lignins are mainly composed of p-hydroxylphenol units with slight amount of guaiacyl and syringyl units. Softwood (gymnosperm) lignins are mostly composed of guaiacyl units with low amount of syringyl and p-hydroxylphenol units. Hardwood (angiosperm) lignins, on the other hand, mainly consist of guaiacyl and syringyl units and low level of p-hydyoxylphenol units. A proposed structure of lignin comprised of coniferyl alcohol was shown as Figure 1.5.

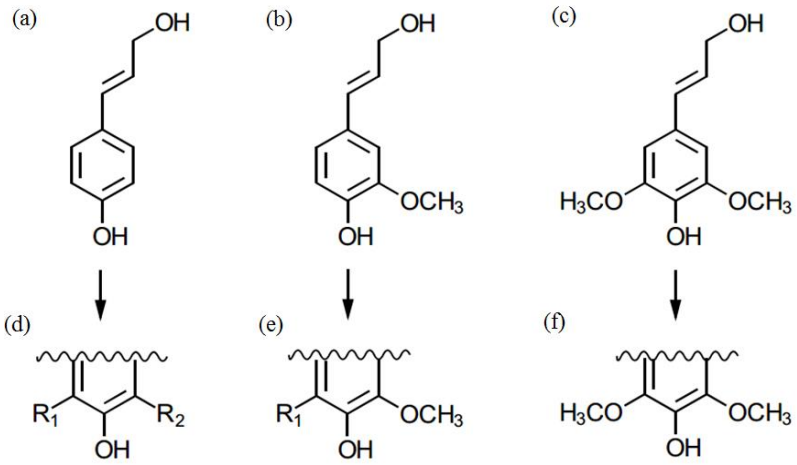

Figure 1.4. Lignin monomers (a) p-coumaryl alcohol, (b) coniferyl alcohol, (c) sinapyl alcohol and the respective units (d) p-hydroxyphenyl, (e) guaiacyl, and (f) syringyl lignins.

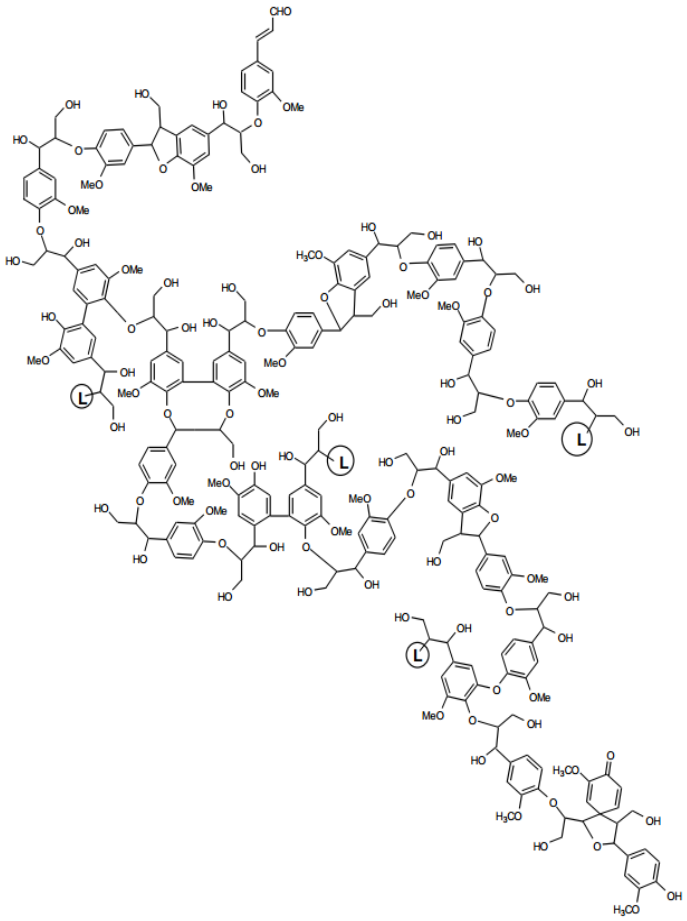

Figure 1.5. Proposed softwood lignin chemical structure.[2]

1.2.2.2 Historical Perspectives of Lignin-Based Carbon Fibers

Generated by the industrial pulping process for approximately 26 to 50 million tons in annual world production,[60-61] lignin was traditionally neglected as the byproduct and considered as a low value biofuel burned for heat and power.[62-67] Recognizing the cost-effective, abundant, and renewable characteristics of lignin, a number of studies have devoted effort to employing lignin for value added products such as activated carbon, plastic materials, and carbon fibers. Until now, the best reported lignin-based carbon fiber from modified technical lignin has exhibited average tensile strength, modulus, and

extensibility at 1.07 GPa, 82.7 GPa, and 2.03%, respectively.[13, 81] Figure 1.6., which illustrates the frequency of lignin-based carbon fiber patents and articles by year, demonstrates the increasing attention that lignin-based carbon fiber has received over the last several decades.

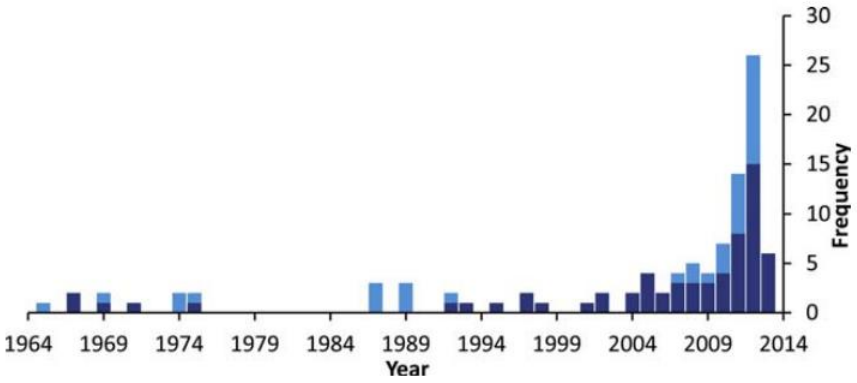

Figure 1.6. Lignin-based carbon fiber-related patents (light) and journal articles (dark) by year.[5]

In the 1960s, Otani et al. demonstrated carbonizing melt- or dry-spun fibers (20 – 30 μm in diameters) comprised of akali lignin, thiolignin, or ligninsulfonate. Interestingly, although Otani et al. stated that carbonized lignin composite fiber with HMWP showed lower mechanical properties after carbonization, they claimed that stronger precursor fiber can be manufactured when incorporating high molecular weight polymers (HMWP) such as polyvinyl alcohol (PVA) and polyacrylonitrile (PAN). They reported tensile strengths of carbonized fibers ranged from 0.147 GPa to 0.785 GPa. In the early 1970s, the Nippon Kayaku Company, which developed and commercialized Kayacarbon lignin carbon fibers, made them available for a brief period. In these products, the lignin and PVA as plasticizer, were dissolved in alkali solution and further dry spun to form precursor fibers.[10-11]

In the early 1990s, Sudo et al. reported utilizing the pitch of hydrogenolysis or phenolysis modified steam-exploded lignin as carbon fiber precursors.[77] The purpose of hydrogenolysis and phenolysis was to remove the hydroxyl and hydroxyl methyl functional group on lignin cross linkages, which could compromise the thermal fluidity of lignin and thus limited spinnability. The authors also investigated the spinnability and thermal stability of the modified lignin pitch and showed resultant carbon fibers with an average diameter of 7.6 ± 2.7 μm and exhibited tensile strength ranging from 0.31 GPa to 0.66 GPa, a modulus of elasticity of 40.7 GPa, and elongation at break ranging from 1.0% to 1.4%. Kubo and coworkers later reported carbonized fibers from hardwood and softwood acetic lignin[82] and Organosolv lignin.[82] Although they observed no major breakthrough from the mechanical properties, interestingly, they found that softwood acetic lignin fiber could be directly carbonized under nitrogen without a thermal stabilization stage. However, the process of softwood acetic lignin fiber under direct carbonization showed porous structures on fiber surface and thus exhibited weak mechanical performance. Owing to the porous structure, Uraki et al. further investigated the possibility of employing direct-carbonize softwood acetic lignin fiber for activated carbon fiber applications.[13] Uraki's work still recommended brief thermal stabilization (1 hour at 250 °C) for softwood acetic lignin fiber to maintain the fibrous shape. They then carbonized the stabilized fibers at 1,000 °C for one hour with nitrogen, followed by a steam activation mixed with nitrogen stream at 900 °C for 40 to 80 minutes in an electric furnace. The activated carbon fiber from softwood acetic lignin showed a surface area ranging from 1,400 – 1,930 m^2/g, which was claimed to be comparable to the highest performance of contemporary commercial activated carbon fibers.[14]

During the early 2000s, Kadla et al. fabricated carbon fibers from Organosolv lignin (Alcell^{TM}), softwood kraft lignin (Indulin AT^{TM}), and hardwood kraft lignin along with the polymer blend with poly(ethylene oxide) (PEO) through melt spinning.[5] They reported lignin blends with PEO to show miscible with lower glass transition temperature (T_g) and better spinnability but all PEO/Alcell fiber and PEO/hardwood lignin blends with ≥ 5% PEO content as thermally unstable. They shows that carbon fiber with diameters from 31 – 46 µm, and tensile strength, modulus, and elongation at break to be 339 – 448 MPa, 33 – 59 GPa, and 0.79% – 1.25, respectively. However, they reported no correlations between carbon fiber mechanical properties and the PEO blend content or molecular weight (100 – 600 Kg/mol). In addition, carbon fibers with melt-spun precursor from blends of hardwood kraft lignin and synthetic polymers such as poly(ethylene terephthalate) (PET) and polypropylene (PP) were also reported by Kubo and Kadla.[83-85] They mixed various ratios of lignin and synthetic polymers and subsequently processed them into pellets that were later thermally extruded, forming precursor fibers. While they reported that the blending with PET/PP decreased the carbon fiber yield, they showed enhanced thermal stability from lignin/PET blends. They showed while structures from the lignin/PP carbon fiber were porous, those from lignin/PET carbon fibers exhibited a smooth surface. Consequently, they observed that lignin/PP carbon fibers exhibited lower mechanical properties than lignin and lignin/PET carbon fibers. They reported that lignin/PET carbon fibers the average tensile strength and modulus of elasticity properties improved 16% and 54%, respectively over those of lignin carbon fibers. Table 1.1 summarizes the mechanical performance of lignin, lignin/PP, and lignin/PET carbon fibers

of Kubo and Kadla's work, among other lignin-based carbon fibers reported from the literature.

PAN has been proposed as a polymer candidate for coextrusion with lignin. Studies have shown that feasible processing and properties utilize the PAN/lignin system for solution-based spinning techniques. In 2011, Zoltek and Weyerhaeuser started a partnership to develop a PAN/lignin composite fiber in pilot-scale production under DOE funding.[1] They spun composite fibers of 15 wt% to 45 wt% of lignin via wet spinning. However, the production of carbon fibers with only up to 25 wt% lignin was successful due to increasing micro-voids in composite fibers with increasing lignin content, shown as Figure 1.7.

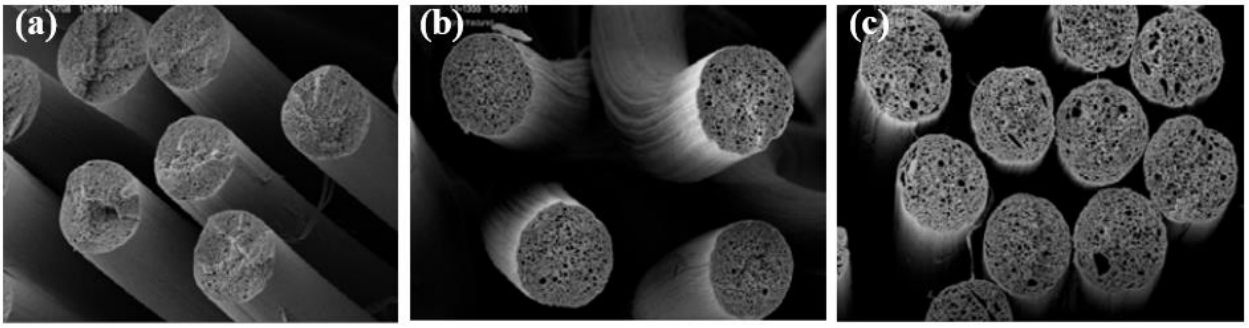

Figure 1.7. PAN/lignin composite fiber with (a) 25%, (b) 35%, and (c) 45 % lignin.[1]

1.2.2.3 Stabilization Scheme of Lignin

Although lignin-based carbon fiber development started in the early 1960s, information regarding the oxidative thermal stabilization mechanisms and conversions of lignin was limited.[41, 89-91] Unlike the conversion reaction of PAN precursors, which undergo oxidation, dehydrogenation, and cyclization under thermal stabilization, those of lignin-based fibers during thermal stabilization are complicated and not well-characterized because of their complex intermonomer linkages. Braun et al. characterized hardwood

kraft lignin fibers during thermal stabilization process by elemental and X-ray photoemission spectroscopic (XPS) analysis. Interestingly, as the β-O-4 linkage (arylglycerol-β-O-4 aryl ether linkage, shown as Figure 1.8) accounts for approximately 40% to 60% of lignin unit linkages, they reported this linkage as having the lowest bond dissociation energy in the lignin structure.[7, 96-98] Therefore, they proposed that the thermal stabilization reaction of the lignin was initiated by the hemolytic cleavage of the β-O-4 bonds in oxidative heating, which formed phenethyl and phenoxy radicals. They claimed that this free-radical chain mechanism would lead to further rearrangement of the lignin structure with direct linkages between aromatic rings and neighboring aliphatic chains, accompanied by the release of CO_2 and water as byproducts of the autoxidation of carbonyl and carboxyl groups. Brodin and Norberg et al. later reported softwood and hardwood lignin fibers stabilized in oxidative and nitrogen environments. Interestingly, they successfully stabilized softwood lignin fibers under an inert environment, but under an oxidative environment, the process of stabilization accelerates. While thermally stabilized in nitrogen, the phenolic-lignin end groups and terminal hydroxymethyl were unable to form carboxyl groups. Thus, no CO_2 was released during stabilization. Proposed lignin reaction schemes under either an oxidative or inert environment are shown in Figure 1.9.[100-103]

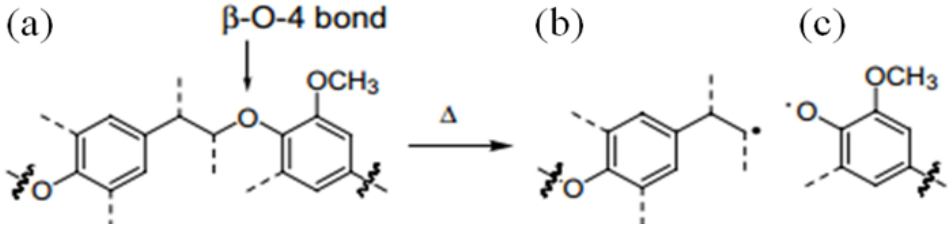

Figure 1.8. (a) Arylglycerol-β-O-4 aryl ether linkage as the dominant interunit linkage in lignins, (b) phenethyl, and (c) phenoxy radicals.[7]

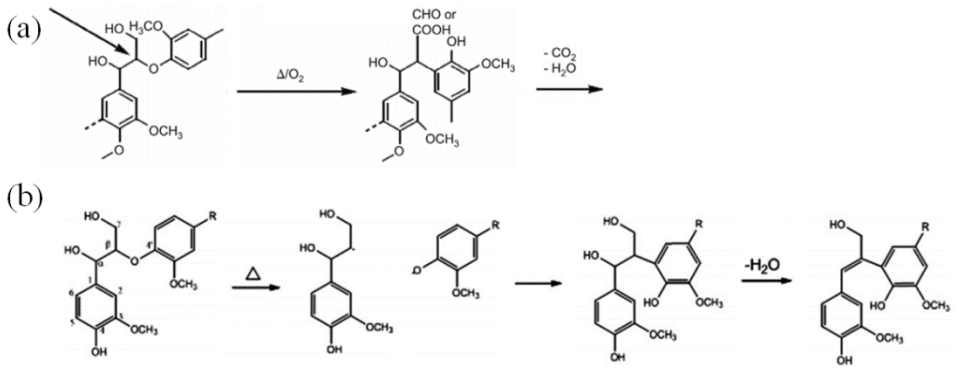

Figure 1.9. Lignin stabilization scheme under (a) oxidative environment[9] and (b) nitrogen.[10]

1.2.2.4 Effects of Lignin on Thermal Stabilization for Polymer Composites

Thermal analysis of lignin-incorporated polymer blends has shown that lignin in polymer can enhance the thermal stability of polymers, tune T_g for processing purposes, and alter enthalpy of the melting process and activation energy for pyrolysis reactions. Previous studies have reported that the altered thermal behavior might be attributed to possible bonding formation or intermolecular interaction between lignin and polymers, which implies that the incorporation of lignin affects the polymer blend thermal stabilization mechanisms during the carbon fiber conversion process. Sazanov et al. investigated the interactions between PAN and lignin under various forms (a dry powder mixture and a solution-cast film) and thermal treatments.[106] According to differential thermal analysis, Sazanov et al. reported peak temperature shifts, a broader peak width, and a decreased peak area on PAN/lignin films when compared to PAN, which they attributed to the catalytic effect of lignin on PAN cyclization. Although they provided few details that elucidate how lignin affects the PAN stabilization mechanism, Sazanov et al. reported that PAN/lignin blend showed a significant difference among the diffusion factors for PAN carbonization kinetics.

Table 1.1. Summary of lignin based carbon fiber mechanical properties

Type of Lignin	Diameter (μm)	Tensile Strength (MPa)	Tensile Modulus (GPa)	Elongation at break (%)
"Modified technical Lignin"[4]	NR	1070	82.7	2.03
Stream-exploded Lignin[10] (Hydrogenolysis)	7.6 ± 2.7	660 ± 230	40.7 ± 6.3	1.63 ± 0.29
Stream-exploded Lignin[11] (Phenolysis)	NR	310 – 460	NR	1.00 – 1.4
Organosolv Lignin (Acetic Acid)[12]	14 ± 1	355 ± 53	39.1 ± 13.3	0.98 ± 0.25
HWKL (Kadla)[13]	46 ± 8	422 ± 80	40 ± 11	1.12 ± 0.22
HWKL/PEO[13]	33 – 63	339 – 458	33 – 59	0.79 – 1.25
Alcell[13]	31 ± 3	388 ± 123	40 ± 14	1.00 ± 0.23
HWKL[14] (Kubo)	46 ± 8	605	61	1.44
HWKL/PP[14] (Up to 50% PP)	44 – 76	155 – 437	28 – 57	0.59 – 0.89
HWKL/PET[14] (Up to 25% PET)	31 – 45	669 – 703	84 – 94	1.06 – 1.13
HWKL[19] (Organic purified)	10 ± 1	520 ± 182	28.6 ± 3.2	NR
Acetylated Softwood Kraft Lignin[20]	~7	1040 ± 100	52 ± 2	2.0 ± 0.2
Softwood/hardwood kraft lignin[22] (LignoBoost)	36 – 78	233 – 377	25 – 33	0.86 – 1.2

1.2.3 Carbon Nanotube (CNT)-Incorporated Carbon Fibers

Since the early 1990s, carbon nanotubes (CNT) have been recognized for their excellent mechanical, thermal, and electrical properties. Typically available in single-walled (SWNT), double-walled (DWNT), and multi-walled (MWNT) geometries, CNTs show diameters ranging from ~1 nm to ~100 nm, depending on the number of walls. Theoretical calculations and experiments have reported SWNT with a Young's modulus and a strength of 0.6-1.3 TPa and 13-52 GPa, respectively. For MWNTs, Yu et al. reported a tensile strength and a modulus on the outermost layer ranging from 11 to 63 GPa and from ~270 to ~950 GPa, respectively. Interestingly, no apparent dependence of tensile strength on the outer shell diameter have been observed. However, an inverse relationship between Young's modulus values and MWNT diameters has been shown. Recognizing the promising mechanical properties of CNTs and the potential reinforcing effects, a number of studies have investigated the property enhancements of materials with the incorporation of CNT.

1.2.3.1 PAN/CNT Composite Carbon Fibers

As a predominant precursor of carbon fibers, polyacrylonitrile (PAN) is one of the promising candidates for polymer/CNT composites. To demonstrate the possibility of producing polymer/SWNT carbon fibers, Ko et al. fabricated electrospun, continuous nanofiber yarns.[116] Not surprisingly, the elastic modulus and thermal stability of fibers improved with increasing CNT loading. However, interactions between PAN and CNT along with the effects of CNT on stabilization and carbonization processes were not clearly reported. For CNT-incorporated PAN fibers, Chae et al. reported reinforcements of PAN fibers with various types of CNT. That is, the incorporation of CNT enhances PAN crystal

orientation, chain extensibility, and crystal sizes and thus improves the tensile properties of PAN fibers.[117] Comparing the PAN fibers with identical processing to PAN/CNT fibers, Chae et al. demonstrated a significant increase in the fiber tensile strength, the modulus, and elongation at break by 70%, 75%, and 110%, respectively.[120-122] In addition, after the carbonization process, they found that CNT improved the orientation and turbostratic carbonaceous structure of the resultant PAN/CNT carbon fibers. This finding demonstrated the templating effect of CNT on polymers and resulted in improved tensile properties of carbon fibers. During the fabrication of PAN/CNT composite carbon fibers, the authors also observed that CNT improved PAN fiber thermal stability and thermal shrinkage. This finding suggested that CNT incorporation could potentially affect the fiber stabilization and carbonization process. Liu et al. later investigated the effects of CNT on thermal stabilization kinetics under various parameters. They reported that the addition of CNT improved the orientation of the stabilized ladder polymer structure, allowed higher stress loading during stabilization, and reduced activation energies for both oxidation and crosslinking reactions.[120-122]

1.2.3.2 Lignin/CNT Composite Carbon Fibers

To investigate the possibilities of improving the thermal conductivity, mechanical performance, and electrical conductivity of lignin fiber systems, CNT have been incorporated into lignin-based fibers. In 2011, Baker et al. reported enhancements on both the tensile strength and the tensile modulus when CNT (up to 10%) were added into continuously melt-spun hardwood lignin, organosolv lignin, or softwood/hardwood lignin-blend carbon fibers.[3] They reported successful CNT dispersion within the melt-spun fiber, shown in Figure 1.10. The authors also reported that CNT could improve fiber stretching

and reduce fiber diameters and thus successfully strengthen both precursor and carbonized fibers. Optimal composite carbon fibers exhibited around 20% and 50% improvement in the tensile strength and the tensile modulus over neat lignin carbon fibers. However, they presented no further details or numerical data of the carbon fiber properties. In a recent literature review, Baker et al. reported improvements of lignin/CNT carbon fiber properties and described them as "poor" when compared to the property enhancement of precursor composite fibers.[3,5] The review article attributed the poor enhancement to the low interfacial adhesion between CNT and lignin carbons according to the "pealed" CNT from the fiber structure during fracturing.[5]

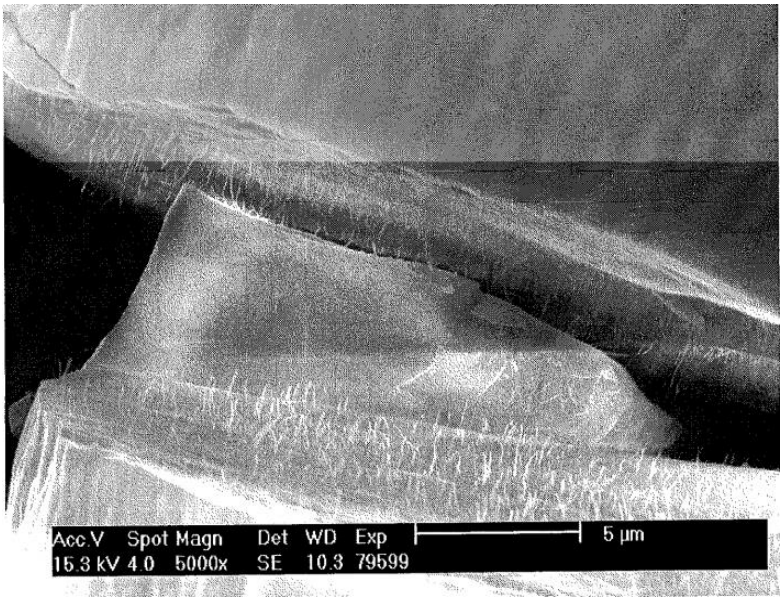

Figure 1.10. Fracture surface of lignin fiber with CNT dispersed therein.[3]

More recently, interest in submicron electrospun lignin-based composite fibers has increased. Teng et al. reported carbonized electrospun lignin-based fiber with the addition of MWNT (1 to 6 wt%).[130-133] In their study, MWNT incorporation (≤ 4 wt% loading) in fibers could improve the tensile moduli of as-spun and thermostabilized fibers and the

elongation at break of carbonized fibers. However, Teng et al. also reported the curling of MWNT-containing fibers during carbonization that later resulted in loss of tensile moduli after carbonization. In addition, TEM images revealed MWNT pullouts from fibers under stress loading, suggesting poor load transfer between lignin and MWNT in fibers. These observations along with the poorly ordered/aligned MWNT in fiber explained the reduction in tensile moduli of the carbonized fibers. Surprisingly, unlike PAN-based carbon fibers, in which electrical conductivity substantially increased with the addition of CNT, no improvement on the electrical conductivity of lignin/MWNT carbon fibers was observed until 6 wt% loading of MWNT.

1.2.4 Fiber Spinning of Solution-Based Lignin/Polymer Blends

Owing to the indefinite molecular structures and complex crosslinking forms of lignin that can limit lignin processability and the resultant fiber properties, recent investigations have called for a better understanding and modulation of the rheological behavior of lignin in melt, gelation, and the molecular assembly with polymers solutions. That is, controlling the syringyl/guaiacyl monolignol ratio in the lignin structure is shown to affect the viscosity of the melt. Poly(ethylene oxide) in solution with lignin can decrease the size of lignin aggregates and regulate lignin molecules to form less-branched, anisotropically cylindrical self-assemblies to enhance processability.[130,134-136] Multiple recent studies have reported that the incorporation of lignin in PAN solution can reduce solution viscosity, affect blend miscibility, solution spinnability, and resultant fiber morphology.[1, 130] However, to date, the fundamental understanding of the interactions between lignin and PAN or other polymers in solution for fiber processing is still limited.

1.3 THESIS OBJECTIVES

To address the barriers for further development of lignin incorporated carbon fibers, the objectives of this study are:

- To develop effective characterizations of the rheological interactions between lignin and polyacrylonitrile (PAN) in composite solutions to allow optimized lignin loading in fiber processing.
- To study the processing, structure, and properties of gel spun PAN, PAN/lignin, and PAN/lignin/carbon nanotubes (CNT) composite fibers.
- To study the stabilization and carbonization behaviors of lignin and CNT incorporated gel-spun PAN-based fibers.
- To study and to develop small-diameter PAN/Lignin composite fibers through bi-component spinning.

1.4 REFERENCES

[1]. Husman, G. In *Development and Commercialization of a Novel Low-cost Carbon Fiber*, Presentation at 2012 DOE Hydrogen and Fuel Cells Program and Vehicle Technologies Program Annual Merit Review and Peer Evaluation Meeting, **2012**.

[2]. Henriksson, G., *Wood chemistry and wood biotechnology*. Walter de Gruyter: **2009**; Vol. 1.

[3]. Baker, F. S.; Baker, D. A.; Menchhofer, P. A. Carbon Nanotube (CNT)-Enhanced Precursor for Carbon Fiber Production and Method of Making a CNT-enhanced Continous Lignin Fiber. US 2011/0285049 A1, **2011**.

[4]. Warren, C. D.; Naskar, A. K. In *Presentation at 2012 DOE Hydrogen and Fuel Cells Program and Vehicle Technologies Program Annual Merit Review and Peer Evaluation Meeting*, May 16, 2012; **2012**.

[5]. Baker, D. A.; Rials, T. G., Recent Advances in Low-Cost Carbon Fiber Manufacture from Lignin. *Journal of Applied Polymer Science* **2013,** *130* (2), 713-728.

[6]. Frank, E.; Hermanutz, F.; Buchmeiser, M. R., Carbon Fibers: Precursors, Manufacturing, and Properties. *Macromolecular Materials and Engineering* **2012,** *297* (6), 493-501.

[7]. Braun, J. L.; Holtman, K. M.; Kadla, J. F., Lignin-based Carbon Fibers: Oxidative Thermostabilization of Kraft Lignin. *Carbon* **2006,** (2), 385.

[8]. Brodin, I.; Ernstsson, M.; Gellerstedt, G.; Sjöholm, E., Oxidative Stabilisation of Kraft Lignin for Carbon Fibre Production. *Holzforschung: International Journal of the Biology, Chemistry, Physics, & Technology of Wood* **2012,** *66* (2), 141-147.

[9]. Norberg, I.; Nordstrom, Y.; Drougge, R.; Gellerstedt, G.; Sjo¨holm, E., A new method for stabilizing softwood kraft lignin fibers for carbon fiber production. *Journal of Applied Polymer Science* **2013,** *128* (6), 3824-3830.

[10]. Sudo, K.; Shimizu, K., A New Carbon Fiber from Lignin. *Journal of Applied Polymer Science* **1992,** *44* (1), 127-134.

[11]. Sudo, K.; Shimizu, K.; Nakashima, N.; Yokoyama, A., A new modification method of exploded lignin for the preparation of a carbon fiber precursor. *Journal of Applied Polymer Science* **1993,** *48* (8), 1485-1491.

[12]. Uraki, Y.; Kubo, S.; Nigo, N.; Sano, Y.; Sasaya, T., Preparation of Carbon Fibers from Organosolv Lignin Obtained by Aqueous Acetic Acid Pulping. *Holzforschung* **1995,** *49* (4), 343-350.

[13]. Kadla, J. F.; Kubo, S.; Venditti, R. A.; Gilbert, R. D.; Compere, A. L.; Griffith, W., Lignin-based Carbon Fibers for Composite Fiber Applications. *Carbon* **2002,** (15), 2913.

[14]. Kubo, S.; Kadla, J. F., Lignin-based Carbon Fibers: Effect of Synthetic Polymer Blending on Fiber Properties. *Journal of Polymers & the Environment* **2005,** *13* (2), 97-105.

[15]. Liu, Y.; Kumar, S., Recent Progress in Fabrication, Structure, and Properties of Carbon Fibers. *Polymer Reviews* **2012,** *52* (3-4), 234-258.

[16]. Barton, B. E.; Patton, J. T.; Hukkanen, E. J.; Bernius, M. T., Two-step sulfonation process for the conversion of polymer fibers to carbon fibers. U.S. Patent Application 14/413,454: **2015**.

[17]. Minus, M. L.; Kumar, S., The Processing, Properties, and Structure of Carbon Fibers. *JOM* **2005,** *57* (2), 52-58.

[18]. Ogale, A. A.; Zhang, M.; Jin, J., Recent advances in carbon fibers derived from biobased precursors. *Journal of Applied Polymer Science* **2016,** *133* (45), 43794 (1-13).

[19]. Baker, D. A.; Gallego, N. C.; Baker, F. S., On the characterization and spinning of an organic-purified lignin toward the manufacture of low-cost carbon fiber. *Journal of Applied Polymer Science* **2012,** *124* (1), 227-234.

[20]. Zhang, M.; Ogale, A. A., Carbon fibers from dry-spinning of acetylated softwood kraft lignin. *Carbon* **2014,** *69*, 626-629.

[21]. Newcomb, B. A.; Giannuzzi, L. A.; Lyons, K. M.; Gulgunje, P. V.; Gupta, K.; Liu, Y.; Kamath, M. G.; McDonald, K.; Moon, J.; Feng, B.; Peterson, G. P.; Chae, H. G.; Kumar, S., High Resolution Transmission Electron Microscopy Study on Polyacrylonitrile/Carbon Nanotube Based Carbon Fibers and the Effect of Structure Development on the Thermal and Electrical Conductivities. *Carbon* **2015,** *93*, 502-514.

[22]. Nordström, Y.; Joffe, R.; Sjöholm, E., Mechanical characterization and application of Weibull statistics to the strength of softwood lignin-based carbon fibers. *Journal of Applied Polymer Science* **2013,** *130* (5), 3689-3697.

[23]. Kumar, S.; Anderson, D. P.; Crasto, A. S., Carbon Fibre Compressive Strength and Its Dependence on Structure and Morphology. *Journal of Materials Science* **1993,** *28* (2), 423-439.

[24]. Masson, J. C., *Acrylic fiber technology and applications*. Marcel Dekker, Inc, New York: **1995**.

[25]. Peebles, L. H., *Carbon Fibers, Formation, Structure and Properties*. CRC, Boca Raton: **1995**.

[26]. Atureliya, S. K.; Bashir, Z., Continuous Plasticized Melt-extrusion of Polyacrylonitrile Homopolymer. *Polymer* **1993,** *34* (24), 5116-5122.

[27]. Daumit, G. P.; Ko, Y. S.; Slater, C. R.; Venner, J. G.; Young, C. C., Melt-spun acrylic fibers possessing a highly uniform internal structure which are particularly suited for thermal conversion to quality carbon fibers. U.S. Patents US5168004: **1992**.

[28]. Chung, D. L., *Carbon Fiber Composites* Butterworth-Heinemann, Boston: **1994**.

[29]. Huang, X. S., Fabrication and Properties of Carbon Fibers. *MATERIALS* **2009,** *2* (4), 2369-2403.

[30]. Kaur, J.; Millington, K.; Smith, S., Producing high-quality precursor polymer and fibers to achieve theoretical strength in carbon fibers: A review. *Journal of Applied Polymer Science* **2016,** *133* (38), 43963 (1-14).

[31]. Shindo, A., Studies on Graphite Fiber. *Journal of Ceramic Association, Japan* **1961,** *69,* C195.

[32]. Shindo, A., On the Carbonization of Polyacrylonitrile Fiber. *Carbon* **1964,** *1* (3), 391-392.

[33]. Hexcel. HexTow® Continuous Carbon Fiber Products [accessed, September 2016]. Available from: http://www.hexcel.com/resources/cont-carbon-fiber-data-sheets.

[34]. Toray. Tensile Strength and Tensile Modulus of T1100G. [accessed, September 2016]. Available from: http://goo.gl/TF4gdX.

[35]. Yakobson, B. I.; Avouris, P., Mechanical Properties of Carbon Nanotubes. In *Carbon Nanotubes*, Springer Berlin Heidelberg: **2001**; Chapter 12, pp 287-327.

[36]. Dumitrica, T.; Hua, M.; Yakobson, B. I., Symmetry-, Time-, and Temperature-dependent Strength of Carbon Nanotubes. *Proceedings of the National Academy of Sciences* **2006,** *103* (16), 6105-6109.

[37]. Chae, H. G.; Newcomb, B. A.; Gulgunje, P. V.; Liu, Y.; Gupta, K. K.; Kamath, M. G.; Lyons, K. M.; Ghoshal, S.; Pramanik, C.; Giannuzzi, L.; Şahin, K.; Chasiotis, I.; Kumar, S., High Strength and High Modulus Carbon Fibers. *Carbon* **2015,** *93*, 81-87.

[38]. Dalton, S.; Heatley, F.; Budd, P. M., Thermal Stabilization of Polyacrylonitrile Fibres. *Polymer* **1999,** *40* (20), 5531-5543.

[39]. Standage, A. E.; Matkowsky, R. D., Thermal Oxidation of Polyacrylonitrile. *European Polymer Journal* **1971,** *7* (7), 775-783.

[40]. Schurz, J., Discoloration Effects in Acrylonitrile Polymers. *Journal of Polymer Science* **1958,** *28* (117), 438-439.

[41]. Fitzer, E.; Müller, D. J., The Influence of Oxygen on the Chemical Reactions During Stabilization of PAN as Carbon Fiber Precursor. *Carbon* **1975,** *13* (1), 63-69.

[42]. Rangarajan, P.; Bhanu, V. A.; Godshall, D.; Wilkes, G. L.; McGrath, J. E.; Baird, D. G., Dynamic Oscillatory Shear Properties of Potentially Melt Processable High Acrylonitrile Terpolymers. *Polymer* **2002,** *43* (9), 2699-2709.

[43]. Takahagi, T.; Shimada, I.; Fukuhara, M.; Morita, K.; Ishitani, A., XPS studies on the chemical structure of the stabilized polyacrylonitrile fiber in the carbon fiber production process. *Journal of Polymer Science Part A: Polymer Chemistry* **1986,** *24* (11), 3101-3107.

[44]. Rahaman, M. S. A.; Ismail, A. F.; Mustafa, A., A review of heat treatment on polyacrylonitrile fiber. *Polymer Degradation and Stability* **2007,** *92* (8), 1421-1432.

[45]. Watt, W.; Johnson, W., Mechanism of Oxidisation of Polyacrylonitrile Fibres. *Nature* **1975,** *257* (5523), 210-212.

[46]. Potter, W. D.; Scott, G., Initiation of Low Temperature Degradation of Polyacrylonitrile. *Nature* **1972,** *236* (63), 30-32.

[47]. Rašković, V.; Marinković, S., Temperature Dependence of Processes During Oxidation of PAN Fibres. *Carbon* **1975,** *13* (6), 535-538.

[48]. Donnet, J. B. B., R. C., *Carbon Fibers*. 2 ed.; Marcel Dekker, New York: **1990**.

[49]. Bashir, Z., A Critical Review of the Stabilisation of Polyacrylonitrile. *Carbon* **1991,** *29* (8), 1081-1090.

[50]. Henrici-Olivé, G.; Olivé, S., Molecular interactions and macroscopic properties of polyacrylonitrile and model substances. In *Chemistry*, Springer Berlin Heidelberg: **1979**; Chapter 3, pp 123-152.

[51]. Grassie, N.; Hay, J. N., Thermal Coloration and Insolubilization in Polyacrylonitrile. *Journal of Polymer Science* **1962,** *56* (163), 189-202.

[52]. Boeriu, C. G.; Bravo, D.; Gosselink, R. J. A.; van Dam, J. E. G., Characterisation of structure-dependent functional properties of lignin with infrared spectroscopy. *Industrial Crops and Products* **2004,** *20* (2), 205-218.

[53]. Sakakibara, A.; Sano, Y., Chemistry of lignin. *Wood and Cellulosic Chemistry, 2nd edn. Marcel Dekker, Inc., New York* **2000**, 109-173.

[54]. Sarkanen, K. V.; Ludwig, C. H., *Lignins: occurrence, formation, structure and reactions*. Wiley Interscience: **1971**.

[55]. SjÖStrÖM, E., LIGNIN. In *Wood Chemistry*, Second ed.; Academic Press: San Diego, **1993**, pp 71-89.

[56]. Glasser, W. G.; Sarkanen, S., *Lignin: properties and materials*. American Chemical Society: **1989**.

[57]. Pearl, I. A., *The chemistry of lignin*. Edward Arnold (Publishers) Ltd.: **1967**.

[58]. Casey, J. P., *Pulp and paper: chemistry and chemical technology*. Interscience Publishers: New York, **1952**.

[59]. Glasser, W. G.; Kelley, S. S., *Concise Encyclopedia of Polymer Science and Engineering*. Wiley-Interscience: Hoboken, New Jersey, **1990**; p 544.

[60]. Ghatak, H. R., Biorefineries from the perspective of sustainability: Feedstocks, products, and processes. *Renewable and Sustainable Energy Reviews* **2011,** *15* (8), 4042-4052.

[61]. Ragauskas, A. J.; Williams, C. K.; Davison, B. H.; Britovsek, G.; Cairney, J.; Eckert, C. A.; Frederick, W. J.; Hallett, J. P.; Leak, D. J.; Liotta, C. L.; Mielenz, J. R.; Murphy, R.; Templer, R.; Tschaplinski, T., The Path Forward for Biofuels and Biomaterials. *Science* **2006,** *311* (5760), 484-489.

[62]. Hu, S.; Zhang, S.; Pan, N.; Hsieh, Y., High energy density supercapacitors from lignin derived submicron activated carbon fibers in aqueous electrolytes. *Journal of Power Sources* **2014,** *270*, 106-112.

[63]. Shen, Q.; Zhang, T.; Zhang, W.; Chen, S.; Mezgebe, M., Lignin-based activated carbon fibers and controllable pore size and properties. *Journal of Applied Polymer Science* **2011,** *121* (2), 989-994.

[64]. Suhas; Carrott, P. J. M.; Ribeiro Carrott, M. M. L., Lignin - from natural adsorbent to activated carbon: A review. *Bioresource Technology* **2007,** *98* (12), 2301-2312.

[65]. Suzuki, M., Activated carbon fiber: Fundamentals and applications. *Carbon* **1994,** *32* (4), 577-586.

[66]. Rodriguez-Mirasol, J.; Cordero, T.; Rodriguez, J. J., Activated carbons from carbon dioxide partial gasification of eucalyptus kraft lignin. *Energy & Fuels* **1993,** *7* (1), 133-138.

[67]. Snowdon, M. R.; Mohanty, A. K.; Misra, M., A Study of Carbonized Lignin as an Alternative to Carbon Black. *ACS Sustainable Chemistry & Engineering* **2014,** *2* (5), 1257-1263.

[68]. Thakur, V. K.; Thakur, M. K.; Raghavan, P.; Kessler, M. R., Progress in Green Polymer Composites from Lignin for Multifunctional Applications: A Review. *ACS Sustainable Chemistry & Engineering* **2014,** *2* (5), 1072-1092.

[69]. Chung, Y.; Olsson, J. V.; Li, R. J.; Frank, C. W.; Waymouth, R. M.; Billington, S. L.; Sattely, E. S., A Renewable Lignin–Lactide Copolymer and Application in Biobased Composites. *ACS Sustainable Chemistry & Engineering* **2013,** *1* (10), 1231-1238.

[70]. Saito, T.; Brown, R. H.; Hunt, M. A.; Naskar, A. K.; Pickel, D. L.; Pickel, J. M.; Messman, J. M.; Baker, F. S.; Keller, M., Turning renewable resources into value-added polymer: Development of lignin-based thermoplastic. *Green Chemistry* **2012,** *14* (12), 3295-3303.

[71]. Jeong, H.; Park, J.; Kim, S.; Lee, J.; Cho, J., Use of Acetylated Softwood Kraft Lignin as Filler in Synthetic Polymers. *Fibers and Polymers* **2012,** *13* (10), 1310-1318.

[72]. Košíková, B.; Gregorová, A.; Osvald, A.; Krajčovičová, J., Role of lignin filler in stabilization of natural rubber–based composites. *Journal of Applied Polymer Science* **2007,** *103* (2), 1226-1231.

[73]. Toriz, G.; Denes, F.; Young, R. A., Lignin-Polypropylene Composites. Part 1: Composites from Unmodified Lignin and Polypropylene. *Polymer Composites* **2002,** *23* (5), 806-813.

[74]. Gregorová, A.; Cibulková, Z.; Košíková, B.; Šimon, P., Stabilization effect of lignin in polypropylene and recycled polypropylene. *Polymer Degradation and Stability* **2005,** *89* (3), 553-558.

[75]. Gregorová, A.; Košíková, B.; Moravčík, R., Stabilization effect of lignin in natural rubber. *Polymer Degradation and Stability* **2006,** *91* (2), 229-233.

[76]. Göran Gellerstedt, E. S. a. I. B., The Wood-Based Biorefinery: A Source of Carbon Fiber? *The Open Agriculture Journal* **2010,** *3*, 119-124.

[77]. Kubo, S.; Uraki, Y.; Sano, Y., Preparation of Carbon Fibers from Softwood Lignin by Atmospheric Acetic Acid Pulping. *Carbon* **1998,** *36* (7–8), 1119-1124.

[78]. Norgren, M.; Edlund, H., Lignin: Recent advances and emerging applications. *Current Opinion in Colloid & Interface Science* **2014,** *19* (5).

[79]. Eckert, R. C.; Abdullah, Z., Carbon fibers from kraft softwood lignin. U.S. Patents 7,678,358 B2: **2010**.

[80]. Otani, S.; Fukuoka, Y.; Igarashi, B.; Sasaki, K., Method for Producing Carbonized Lignin Fiber. U.S. Patents 3461082: **1969**.

[81]. Fukuoka, Y., Carbon fiber made from lignin (kayacarbon). *Japan Chemical Quarterly* **1969,** *5* (3), 63-66.

[82]. Uraki, Y.; Nakatani, A.; Kubo, S.; Sano, Y., Preparation of Activated Carbon Fibers with Large Specific Surface Area from Softwood Acetic Acid Lignin. *J Wood Sci* **2001,** *47* (6), 465-469.

[83]. Seydibeyoğlu, M. Ö., A Novel Partially Biobased PAN-Lignin Blend as a Potential Carbon Fiber Precursor. *Journal of Biomedicine and Biotechnology* **2012,** *2012*, 1-8.

[84]. Maradur, S. P.; Kim, B. H.; Yang, K. S.; Kim, C. H.; Kim, S. Y.; Kim, W. C., Preparation of Carbon Fibers from a Lignin Copolymer with Polyacrylonitrile. *Synthetic Metals* **2012,** *162* (5-6), 453-459.

[85]. Lehmann, A.; Ebeling, H.; Fink, H. P., Method for the production of lignin-containing precursor fibres and also carbon fibres. Application WO 2012/156443. **2013**.

[86]. Paulauskas, F. L.; Naskar, A. K.; Ozcan, S.; Keiser, J. R.; Gorog, J. P. *CRADA Final Report: Materials Development For Pulp and Paper Mills, Task 9 Proof of Commercial Concept: Commodity Carbon Fibers From Weyerhaeuser Lignin Based Fibers*; ORNL/TM-2010/171; **2010**.

[87]. Bissett, P. J.; Herriott, C. W., Lignin/Polyacrylonitrile-Containing Dopes, Fibers, and Methods of Making Same. U.S. Patents 2012/0003471: **2012**.

[88]. Ragauskas, A. J.; Beckham, G. T.; Biddy, M. J.; Chandra, R.; Chen, F.; Davis, M. F.; Davison, B. H.; Dixon, R. A.; Gilna, P.; Keller, M.; Langan, P.; Naskar, A. K.; Saddler, J. N.; Tschaplinski, T. J.; Tuskan, G. A.; Wyman, C. E., Lignin Valorization: Improving Lignin Processing in the Biorefinery. *Science* **2014,** *344* (6185).

[89]. Fitzer, E.; Frohs, W.; Heine, M., Optimization of Stabilization and Carbonization Treatment of PAN Fibres and Structural Characterization of the Resulting Carbon Fibres. *Carbon* **1986,** *24* (4), 387-395.

[90]. Shimada, I.; Takahagi, T.; Fukuhara, M.; Morita, K.; Ishitani, A., FT-IR Study of the Stabilization Reaction of Polyacrylonitrile in the Production of Carbon Fibers. *Journal of Polymer Science Part A: Polymer Chemistry* **1986,** *24* (8), 1989-1995.

[91]. Gupta, A. K.; Paliwal, D. K.; Bajaj, P., Effect of an acidic comonomer on thermooxidative stabilization of polyacrylonitrile. *Journal of Applied Polymer Science* **1995,** *58* (7), 1161-1174.

[92]. Lundquist, K., NMR Studies of Lignins. 2. Interpretation of the ^{1}H NMR Spectrum of Acetylated Birch Lignin. *Acta Chemica Scandinavia B* **1979,** *33*, 27-30.

[93]. Lundquist, K.; Stern, K., Analysis of lignins by 1H NMR spectroscopy. *Nordic Pulp & Paper Research Journal* **1989,** *4* (3), 210-213.

[94]. Britt, P. F.; Buchanan, A. C.; Malcolm, E. A., Thermolysis of Phenethyl Phenyl Ether: A Model for Ether Linkages in Lignin and Low Rank Coal. *The Journal of Organic Chemistry* **1995,** *60* (20), 6523-6536.

[95]. Britt, P. F.; Buchanan, A. C.; Malcolm, E. A., Impact of Restricted Mass Transport on Pyrolysis Pathways for Aryl Ether Containing Lignin Model Compounds. *Energy & Fuels* **2000,** *14* (6), 1314-1322.

[96]. Nimz, H., A New Type of Rearrangement in the Lignin Field. *Angewandte Chemie International Edition in English* **1966,** *5* (9), 843-843.

[97]. Gellerstedt, G.; Pettersson, B., Autoxidation of lignin. *Svensk Papperstidning-Nordisk Cellulosa* **1980,** *83* (11), 314-318.

[98]. Fenner, R. A.; Lephardt, J. O., Examination of the thermal decomposition of kraft pine lignin by Fourier transform infrared evolved gas analysis. *Journal of Agricultural and Food Chemistry* **1981,** *29* (4), 846-849.

[99]. Brodin, I.; Gellerstedt, G.; Sjöholm, E., The behavior of kraft lignin during thermal treatment. *Journal of Analytical and Applied Pyrolysis* **2010,** *87* (1), 70-77.

[100]. Corradini, E.; Pineda, E. A. G.; Hechenleitner, A. A. W., Lignin-poly (vinyl alcohol) blends studied by thermal analysis. *Polymer Degradation and Stability* **1999,** *66* (2), 199-208.

[101]. Wang, J.; Manley, R.; Feldman, D., Synthetic polymer-lignin copolymers and blends. *Progress in Polymer Science* **1992,** *17* (4), 611-646.

[102]. Kadla, J. F.; Kubo, S., Lignin-based polymer blends: analysis of intermolecular interactions in lignin–synthetic polymer blends. *Composites Part A: Applied Science and Manufacturing* **2004,** *35* (3), 395-400.

[103]. Canetti, M.; Bertini, F.; De Chirico, A.; Audisio, G., Thermal degradation behaviour of isotactic polypropylene blended with lignin. *Polymer Degradation and Stability* **2006,** *91* (3), 494-498.

[104]. Sazanov, Y. N.; Kostycheva, D. M.; Fedorova, G. N.; Ugolkov, V. L.; Kulikova, E. M.; Gribanov, A. V., Composites of lignin and polyacrylonitrile as carbon precursors. *Russian Journal of Applied Chemistry* **2008,** *81* (7), 1220-1223.

[105]. Sazanov, Y. N.; Fedorova, G. N.; Kulikova, E. M.; Kostycheva, D. M.; Novoselova, A. V.; Gribanov, A. V., Cocarbonization of polyacrylonitrile with lignin. *Russian Journal of Applied Chemistry* **2007,** *80* (4), 619-622.

[106]. Iijima, S., Helical Microtubules of Graphitic Carbon. *Nature* **1991,** *354* (6348), 56-58.

[107]. Salvetat, J. P.; Bonard, J. M.; Thomson, N. H.; Kulik, A. J.; Forró, L.; Benoit, W.; Zuppiroli, L., Mechanical Properties of Carbon Nanotubes. *Appl Phys A* **1999,** *69* (3), 255-260.

[108]. Tombler, T. W.; Zhou, C.; Alexseyev, L.; Kong, J.; Dai, H.; Liu, L.; Jayanthi, C. S.; Tang, M.; Wu, S., Reversible electromechanical characteristics of carbon nanotubes under local-probe manipulation. *Nature* **2000,** *405* (6788), 769-772.

[109]. Yu, M. F.; Files, B. S.; Arepalli, S.; Ruoff, R. S., Tensile Loading of Ropes of Single Wall Carbon Nanotubes and their Mechanical Properties. *Physical Review Letters* **2000,** *84* (24), 5552-5555.

[110]. Yu, M. F.; Lourie, O.; Dyer, M. J.; Moloni, K.; Kelly, T. F.; Ruoff, R. S., Strength and Breaking Mechanism of Multiwalled Carbon Nanotubes Under Tensile Load. *Science* **2000,** *287* (5453), 637-640.

[111]. Baughman, R. H.; Zakhidov, A. A.; de Heer, W. A., Carbon Nanotubes - the Route Toward Applications. *Science* **2002,** *297* (5582), 787-792.

[112]. Song, K.; Zhang, Y.; Meng, J.; Green, E.; Tajaddod, N.; Li, H.; Minus, M. L., Structural Polymer-Based Carbon Nanotube Composite Fibers: Understanding the Processing–Structure–Performance Relationship. *Materials* **2013,** *6* (6), 2543-2577.

[113]. Basu-Dutt, S.; Minus, M. L.; Jain, R.; Nepal, D.; Kumar, S., Chemistry of Carbon Nanotubes for Everyone. *Journal of Chemical Education* **2012,** *89* (2), 221-229.

[114]. Min, B. G.; Chae, H. G.; Minus, M. L.; Kumar, S., Polymer/Carbon Nanotube Composite Fibers—An Overview. *Functional Composites of Carbon Nanotubes and Applications* **2009**, 43-73.

[115]. Coleman, J. N.; Khan, U.; Blau, W. J.; Gun'ko, Y. K., Small but Strong: A Review of the Mechanical Properties of Carbon Nanotube–Polymer Composites. *Carbon* **2006,** *44* (9), 1624-1652.

[116]. Ko, F.; Gogotsi, Y.; Ali, A.; Naguib, N.; Ye, H.; Yang, G. L.; Li, C.; Willis, P., Electrospinning of Continuous Carbon Nanotube-Filled Nanofiber Yarns. *Advanced Materials* **2003,** *15* (14), 1161-1165.

[117]. Chae, H. G.; Sreekumar, T. V.; Uchida, T.; Kumar, S., A Comparison of Reinforcement Efficiency of Various Types of Carbon Nanotubes in Polyacrylonitrile Fiber. *Polymer* **2005,** *46* (24), 10925-10935.

[118]. Chae, H. G.; Minus, M. L.; Kumar, S., Oriented and Exfoliated Single Wall Carbon Nanotubes in Polyacrylonitrile. *Polymer* **2006,** *47* (10), 3494-3504.

[119]. Chae, H. G.; Minus, M. L.; Rasheed, A.; Kumar, S., Stabilization and Carbonization of Gel Spun Polyacrylonitrile/Single wall Carbon Nanotube Composite Fibers. *Polymer* **2007,** *48* (13), 3781-3789.

[120]. Liu, Y.; Chae, H. G.; Kumar, S., Gel-spun Carbon Nanotubes/Polyacrylonitrile Composite Fibers. Part I: Effect of Carbon Nanotubes on Stabilization. *Carbon* **2011,** *49*, 4466-4476.

[121]. Liu, Y.; Chae, H. G.; Kumar, S., Gel-spun Carbon Nanotubes/Polyacrylonitrile Composite Fibers. Part III: Effect of Stabilization Conditions on Carbon Fiber Properties. *Carbon* **2011,** *49*, 4487-4496.

[122]. Liu, Y.; Chae, H. G.; Kumar, S., Gel-spun Carbon Nanotubes/Polyacrylonitrile Composite Fibers. Part II: Stabilization Reaction Kinetics and Effect of Gas Environment. *Carbon* **2011,** *49*, 4477-4486.

[123]. Dallmeyer, I.; Lin, L. T.; Li, Y.; Ko, F.; Kadla, J. F., Preparation and Characterization of Interconnected, Kraft Lignin-Based Carbon Fibrous Materials by Electrospinning. *Macromolecular Materials and Engineering* **2013,** *298* (5), 540-551.

[124]. Seo, D. K.; Jeun, J. P.; Kim, H. B.; Kang, P. H., Preparation and characterization of the carbon nanofiber mat produced from electrospun PAN/lignin precursors by electron beam irradiation. *Rev. Adv. Mater. Sci* **2011,** *28*, 31-34.

[125]. Lallave, M.; Bedia, J.; Ruiz-Rosas, R.; Rodríguez-Mirasol, J.; Cordero, T.; Otero, J. C.; Marquez, M.; Barrero, A.; Loscertales, I. G., Filled and Hollow Carbon Nanofibers by Coaxial Electrospinning of Alcell Lignin without Binder Polymers. *Advanced Materials* **2007,** *19* (23), 4292-4296.

[126]. Lai, C.; Zhou, Z.; Zhang, L.; Wang, X.; Zhou, Q.; Zhao, Y.; Wang, Y.; Wu, X.; Zhu, Z.; Fong, H., Free-standing and mechanically flexible mats consisting of electrospun carbon nanofibers made from a natural product of alkali lignin as binder-free electrodes for high-performance supercapacitors. *Journal of Power Sources* **2014,** *247* (0), 134-141.

[127]. Poursorkhabi, V.; Mohanty, A. K.; Misra, M., Electrospinning of Aqueous Lignin/Poly(ethylene oxide) Complexes. *Journal of Applied Polymer Science* **2015,** *132* (2), 41260 (1-9).

[128]. Teng, N.; Dallmeyer, I.; Kadla, J. F., Incorporation of Multiwalled Carbon Nanotubes into Electrospun Softwood Kraft Lignin-Based Fibers. *Journal of Wood Chemistry and Technology* **2013,** *33* (4), 299-316.

[129]. Ra, E. J.; An, K. H.; Kim, K. K.; Jeong, S. Y.; Lee, Y. H., Anisotropic electrical conductivity of MWCNT/PAN nanofiber paper. *Chemical Physics Letters* **2005,** *413* (1–3), 188-193.

[130]. Oroumei, A.; Fox, B.; Naebe, M., Thermal and Rheological Characteristics of Biobased Carbon Fiber Precursor Derived from Low Molecular Weight Organosolv Lignin. *ACS Sustainable Chemistry & Engineering* **2015**.

[131]. Sun, Q.; Khunsupat, R.; Akato, K.; Tao, J.; Labbe, N.; Gallego, N. C.; Bozell, J. J.; Rials, T. G.; Tuskan, G. A.; Tschaplinski, T. J.; Naskar, A. K.; Pu, Y.; Ragauskas, A. J., A study of Poplar Organosolv Lignin After Melt Rheology Treatment as Carbon Fiber Precursors. *Green Chemistry* **2016**.

[132]. Imel, A. E.; Naskar, A. K.; Dadmun, M. D., Understanding the Impact of Poly(ethylene oxide) on the Assembly of Lignin in Solution toward Improved Carbon Fiber Production. *ACS Applied Materials & Interfaces* **2016,** *8* (5), 3200-3207.

[133]. Akato, K.; Tran, C. D.; Chen, J.; Naskar, A. K., Poly(ethylene oxide)-Assisted Macromolecular Self-Assembly of Lignin in ABS Matrix for Sustainable Composite Applications. *ACS Sustainable Chemistry & Engineering* **2015,** *3* (12), 3070-3076.

[134]. Ding, R.; Wu, H.; Thunga, M.; Bowler, N.; Kessler, M. R., Processing and Characterization of Low-cost Electrospun Carbon Fibers from Organosolv Lignin/Polyacrylonitrile Blends. *Carbon* **2016,** *100*, 126-136.

[135]. Jia, Z.; Lu, C.; Liu, Y.; Zhou, P.; Wang, L., Lignin/Polyacrylonitrile Composite Hollow Fibers Prepared by Wet-Spinning Method. *ACS Sustainable Chemistry & Engineering* **2016,** *4* (5), 2838-2842.

[136]. Husman, G. In *Development and Commercialization of a Novel Low-Cost Carbon Fiber*, Presentation at 2014 DOE Hydrogen and Fuel Cells Program and Vehicle Technologies Office Annual Merit Review and Peer Evaluation Meeting, **2014**.

CHAPTER 2

RHEOLOGICAL BEHAVIOR OF POLYACRYLONITRILE AND POLYACRYLONITRILE/LIGNIN BLENDS

2.1 INTRODUCTION

Throughout the research and development of advanced textiles, high-performance fibers such as Kevlar®, Dyneema®, Spectra®, and carbon fibers have attracted great attention due to their high specific strength, modulus, and versatile applications. While the exceptional mechanical properties of high-performance fibers are attributed to the highly aligned molecular structure, and minimized defects, voids, and polymer chain entanglements in fiber structure, processing optimization plays a decisive role of the resultant fiber properties. Currently, Kevlar®, Dyneema®, Spectra®, and polyacrlonitrile fibers as carbon fiber precursors are all manufactured from solutions that typically comprised of 5-20 wt% polymers dissolved in designated solvents.[3-7] In order to understand the polymer molecular behavior in solutions and ensure the fiber fabrication quality, rheological characterizations of the solution serve as a critical guidance toward further development. In the past decades, on the basis to advance polyacrylonitrile (PAN) based carbon fiber performance, investigation of PAN rheological systems related to solution homogeneity, spinnabiliy, gelation behavior, and coagulation conditions have been an unceasing research focus. Recently, surging interests in low-cost carbon fibers have called for more cost-effective alternatives for carbon fiber precursor materials and conversion processes. Lignin, as an abundant biorefinery byproduct and a melt-spinnable material, has

received increasing attentions for its utilization in carbon fiber. However, no demonstration of melt-spun lignin-based carbon fibers has been reported to date to meet the performance target of low cost carbon fibers set by the U.S. Department of Energy.[10-15] More recently, lignin has been proposed to be processed in solution state with other polymers, specifically with PAN, to form blend fiber with further conversion into carbon fibers. Nonetheless, the addition of lignin is shown to reduce polymer solution viscosity and affect spinnability.[12-13] Furthermore, lignin/polymer blends have also been reported with porous structure,[17] phase separation,[18] reduced drawability,[19-20] and thus limited the mechanical performance of resultant fibers.

In order to fully render the potential of mechanical performance of lignin incorporated fibers and the derived carbon fibers, understanding of the interactions between lignin and polymers in solutions or melts is critically desired. In this work, fundamental study of PAN, and PAN/annual plant lignin (APL) solutions with APL incorporation up to 37.5 wt% (with respect to total solid content) are conducted through dynamic shear rheology. Interactions between PAN and APL are depicted based on the characteristics of solution thermo-reversibility, miscibility, and viscoelastic behavior.

2.2 EXPERIMENTAL

2.2.1 Materials and Solution Preparation

Polyacrylonitrile-co-methacrylic acid (PAN-co-MAA; 4 wt% MAA, Mv = 247,000 g/mol) was acquired from Exlan, Co. (Osaka, Japan) and the sulfur free, annual plant lignin (APL) powder Protobind 2400 from the soda pulping process was provided by GreenValue (Media, PA). Organic solvent dimethylformamide (DMF) was obtained from Sigma-Aldrich and distilled before use. For PAN solution, PAN slurry is initially prepared by

adding polymer powder into DMF in a glass reactor with a solid concentration of 15 g/dL, followed by eight hours of stirring at 200 rpm at room temperature to prevent polymer agglomeration. After the stirring process, the slurry is slowly heated to 80 °C in silicone oil bath under continuous stirring at 200 rpm. The solution was then maintained under the same conditions for five hours before collection. Throughout the solution preparation, a nitrogen stream of 10 standard cubic feet per hour (SCFH) was introduced to avoid solution oxidation in glass reactor. Collected PAN solution then undergoes a 20-minute degas process under vacuum at 60°C before further characterizations. For PAN/APL composite solutions, APL solids were first dissolved in DMF by orbital shaker (MaxQ 4450, Thermo Scientific.) at 180 rpm and maintained at 40°C for eight hours before the subsequent addition of PAN polymer powder to form PAN/APL slurry in a glass reactor. PAN/APL solutions were then prepared under identical stirring, heating, and degas procedures to PAN solution. In this study, 3.5 g and 9 g of lignin solids are dissolved in 1 dL of DMF with control PAN solids (15 g/dL) to form PAN/APL1 and PAN/APL2 solutions with total solid content of 18.5 g/dL (18.9 wt% lignin in solids) and 24 g/dL (37.5 wt% lignin in solids), respectively.

2.2.2 Solution Characterizations

Rheology characterizations of all solutions are conducted using Discovery Hybrid Rheometer (TA Instruments) in parallel plate geometry, with a 60-mm plate on top and Peltier plate on the bottom with a gap size of 1 mm in between. Isochronal temperature scans of solutions at 1 rad/s from 60°C to 0°C, and then back to 60°C at a rate of 2°C/min were performed to investigate solution themo-reversibility, and storage modulus (G') and loss modulus (G") response to temperature. Dynamic frequency sweep measurements from

0.1 rad/s to 100 rad/s of each solution were performed at a temperature ranging from -7 °C to 56 °C (± 0.05 °C), with an increment of 7 °C. This temperature range is chosen in order to investigate the polymer behavior from solution state to viscoelastic stretching of as-spun dope, and during coagulation. During sample loading, a thin layer of silicone oil was applied to cover the exposed surface of solution to prevent solvent evaporation and moisture absorption during experiment.

2.3 RESULTS AND DISCUSSION

Isochronal temperature scans of PAN solution and PAN/APL blend solutions at an oscillatory frequency of 1 rad/s are shown as Figure 2.1. In each trial, solution sample undergoes a cooling scan from 60 °C to 0 °C, followed by a reheating scan from 0 °C to 60 °C. For PAN solution (Figure 2.1a.), storage modulus (G') increases with a decrease in temperature during cooling scan due to the reduced mobility of polymer chains and vice versa during the reheating scan. Throughout the cooling and subsequent reheating process between 60 °C and 0 °C, PAN solution exhibits thermo-reversibility with the recovery in G' and G" with respect to temperature gradient. In both cooling and reheating process, G" > G' in the entire temperature range, indicating the dominance of liquid-like behavior. For PAN/APL1 solution (18.9 wt% lignin, Figure 2.1b.), as G" of PAN/APL1 solution still recover with thermo-reversibility, G' of PAN/APL1 during reheat deviates from the PAN G' curve with enhanced elasticity compared to the cooling scan and exhibits an upturn starting around 37 °C. This G' upturn along with the change of G' curve slope around 37 °C imply a possible binodal temperature of the blend during reheating process.[19] In the case of PAN/APL2 (Figure 2.1c) solution, this effect is manifested with higher APL content in solution, where the reheat G' curve further deviates from the original G' curve of cooling

scan. In addition, G' upturn magnitude has increased and caused a local minimum around 37 °C for the PAN/APL2. When the higher magnitude of the G' upturn is attributed to the strong dynamic asymmetry of the constituent components (PAN and lignin in this case),

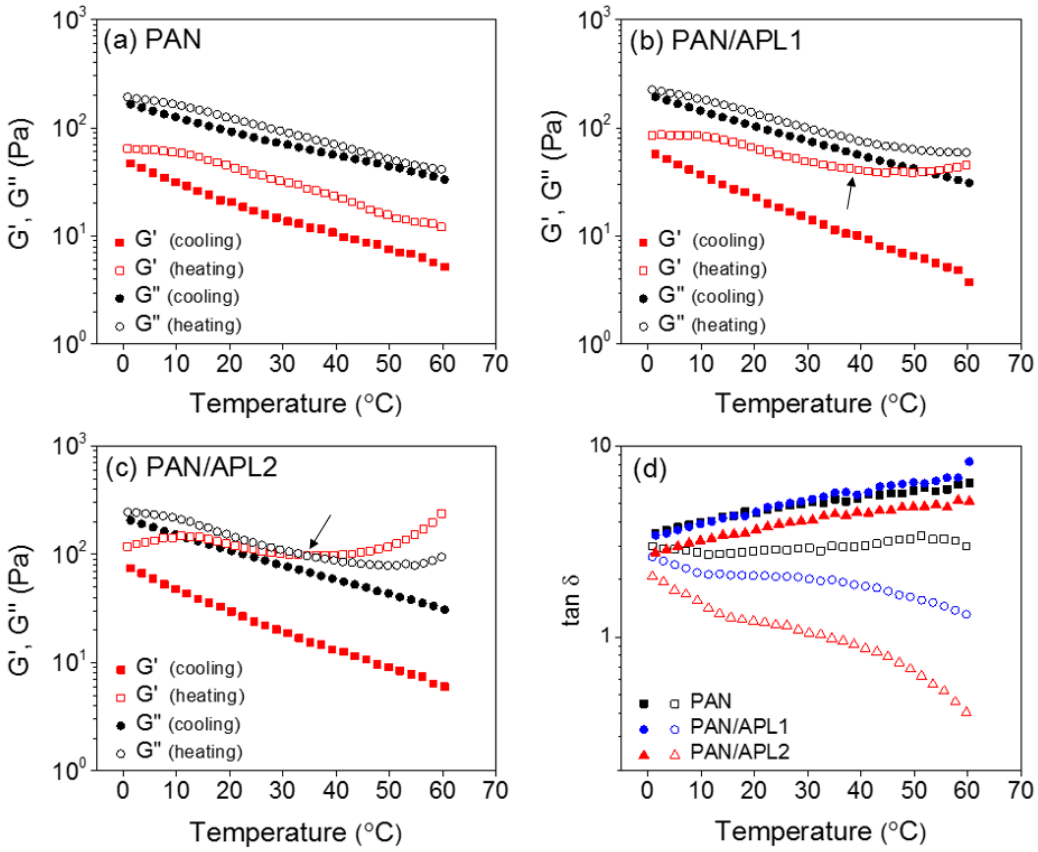

Figure 2.1. Storage modulus (G') and loss modulus (G") of (a) PAN, (b) PAN/APL1, and (c) PAN/APL2 solutions under isochronal temperature scans. Filled symbols represent the cooling scan and empty symbols represent the subsequent heating scan. Solution tan δ values are summarized in (d).

the minimum around 37 °C in G' curve suggests a spinodal point of the blend where minority-component rich domain and majority-component rich domain develop to alter solution G' behavior.[3, 22-25] Moreover, a crossover point of G' and G" is observed around

37 °C, suggesting formation of physical gel network through the thermo-rheological interactions between lignin and PAN. To monitor interactions between the elastic component (G') and the viscous component (G") of the solutions, loss tangent (tan δ) curves of PAN, PAN/APL1, and PAN/APL2 during isochronal temperature scans are shown in Figure 2.1d. In the initial cooling scan, PAN, PAN/APL1, and PAN/APL2 exhibited comparable tan δ magnitude and slope, indicating a similar response between the elastic and viscous components. During the reheating process, deviations of tan δ curve are then observed from the PAN/APL1 and PAN/APL2 solutions. Note that the emergence of G'/G" crossover point is not observed in the temperature scan of PAN or PAN/APL1 solutions but only for PAN/APL2, and the altered behavior of G' and tan δ with the increasing lignin content is only shown during the reheating scan but not in the initial cooling scan. These results suggest that the presence of lignin promotes solution sensitivity on temperature gradient, and induce polymer gel-network formation during quenching.

Complex viscosity, storage modulus G', and loss modulus G" of PAN, PAN/APL1, and PAN/APL2 solutions are presented in Figure 2.2, Figure 2.3, and Figure 2.4, respectively. For all solutions, strong dependence of solution viscosity on the applied temperature as well as the similar shear thinning behavior at increasing oscillatory frequencies is observed. Around room temperature (21 °C), PAN exhibits slopes of G' versus ω (1.654), and G" versus ω (0.992) log-log plots at the terminal region when $\omega \rightarrow 0$, in accordance with the scaling law of $G' \sim \omega^2$ and $G'' \sim \omega^1$. By comparison, PAN/APL1 exhibits the corresponding slopes of 1.446 and 0.981 and PAN/APL2 shows the respective slopes of 1.426 and 0.974. The decreasing slopes of G' versus ω, and G" versus ω with increasing APL content suggest that APL molecules in the composite solutions promote

more solid-like behavior of the solutions. As the deviation of scaling law with the presence of lignin implies intermolecular interactions between the blend components, it is of interests to investigate the blend miscibility and PAN chains behavior in the vicinity of lignin.

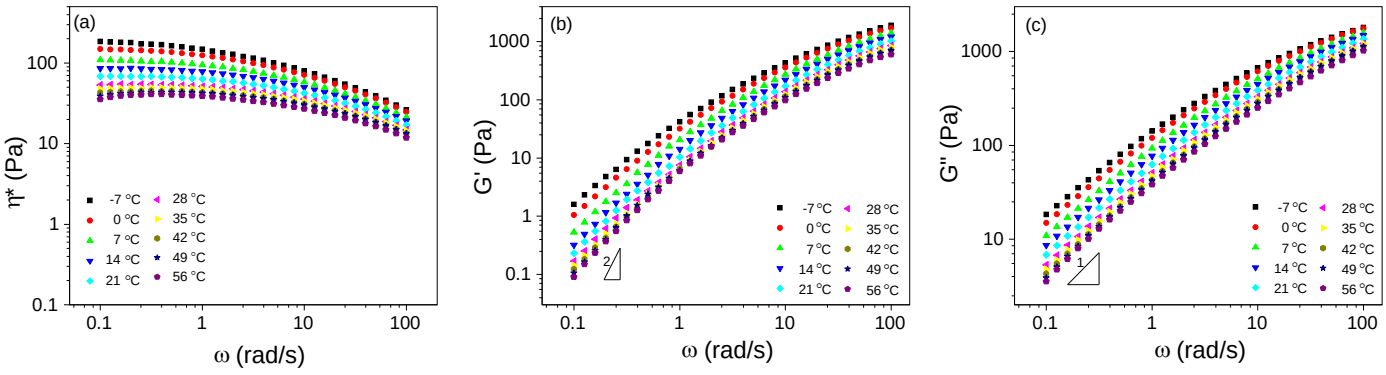

Figure 2.2. PAN solution viscosity (a), storage modulus G' (b), and loss modulus G" (c) at various temperatures.

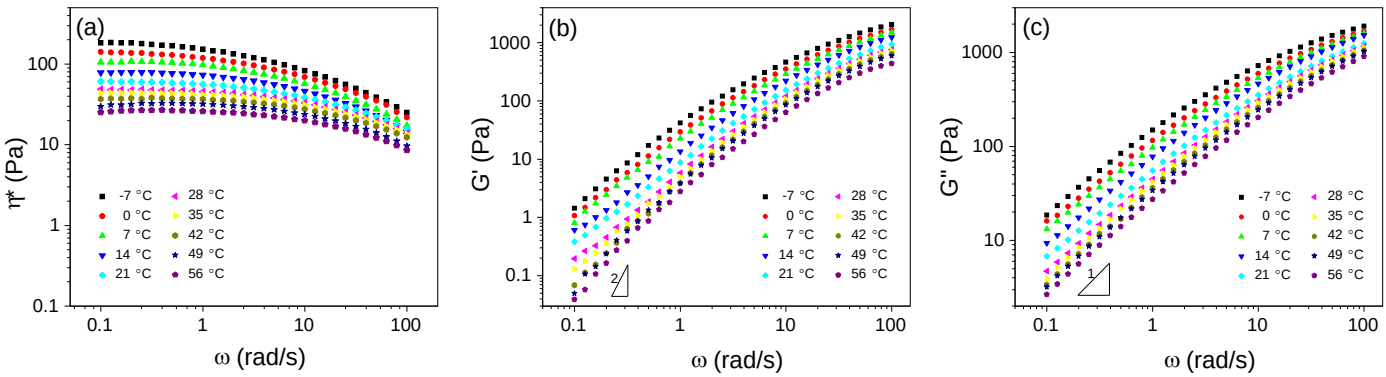

Figure 2.3. PAN/APL1 solution viscosity (a), storage modulus G' (b), and loss modulus G" (c) at various temperatures.

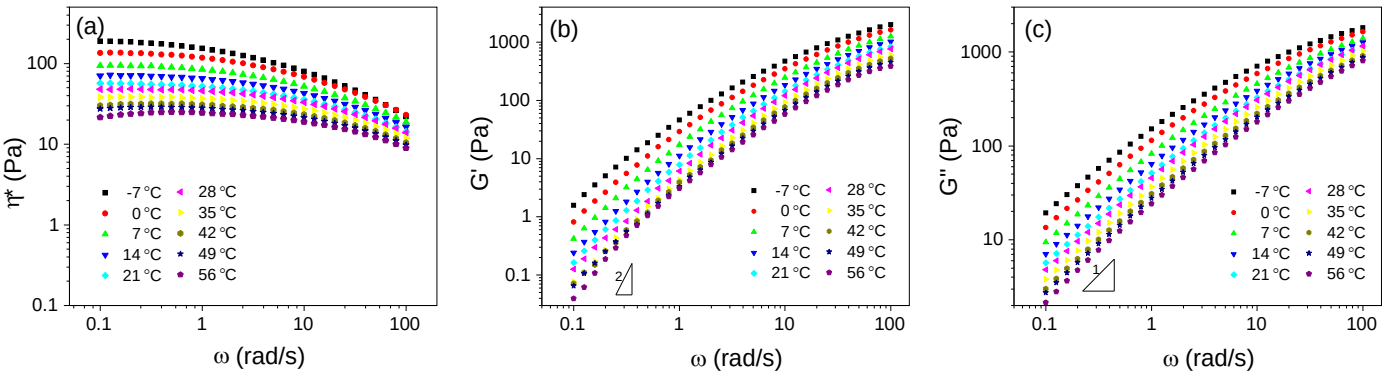

Figure 2.4. PAN/APL2 solution viscosity (a), storage modulus G' (b), and loss modulus G" (c) at various temperatures.

Homogeneity of polymer melts or solutions is often characterized by the slope of G' versus G" log-log plot (Han plot), where a theoretical slope value of 2 indicates a homogeneous, monodisperse, and entangled polymer solution or melt. While the ratio of the amount of energy stored (G') to the amount of energy dissipated (G") in the polymer blends are found to be independent of the blend composition ratio, the slope of G' versus G" log-log plot is also useful to evaluate polymer blend miscibility. The log-log plots of G' versus G" for PAN, PAN/APL1, and PAN/APL2 solutions are shown in Figure 2.5. PAN solution (Figure 2.5a) exhibits a consistent slope of 1.57 (± 0.03) that is independent of applied temperature, confirming a homogeneous, monodisperse polymer solution. For PAN/APL blends (Figure 2.5b and Figure 2.5c), consistency of log G' versus log G" curves with independence on temperature and blend composition is also observed, rendering a slope value for PAN/APL1 (1.56 ± 0.03) and PAN/APL2 (1.57 ± 0.04), respectively. Note that while lignin is an amorphous, three-dimensional matrix which is distinct from PAN molecular structure, PAN and PAN/APL blends (with up to 37.5 wt% lignin) exhibit similar

slope from the log G' versus log G" curves. The temperature-independent, and the composition-independent slope value (~1.57) of PAN, PAN/APL1, and PAN/APL2 solutions confirms the single-phase, miscible blend at each temperature of investigation.[29] This implies that no existence of PAN-rich or lignin-rich domain is observed during the

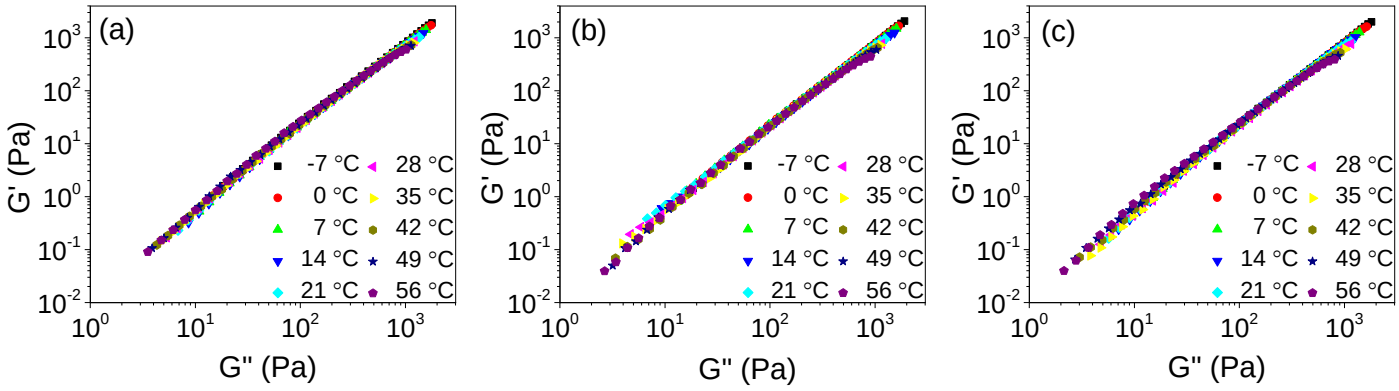

Figure 2.5. Log-log plot of G' versus G" for (a) PAN, (b) PAN/APL1, and (c) PAN/APL2 solutions at various temperatures.

isothermal dynamic frequency sweep at all temperatures.

To characterize the intermolecular interactions between PAN and lignin in solution, *Eq.* 2.1 provides Arrhenius relationship between temperature (T) and zero-shear viscosity (η_0) of polymer melts or solutions in terms of activation energy (E_a) that describe the polymer chain restrictive force to flow.[31-32] For dynamic shear rheology, η_0 can be directly obtained from the complex viscosity, η^*, where $\omega \rightarrow 0$. η_0^* (η_0 obtained from complex viscosity) of PAN, PAN/APL1, and PAN/APL2 solutions at various temperatures are shown in Figure 2.6a.

$$Eq.2.1 \qquad \eta_0 = Ae^{\frac{E_a}{RT}}, \quad (R = universial\ gas\ constant)$$

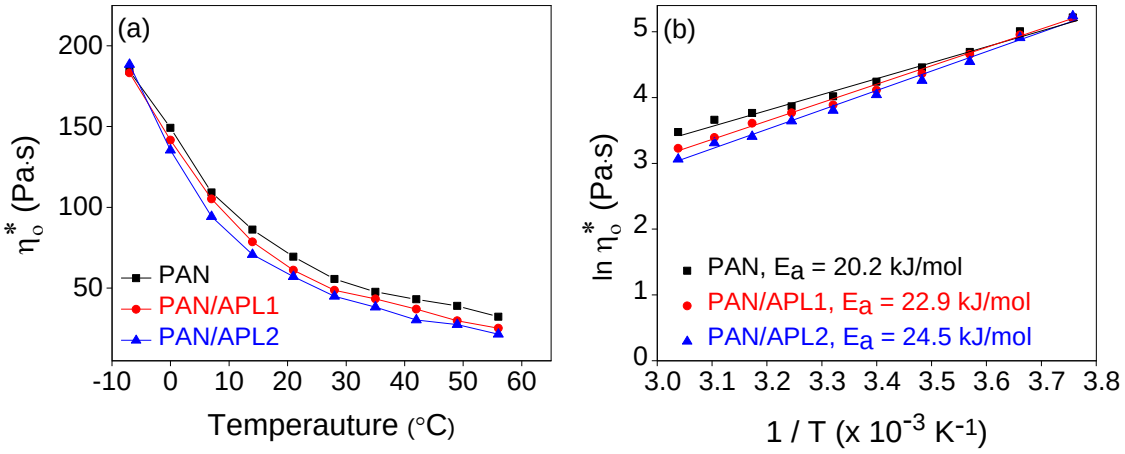

Figure 2.6. Zero-shear viscosity (η*, where $\omega \rightarrow 0$) of PAN, PAN/APL1, and PAN/APL2 solutions at various temperatures (a), and plot for solution activation energy, (b).

For PAN, PAN/APL1, and PAN/APL2 solutions, η_0* is shown to decrease at higher temperatures. With the incorporation of lignin, PAN/APL1 blend (3.5 g/dL lignin + 15 g/dL PAN solid content) shows similar viscosity compared to PAN solution (15 g/dL PAN solid content) at – 7 °C. At increasing temperatures (0 to 56 °C), PAN/APL1 consistently exhibits lower viscosities than PAN solution. This effect is further manifested by PAN/APL2 when higher loading of lignin is present in solution (9 g/dL lignin + 15 g/dL PAN solid content). Figure 2.6b illustrates the linear relationship between ln η_0* and 1/T along with calculated activation energies from the slopes and Eq. 1. Interestingly, despite the reduced viscosities of PAN/APL blends, solution activation energies are found to increase with increasing lignin content (PAN/APL2 > PAN/APL1 > PAN). This suggests interaction between lignin molecules and the PAN on the side chains to cause long-chain branching, where the branches increase chain segment size and rigidity to cause higher activation energies regardless the lower solution viscosities compared to the linear, short-

side-chain analogues.[33] While the activation energy is also closely related to polymer entanglements, an alternative interpretation for the aforementioned discussions of activation energy is that the activation energy increase can be attributed to the physical entanglements between APL and PAN molecules instead of possible PAN/APL chemical interactions. To verify the argument, solution apparent yield stress, or critical stress where a structural breakdown of a viscoelastic liquid occurs are evaluated. *Eq.* 2.2 is the modified Casson equation that determines the critical stress of polymer melt or solution, in which *G",* σ_0, *k*, and ω are the loss modulus, yield stress, viscosity coefficient, and angular frequency, respectively.

$$Eq.2.2 \qquad \sqrt{G"} = \sqrt{\sigma_0} + \sqrt{k\omega}$$

To describe the relationship between loss modulus G" and angular frequency ω, modified Casson plots for PAN, PAN/APL1, and PAN/APL2 solutions are shown in Figure 2.7. The intercept of $\sqrt{G"}$ obtained from the linear extrapolation of each dynamic frequency sweep can be used to obtain the solution critical stress. Comparison of the solution critical stresses at various temperatures are then summarized in Table **2.1** and illustrated in Figure 2.8. For all solutions, critical stress decreases at higher temperatures, indicating that break-up stress of molecular associations for the physical structure in solution decreases at higher temperatures. At the same time, solution critical stress is shown to decrease with increasing lignin content in the solution throughout the entire temperature range. This suggests that the presence of APL does not contribute to prevent physical

structural breakdown of polymers in solution, which disapproves the proposition of solution activation energy increases due to the entanglements between PAN and APL.

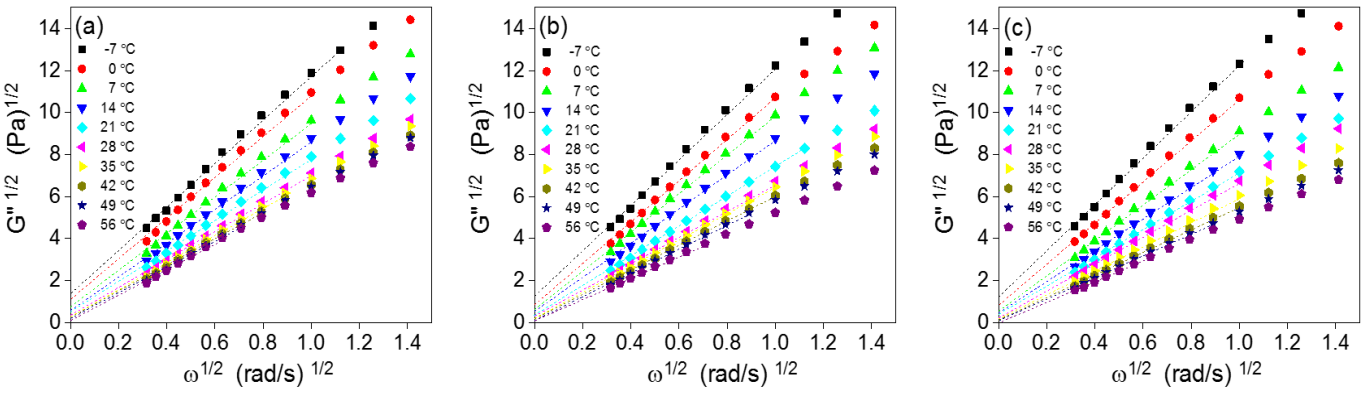

Figure 2.7. Modified Casson plot for (a) PAN, (b) PAN/APL1, and (c) PAN/APL2 solution at various temperatures.

Table 2.1. Solution critical stress at various corresponding temperatures

Temperature (°C)	Solution critical stress (Pa)		
	PAN	PAN/APL1	PAN/APL2
-7	2.597	2.231	1.490
0	1.541	1.282	0.859
7	0.565	0.376	0.291
14	0.437	0.316	0.209
21	0.257	0.172	0.136
28	0.122	0.088	0.051
35	0.077	0.041	0.034
42	0.069	0.034	0.015
49	0.040	0.018	0.013
56	0.033	0.017	0.003

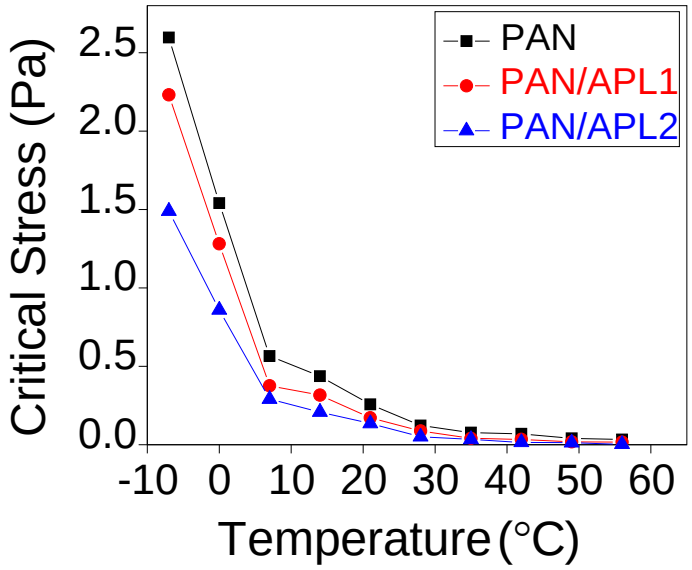

Figure 2.8. Comparison of the solution critical stresses at various temperatures

Solution relaxation time (λ) under dynamic shear can be calculated according to *Eq*. 2.3, where J' and $[\eta^*]$ and are the solution compliance and magnitude of complex viscosity, respectively.[31, 36] To obtain the characteristic relaxation time of the solution in terminal region, the longest relaxation time λ_0, (where $\omega \rightarrow 0$) of PAN, PAN/APL1, and PAN/APL2 solutions at various temperatures are shown in Figure 2.9. For entangled polymers, λ_0 is closely related to the onset of nonlinear pseudoplastic region.[3] Therefore, it is no surprise to see λ_0 exhibits a clear shift to lower values with increasing temperatures for all solutions in this study, indicating a manifested pseudoplastic solution behavior at higher temperatures. With 18.9% of lignin incorporation, PAN/APL1 exhibits no significant difference of relaxation time compared to PAN solution. However, when the lignin incorporation is increased to 37.5%, PAN/APL2 solution shows a general trend in

decreasing relaxation time in comparison to the other two solutions at respective temperatures. In an analogy of using reptation model to describe PAN relaxation in solution,[37-38] here the reduction of longest relaxation time λ_0 can be considered as a decrease in reptation time, or less disentanglement hindrance on the polymer chains. This result agrees with the aforementioned observations of reduced viscosities and critical stresses of PAN/APL solutions.

$$Eq.\,2.3 \qquad J' = \frac{G'}{([\eta^*]\omega)^2} = \frac{\lambda}{[\eta^*]}$$

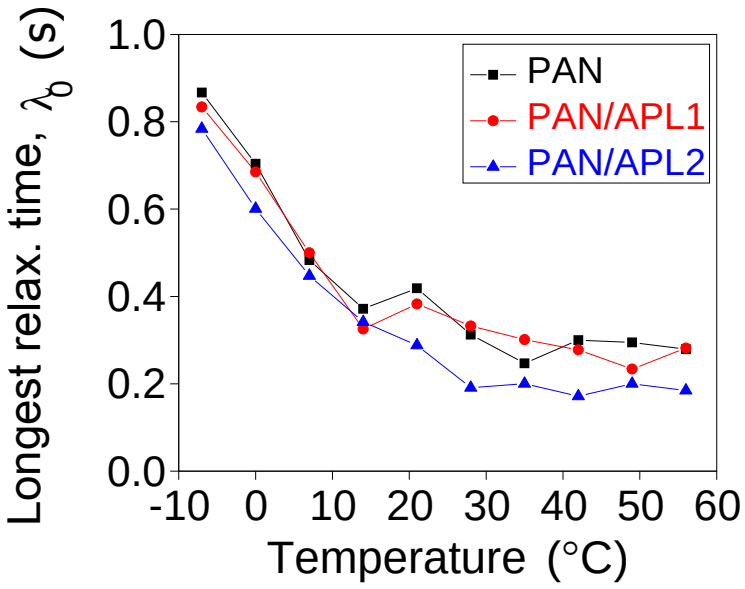

Figure 2.9. Longest relaxation time, λ_0 of PAN, PAN/APL1, and PAN/APL2 solutions.

In a solution-based, wet spinning process of fiber manufacturing, the spinning dope generally undergoes a high-speed shearing deformation into a quenching medium at a relatively low temperature than the as-spun extrudate. During processing, polymer chains in fiber structure experience disentanglement, chain alignment and extension to render enhanced mechanical performance.[39-40] While the polymer chain rearrangement can

complete in a very short time frame during fiber spinning process, it is difficult to monitor the real-time polymer behaviors in solution. As an approach to envision the polymer response to high-speed shearing undertaken at reducing temperatures, tan δ of PAN, PAN/APL1, and PAN/APL2 solutions from dynamic frequency measurements at -7 °C to 56 °C under an oscillatory frequency of 100 rad/s are illustrated in Figure 2.10. All solutions exhibit a similar trend where tan δ decreases with decreasing temperatures, corresponding to a transition towards more solid-like dominance behavior during coagulation. From 21 to 56 °C, PAN/APL2 exhibits respectively higher tan δ than PAN/APL1 and PAN solutions, indicating that lignin incorporation promotes a viscous-component dominance in solution structure at the designated temperatures. In lower temperatures, interestingly, tan δ values of the solutions converge around 14 °C and further exhibit inverted order of tan δ values (PAN > PAN/APL1 > PAN/APL2). This converging temperature of a constant tan δ value suggests the physical crosslink development, or a possible gel point induced by polymer chains.[18] Furthermore, under the shearing process at a decreasing temperature to -7 °C, the magnitudes of tan δ values (PAN > PAN/APL1 > PAN/APL2) imply that the incorporation of lignin promotes the PAN physical network formation and the elastic-component dominance during decreasing temperatures. A possible explanation for the observation is, since lignin incorporation is shown to reduce solution relaxation time, the elastic component in the PAN/APL solutions is therefore more sensitive to the temperature gradient during solid-like (high frequency) motions. In a rapidly cooling, high-speed shearing process, the PAN/APL solution is expected to undergo an accelerated transition from viscous-component dominance to elastic-component dominance. This is a close analogy to the event of fiber spinning process, where

the spinning dope can be extruded into a quenching medium (e.g., air or bath) and undergoes stretching (high-speed shearing) and coagulation (quenching) simultaneously. As a result, the phenomenon of excessively rapid coagulating characteristic was reported to cause noncoherent gels during acrylic fiber process and thus reduce the fiber stretchability when compared to fiber processed with mild coagulation.

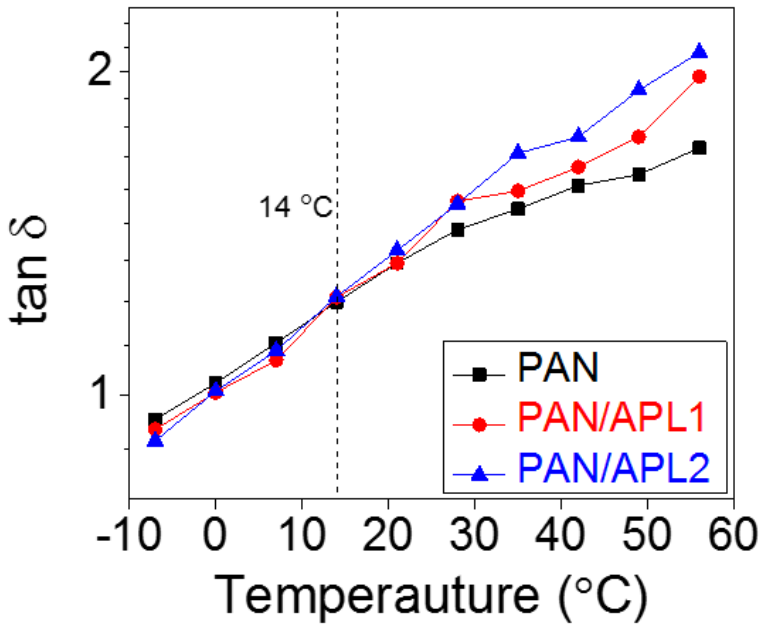

Figure 2.10. Solution loss tangent (tan δ) of PAN, PAN/APL1, and PAN/APL2 from dynamic frequency measurements under an oscillatory frequency of 100 rad/s at various temperatures.

2.4 CONCLUSIONS

Fundamental study of PAN and PAN/APL rheological systems with up to 37.5 wt% lignin incorporation is provided herein as an approach to elucidate the interactions between PAN and lignin during fiber processing. According to the results, lignin incorporation can

induce PAN side chain branching and reduce solution viscosity, critical stress, and relaxation time. Compared to PAN solution, PAN/APL composite solutions exhibit inverted behavior from more liquid-like structure to more gel-like (or solid-like) structure under high-speed shearing and quenching process. This result suggests that PAN coagulation mechanism during fiber manufacturing process is hastened with the incorporation of lignin. While polymeric fibers such as polyethylene and PAN are shown to exhibit enhanced mechanical properties with proper processing or drawing during gel-state of the extrudate, these results indicate that operation windows such as gel-state drawing temperature or coagulating temperature must be carefully tailored for PAN/APL systems. Isochronal frequency scans of PAN/APL blends display a poor thermo-reversibility during reheating process after a precedent cooling scan, indicating the proper coagulation parameters of the PAN/APL extrudate should be identified to avoid formation of PAN-rich or lignin-rich domains that can potentially disturb later drawing stages.

2.5 REFERENCES

[1]. Chae, H. G.; Kumar, S., Making Strong Fibers. *Science* **2008,** (5865), 908.

[2]. Gupta, V. B., Kothari, V.K. (Eds.), *Manufactured Fibre Technology*. Chapman & Hall: New York, **1997**.

[3]. Newcomb, B. A.; Gulgunje, P. V.; Liu, Y.; Gupta, K.; Kamath, M. G.; Pramanik, C.; Ghoshal, S.; Chae, H. G.; Kumar, S., Polyacrylonitrile Solution Homogeneity Study by Dynamic Shear Rheology and the Effect on the Carbon Fiber Tensile Strength. *Polymer Engineering & Science* **2016**.

[4]. Tan, L.; Pan, D.; Pan, N., Rheological Study on Thermal-induced Gelation Behavior of Polyacrylonitrile Solution. *Journal of Polymer Research* **2009,** *16* (4), 341-350.

[5]. Tan, L.; Pan, D.; Pan, N., Gelation Behavior of Polyacrylonitrile Solution in Relation to Aging Process and Gel Concentration. *Polymer* **2008,** *49* (26), 5676-5682.

[6]. Malkin, A.; Ilyin, S.; Roumyantseva, T.; Kulichikhin, V., Rheological Evidence of Gel Formation in Dilute Poly(acrylonitrile) Solutions. *Macromolecules* **2013,** *46* (1), 257-266.

[7]. Morris, E. A.; Weisenberger, M. C.; Bradley, S. B.; Abdallah, M. G.; Mecham, S. J.; Pisipati, P.; McGrath, J. E., Synthesis, Spinning, and Properties of Very High Molecular Weight Poly(acrylonitrile-co-methyl acrylate) for High Performance Precursors for Carbon Fiber. *Polymer* **2014,** *55* (25), 6471-6482.

[8]. Ragauskas, A. J.; Beckham, G. T.; Biddy, M. J.; Chandra, R.; Chen, F.; Davis, M. F.; Davison, B. H.; Dixon, R. A.; Gilna, P.; Keller, M.; Langan, P.; Naskar, A. K.; Saddler, J. N.; Tschaplinski, T. J.; Tuskan, G. A.; Wyman, C. E., Lignin Valorization: Improving Lignin Processing in the Biorefinery. *Science* **2014,** *344* (6185).

[9]. Baker, D. A.; Rials, T. G., Recent Advances in Low-Cost Carbon Fiber Manufacture from Lignin. *Journal of Applied Polymer Science* **2013,** *130* (2), 713-728.

[10]. Ding, R.; Wu, H.; Thunga, M.; Bowler, N.; Kessler, M. R., Processing and Characterization of Low-cost Electrospun Carbon Fibers from Organosolv Lignin/Polyacrylonitrile Blends. *Carbon* **2016,** *100*, 126-136.

[11]. Liu, H. C.; Chien, A. T.; Newcomb, B. A.; Liu, Y.; Kumar, S., Processing, Structure, and Properties of Lignin- and CNT-Incorporated Polyacrylonitrile-Based Carbon Fibers. *ACS Sustainable Chemistry & Engineering* **2015,** *3* (9), 1943-1954.

[12]. Husman, G. In *Development and Commercialization of a Novel Low-Cost Carbon Fiber*, Presentation at 2014 DOE Hydrogen and Fuel Cells Program and Vehicle Technologies Office Annual Merit Review and Peer Evaluation Meeting, **2014**.

[13]. Dong, X.; Lu, C.; Zhou, P.; Zhang, S.; Wang, L.; Li, D., Polyacrylonitrile/lignin Sulfonate Blend Fiber for Low-cost Carbon Fiber. *RSC Advances* **2015,** *5* (53), 42259-42265.

[14]. Xia, K.; Ouyang, Q.; Chen, Y.; Wang, X.; Qian, X.; Wang, L., Preparation and Characterization of Lignosulfonate–Acrylonitrile Copolymer as a Novel Carbon Fiber Precursor. *ACS Sustainable Chemistry & Engineering* **2016,** *4* (1), 159-168.

[15]. Liu, H. C.; Chien, A. T.; Newcomb, B. A.; Bakhtiary Davijani, A. A.; Kumar, S., Stabilization Kinetics of Gel Spun Polyacrylonitrile/lignin Blend Fiber. *Carbon* **2016,** *101*, 382-389.

[16]. Husman, G. In *Development and Commercialization of a Novel Low-cost Carbon Fiber*, Presentation at 2012 DOE Hydrogen and Fuel Cells Program and Vehicle Technologies Program Annual Merit Review and Peer Evaluation Meeting, **2012**.

[17]. Thunga, M.; Chen, K.; Grewell, D.; Kessler, M. R., Bio-renewable Precursor Fibers from Lignin/Polylactide Blends for Conversion to Carbon Fibers. *Carbon* **2014,** *68*, 159-166.

[18]. Qian, B.; Pan, D.; Wu, Z., The mechanism and characterstics of dry-jet wet-spinning of acrylic fibers. *Advances in Polymer Technology* **1986,** *6* (4), 509-529.

[19]. Kapnistos, M.; Hinrichs, A.; Vlassopoulos, D.; Anastasiadis, S. H.; Stammer, A.; Wolf, B. A., Rheology of a Lower Critical Solution Temperature Binary Polymer Blend in the Homogeneous, Phase-Separated, and Transitional Regimes. *Macromolecules* **1996,** *29* (22), 7155-7163.

[20]. Sharma, J.; Clarke, N., Miscibility Determination of a Lower Critical Solution Temperature Polymer Blend by Rheology. *The Journal of Physical Chemistry B* **2004,** *108* (35), 13220-13230.

[21]. Li, L.; Aoki, Y., Rheological Images of Poly(vinyl chloride) Gels. 1. The Dependence of Sol−Gel Transition on Concentation. *Macromolecules* **1997,** *30* (25), 7835-7841.

[22]. Han, C. D.; Jhon, M. S., Correlations of the First Normal stress Difference with Shear Stress and of the Storage Modulus with Loss Modulus for Homopolymers. *Journal of Applied Polymer Science* **1986,** *32* (3), 3809-3840.

[23]. Neumann, C.; Loveday, D. R.; Abetz, V.; Stadler, R., Morphology, Dynamic Mechanical Properties, and Phase Behavior of ABC-Triblock Copolymers with Two Semicompatible Elastomer Blocks. *Macromolecules* **1998,** *31* (8), 2493-2500.

[24]. Yoon, P. J.; Han, C. D., Effect of Thermal History on the Rheological Behavior of Thermoplastic Polyurethanes. *Macromolecules* **2000,** *33* (6), 2171-2183.

[25]. Chae, H. G.; Kim, B. C.; Im, S. S.; Han, Y. K., Effect of Molecular Weight and Branch Structure on the Crystallization and Rheological Properties of Poly(butylene adipate). *Polymer Engineering & Science* **2001,** *41* (7), 1133-1139.

[26]. Han, C. D.; Chuang, H. K., Criteria for rheological compatibility of polymer blends. *Journal of Applied Polymer Science* **1985,** *30* (11), 4431-4454.

[27]. Hong, S. M.; Kim, B. C.; Hwang, S. S.; Kim, K. U., Rheological and Physical Properties of Polyarylate/LCP Blend Systems. *Polymer Engineering & Science* **1993,** *33* (10), 630-639.

[28]. Lee, H. M.; Park, O. O., Rheology and Dynamics of Immiscible Polymer Blends. *Journal of Rheology* **1994,** *38* (5), 1405-1425.

[29]. Rosen, S. L., *Fundamental Principles of Polymeric Materials*. Wiley: New York, **1993**.

[30]. Li, L.; Uchida, H.; Aoki, Y.; Yao, M. L., Rheological Images of Poly(vinyl chloride) Gels. 2. Divergence of Viscosity and the Scaling Law before the Sol−Gel Transition. *Macromolecules* **1997,** *30* (25), 7842-7848.

[31]. Vega, J. F.; Santamaría, A.; Muñoz-Escalona, A.; Lafuente, P., Small-Amplitude Oscillatory Shear Flow Measurements as a Tool To Detect Very Low Amounts of Long Chain Branching in Polyethylenes. *Macromolecules* **1998,** *31* (11), 3639-3647.

[32]. Shroff, R. N.; Mavridis, H., Long-Chain-Branching Index for Essentially Linear Polyethylenes. *Macromolecules* **1999,** *32* (25), 8454-8464.

[33]. Dealy , J. M.; Wissbrun, K. F., *Melt Rheology and Its Role in Plastics Processing*. Springer: New York, **1990**.

[34]. Wissbrun, K. F.; Griffin, A. C., Rheology of a Thermotropic Polyester in the Nematic and Isotropic States. *Journal of Polymer Science: Polymer Physics Edition* **1982,** *20* (10), 1835-1845.

[35]. Lyoo, W. S.; Kim, J. H.; Choi, J. H.; Kim, B. C.; Blackwell, J., Role of Degree of Saponification in the Shear-Induced Molecular Orientation of Syndiotacticity-Rich Ultrahigh Molecular Weight Poly(vinyl alcohol). *Macromolecules* **2001,** *34* (12), 3982-3987.

[36]. Graessley, W. W., Effect of Long Branches on the Flow Properties of Polymers. *Accounts of Chemical Research* **1977,** *10* (9), 332-339.

[37]. Smith, P.; Lemstra, P. J., Ultra-high-strength Polyethylene Filaments by Solution Spinning/Drawing. *Journal of Materials Science* **1980,** *15* (2), 505-514.

[38]. Smith, P.; Lemstra, P. J., Ultrahigh-strength Polyethylene Filaments by Solution Spinning/drawing, 2. Influence of Solvent on the Drawability. *Die Makromolekulare Chemie* **1979,** *180* (12), 2983-2986.

[39]. Winter, H. H.; Chambon, F., Analysis of Linear Viscoelasticity of a Crosslinking Polymer at the Gel Point. *Journal of Rheology* **1986,** *30* (2), 367-382.

[40]. Ferry, J. D., *Viscoelastic Properties of Polymers*. Wiley: New York,, **1980**.

CHAPTER 3

STABILIZATION KINETICS OF GEL SPUN POLYACRYLONITRILE/LIGNIN BLEND FIBERS

3.1 INTRODUCTION

Throughout the development and increasing demand of carbon fibers, polyacrylonitrile (PAN) has been the predominant precursor for the production of high performance carbon fibers and this accounts for more than 90% of the commercial carbon fibers.[2] Owing to the relatively high cost, applications of carbon fibers are rather limited. [3] While significant cost reductions have been achieved in carbon fiber production over the last three decades, further cost reductions will significantly increase carbon fiber usage, especilaly in the automotive sector. Current market demand for low-cost carbon fiber is approximately 300 million kg per year,[4-5] As one of the most abundant reneawable materials on earth and the byproduct of pulp and paper industry, lignin has been considered an attractive cost-effective alternative to PAN for carbon fiber precursors . To-date, lignin-based carbon fibers have exhibited relatively low mechanical properties compared to the PAN-based carbon fibers.[6-11] Although numerous efforts have been devoted to lignin dervied carbon fibers since 1960s, understanding of the fundamental chemistry of this process is still limited and requires further development in translational biorefinery research.[13-18]

Over the last decade, there has been interest, in both academic and industrial laboratories, to integrate the cost advantages of lignin and the good mechanical properties

of PAN. As a result, PAN/lignin blend based carbon fibers have been processed with comparable mechanical performance to that of the control PAN-based carbon fibers.[19, 21] In one of the reports, it has been suggested that the incorporation of lignin could potentially increase PAN stabilization efficiency . In two separate studies it was suggested that lignin incorporation could initiate PAN stabilization process at a realtively lower temperature.[22-23] However, no details regarding the reaction mechanisms and kinetics were discussed in these studies. Therefore, in this study we report for the first time, the stabilization reaction kinetics of gel spun PAN/lignin blend fibers.

3.2 EXPERIMENTAL

3.2.1 Materials and fiber processing

PAN-co-MAA (96/4, M_v = 247,000 g/mol) was acquired from Exlan, Co. (*Japan*). Softwood kraft lignin (Indulin AT) was provided by MeadWestvaco (*Richmond, VA*). Kraft lignin typically has relatively higher (typically higher than 2 wt%) sulfur content.[19] For comparison, we note that in our previous work,[25] annual plant lignin with soda pulping process was used and that lignin contained about 0.5 wt% sulfur.[26-30] As-received lignin powder was first treated with diluted HCl and distilled water repeatedly, followed by multiple washes with methanol to filter the insoluble fraction. Methanol-treated lignin was then washed with distilled water repeatedly and dried under vacuum at 60 °C overnight before use. Dimethylformamide (DMF) was obtained from Sigma-Aldrich. Co. and used as received. For solution preparation, PAN and lignin solids are dissolved into DMF within a glass reactor maintained at 80 ˚C. PAN solution is prepared at a solid concentration of 15 g/dL. When preparing for PAN/lignin solution, 5 g/dL of lignin solid was dissolved in

DMF while PAN solid concentration remained unchanged. (PAN : lignin solid content ratio = 75:25.) A spinning system designed by Hills, Inc. and a spinnerette with a 200 μm diameter hole were used for fiber spinning. Fibers were spun through an air gap of 30 mm into a methanol coalgulation bath maintained at -50˚C. As-spun fibers were collected at a spin draw ratio of 3 and subsequently kept immersed in methanol at -30 ˚C for 36 hours to ensure gelation before further fiber drawings. Post-spin fiber drawing was frist performed in ambient condition and later in a glycerol bath maintained at 165 ˚C. All fibers in the current study were drawn to total draw ratio of 10, and the diameter of PAN and PAN/softwood kraft lignin (SWL) fibers were 21.7 μm and 21.2 μm, respectively.

3.2.2 Characterizations

Dynamic mechanical anaylysis (DMA) was performed on precursor fibers at a frequncy of 1 Hz using a RSA III solid analyzer. 30-filament fiber bundles were used at a gauge length of 25.4 mm at a heating rate of 1 ˚C/min from 30 ˚C to 200 ˚C. Tensile properties of precursor fibers were tested via FAVIMAT on single filaments at 25.4 mm gauge length and a strain rate of 1 %/s. At least 20 fibers were tested in each case. Scanning electron microscope (SEM) images of the fibers were collected using Zeiss Ultra 60 FE-SEM at an accelerating voltage of 5 kV. Fourier transform Infrared spectra (FTIR) of SWL powder, PAN fiber and PAN/SWL fiber are collected on Spectrum One from PerkinElmer with a resolution of 1 cm^{-1}. To study the fiber structure, Wide angle X-ray diffraction (WAXD) patterns were obtained by Rigaku Micromax-002 and Rigaku IV++ detecting system with operating parameters of 45 kV, 0.65 mA and λ = 1.5418 Å. Softwares AreaMax V1.00 and MDI Jade 6.1 were used to analyze the WAXD patterns. Thermo-mechanical analysis (TMA Q400, TA Instruments) was conducted with 10-filament fiber

bundles at various applied stresses and heating rates (1, 3, and 5 °C/min) to 325 °C under nitrogen and air environment. Differential scanning calorimetry (TA Instrument Q2000) under oxidative and nitrogen environments at various heating rates rates (5, 10, and 15 °C/min) from 25 °C to 400 °C were performed on fibers in order to differentiate stabilization reactions.

3.3 RESULTS AND DISCUSSIONS

Mechanical properties and structural parameters of precursor fibers are summarized in Table 3.1, and the SEM images of the tensile fractured fiber surfaces and the FTIR spectra of the precursor fibers are shown in Figure B.1 and Figure B.2, respectively, in appendix B. The tensile properties of the PAN and PAN/SWL fibers are comparable to each other. PAN/SWL fiber has a lower PAN crystal size than PAN fiber and similar PAN crystal orientation. Storage modulus and tan δ curves along with the loss modulus of the fibers from DMA were shown in Figure 3.1. PAN/SWL exhibited higher storage modulus over entire temperature range, which agrees with tensile testing results. The PAN tan δ peak at ~ 90 °C is attributed to β_c relaxation of the polymer chain motion in the para-crystalline region. In the current study, PAN and PAN/SWL fiber exhibited relatively unchanged meridional peak postions obtained from WAXD (Table 3.1), suggesting that there was no significant effect on polymer chain conformation by incorporating SWL in the fiber. Interestingly, DMA of PAN/SWL fiber shows a noticeably reduced tan δ peak magnitude (Figure 3.1a) and a dimished shoulder on loss modulus curve ~ 90 °C (Figure 3.1b) as compared to the PAN fiber, implying a suppressed β_c relaxation that can result from anti-plasticization effect . While antiplasticization effect is critically dependent

on the additive species, it is interesting that antiplasticization is observed between pre-treated softwood lignin and PAN copolymer in the current study.

Table 3.1. Peak temperatures from DSC data for PAN and PAN/SWL fibers

	PAN	PAN/SWL
Tensile modulus (GPa)	14.7 ± 0.8	16.0 ± 0.6
Tensile strength (MPa)	624 ± 61	776 ± 50
Strain to failure (%)	8.7 ± 0.5	8.6 ± 0.4
Facture toughness (MPa)	31.3 ± 3.0	37.2 ± 4.8
f_{PAN} [a]	0.82	0.82
Crystal size [b] (nm)	11.8	9.3
$d_{2\theta \approx 17°}$ [c] (Å)	5.243	5.263
$d_{2\theta \approx 30°}$ [d] (Å)	3.031	3.045
$2\theta_{meridional\ scan}$ [e] (°)	39.14	39.13

[a] Herman's orientation factor of PAN, calculated from Azimuthal scan of PAN (2 0 0), (1 1 0) planes.
[b] The crystal size of PAN calculated using WAXD peak at 2θ ≈ 17˚.
[c] Equatorial PAN d-spacing. (for 2θ~17° diffraction peak)
[d] Equatorial PAN d-spacing. (for 2θ~30° diffraction peak)
[e] PAN peak position from meridional scan.

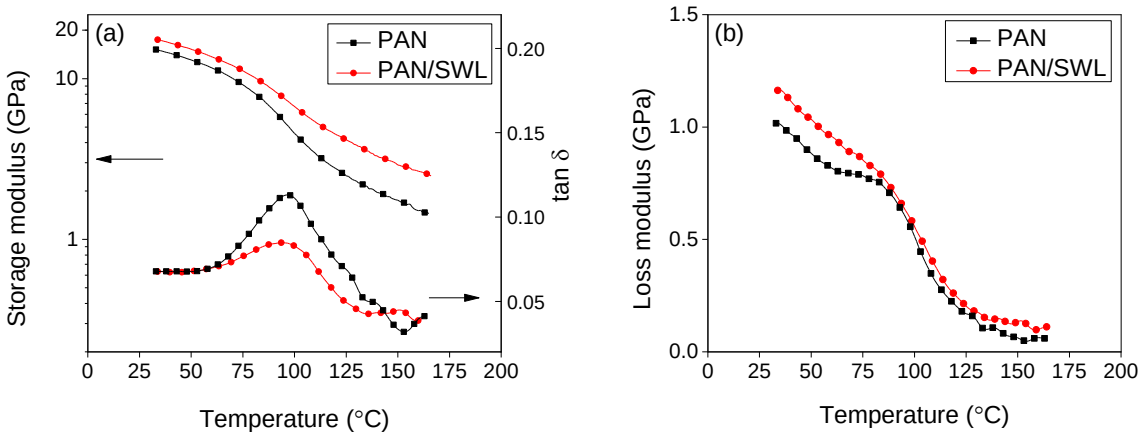

Figure 3.1. Storage modulus and tan δ (a) and loss modulus (b) of PAN and PAN/SWL fibers.

Thermal stabilization is a critical processing stage during PAN-based carbon fiber manufacturing. During stablization, PAN fibers undergo complex reactions including oxidation, cyclization, and crosslinking that transform PAN polymer chains into stabilized

ladder polymer strcuture. While the cyclization reaction can be initiated with or without the presence of oxygen, oxidation and crosslinking can only occur under an oxidative environment, this allows separation and monitoring of the individual stabilization reactions under inert or oxidative environments by differential scanning calorimetry (DSC). When the PAN fiber was stabilized under an oxidative condition, a broad exothermic peak constituted by multiple peaks from concurrent reactions were observed as Figure **3.2**a. When the PAN fiber was run in a nitrogen environment, a single narrower peak corresponding to the cyclization reaction appeared as shown in Figure **3.2**b.[39] While quickly quenched the sample from nitrogen run back to room temperature followed by a rerun in an oxidative environment by DSC, two broad peaks were then evolved. These peaks were assigned to oxidation and crosslinking reactions, with respective order of increasing temperatures.[41-42]

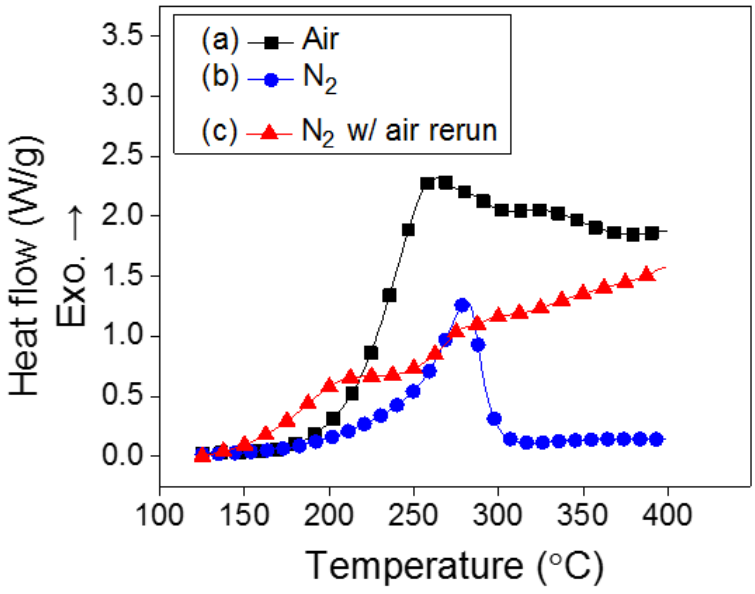

Figure 3.2. DSC curves of PAN fibers at a heating rate of 5 °C/min in (a) air, (b) nitrogen, and (c) nitrogen run followed by rerun in air environments.

To analyze the effects of lignin on stabilization reactions and kinetics by DSC, PAN and PAN/SWL fibers were run in nitrogen first and then rerun in air with heating rates of 5, 10, and 15 °C/min, shown as Figure **3.3**. In heat treatments under nitrogen, a single exothermic peak were observed from both PAN and PAN/SWL fibers, attributed to the cyclization reaction. Shown as Figure **3.3** a and b, PAN/SWL fibers exhibited lower exothermic heat flow magnitude than PAN fiber. While fast heat release during the reaction could result in local overheating , this suggested that the incorporation of lignin can alleviate excessive heat release during cyclization.

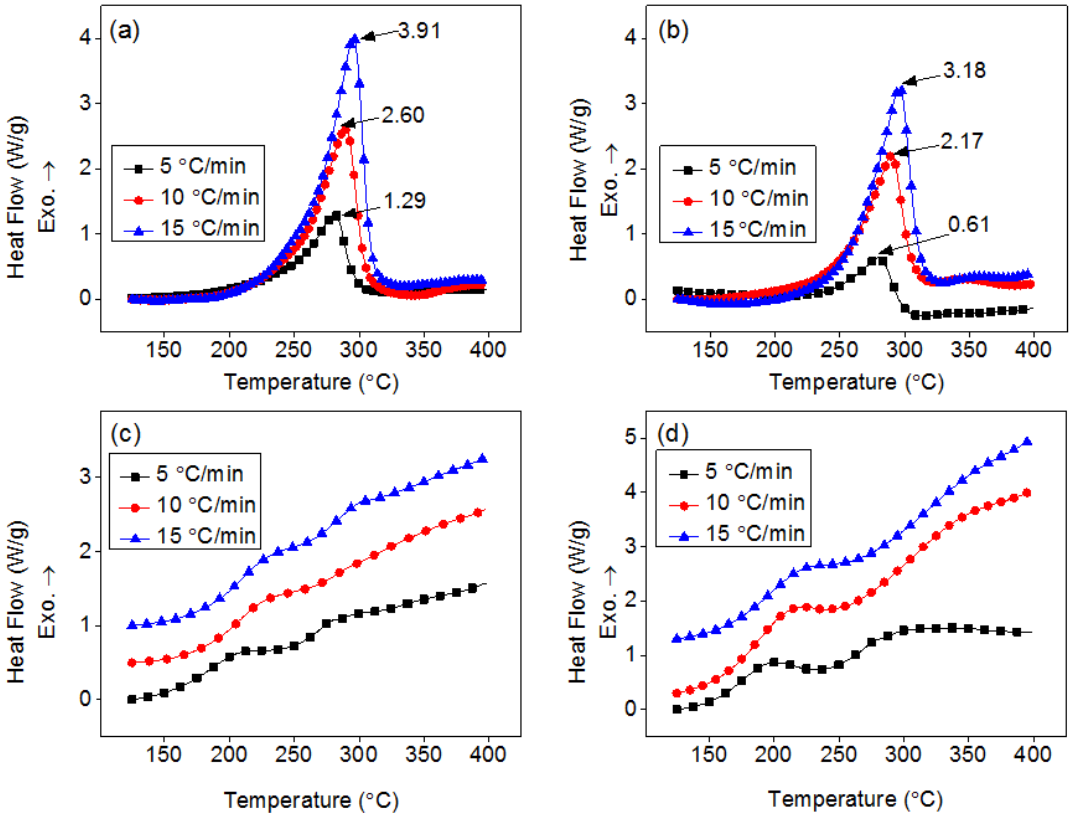

Figure 3.3. DSC curves at various heating rates with (a) PAN fiber in nitrogen, (b) PAN/SWL fiber in nitrogen, and (c) PAN and (d) PAN/SWL fibers rerun in air after runs in nitrogen.

To further investigate reaction activation energies and reaction kinetics from DSC, peak temperatures of cyclization (in nitrogen), oxidation (in air), and crosslinking (in air) were collected and listed in Table 3.2 for calculations by the Kissinger method (*Eq.* 3.1) and Ozawa method (*Eq.* 3.2), where φ, T_p, E_a, R are heating rate (°C/min), peak temperature (Kelvin), activation enegy, and univsersial gas constant (8.3145 $\frac{J}{mol \cdot K}$), respectively.[43] With the determination of activation energies, a pre-exponential factor for the Arrhenius equation $A = \frac{\varphi E_a}{RT_p^2} \cdot e^{E_a/RT_p}$ can be calculated to further describe the reaction rates with rate constant $k = A \cdot e^{-E_a/RT}$.[36-37, 45]

$$-\frac{E_a}{R} = \frac{d(ln\frac{\varphi}{T_p^2})}{d\left(\frac{1}{T_p}\right)} \qquad Eq.\,3.1$$

$$-\frac{E_a}{R} = \frac{1}{0.4567}\frac{d(log\varphi)}{d\left(\frac{1}{T_p}\right)} \qquad Eq.\,3.2$$

Table 3.2. Peak temperatures from DSC data for PAN and PAN/SWL fibers

	PAN peak temp. (°C)			PAN/SWL peak temp. (°C)		
Heating Rate (°C/min)	In N_2	Rerun in Air		In N_2	Rerun in Air	
	$T_{cyclization}$	$T_{oxidation}$	$T_{crosslink}$	$T_{cyclization}$	$T_{oxidation}$	$T_{crosslink}$
5	281.0	205.6	278.0	279.8	194.4	271.3
10	290.2	220.9	291.1	290.3	210.5	302.2
15	296.0	228.2	299.1	296.4	218.8	313.5

Plots of the Kissinger method of PAN and PAN/SWL fibers for activation energy determination are shown in Figure 3.4 and the reaction kinetics of the cyclization, oxidation, and crosslinking reactions are summarized in Table 3.3. According to the results

from the Kissinger method, PAN fiber exhibited cyclization, oxidation and crosslinking activation energies of 183.1 kJ/mol, 87.7 kJ/mol, and 127.0 kJ/mol, respectively. With the incorporation of lignin, the corresponding activation energies were calculated as 163.7 kJ/mol, 77.4 kJ/mol, and 57.3 kJ/mol which are equivalent to 10.6 %, 11.7%, and 54.9% reduction in the respective activation energies. The decrease in activation energies implies that lignin participates in (or at least influences) the PAN cyclization, oxidation, and crosslinking reactions. Interestingly, note that when PAN/SWL fiber exhibited significantly lower crosslinking reaction activation energy than PAN fiber, the crosslinking reaction peaks of PAN/SWL fiber shift to higher temperatues with noticeably broader widths than PAN crosslinking peaks at the same heating rates. These observations in the PAN/SWL crosslinking reaction peaks suggest that lignin participates in PAN crosslinking reaction during thermal stabilization process. While crosslinking during stabilization can promote better load sharing between polymer chains and thus allows more stretching during carbon fiber processing , the significantly lower PAN/SWL crosslinking activation energy than PAN fiber suggests that earlier stage crosslinking can be initiated with the addition of lignin to allow increased stretching during stabilization process. Cyclization, oxidation and crosslinking reaction rate constants of PAN and PAN/SWL fibers were calculated using Arrhenius equation and the results are summarized in Table 3.3. Calculations according to the results from Kissinger and Ozawa methods show that PAN/SWL fiber exhibits approximately 18% to 24% higher rate constants for all reactions than PAN fiber at 250 °C. The increased reaction rate constants agree with the observation of lower activation energies previously discussed. The reduced activation energies along with the increased reaction rate constants of PAN/SWL fiber suggest reduced processing

time and reduced energy requirment for carbon fiber manufacturing with the incorporation of lignin in PAN as compared to only PAN.

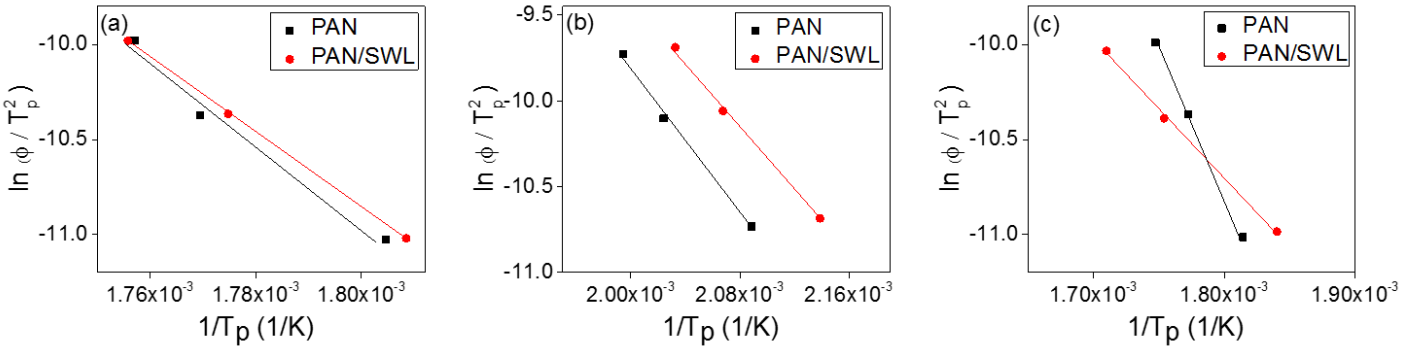

Figure 3.4. Plotting for activation energies of (a) cyclization, (b) oxidation, and (c) crosslinking reactions for PAN and PAN/SWL fiber by Kissinger method.

Table 3.3. Activation energies and reaction kinetics parameters of PAN and PAN/SWL fibers from DSC

		Kissinger method			Ozawa method		
	Reaction	E_a (kJ/mol)[a]	A (s^{-1})[b]	$k_{250°C}$ (s^{-1})[c]	E_a (kJ/mol)[a]	A (s^{-1})[b]	$k_{250°C}$ (s^{-1})[c]
PAN	Cyclization	183.1	6.5×10^{16}	0.034	183.0	6.3×10^{16}	0.034
	Oxidation	87.7	8.6×10^{8}	1.483	91.2	2.1×10^{9}	1.658
	Crosslinking	127.0	2.7×10^{11}	0.057	129.6	5.0×10^{11}	0.056
PAN/SWL	Cyclization	163.7	9.4×10^{14}	0.042	164.5	1.1×10^{15}	0.039
	Oxidation	77.4	9.4×10^{7}	1.757	81.2	2.6×10^{8}	2.042
	Crosslinking	57.3	3.7×10^{4}	0.069	63.4	1.6×10^{5}	0.072

[a] Reaction activation energy.
[b] Pre-exponential factor.
[c] Reaction rate constant calculated at 250 °C.

During stabilization reactions, fiber shrinkages were often observed from PAN-based fibers. Previous studies show that the fiber shrinkage can be categorized as entropic relaxation stage (100 – 175 ˚C) within the amorphous polymer phase and the chemical reaction stage (> 175 ˚C) resulting from cyclization to form ladder structure. Since

oxidation and crosslinking would require oxidative environment to proceed, fiber shrinkage kinetics due to cyclization reaction can thus be monitored through thermo-mechanical analysis under inert environment. Previous studies on PAN cyclization activation energies from fiber shrinkages were performed under prolonged isothermal residence in nitrogen, and were shown comparable to the corresponding DSC results. Although the findings successfully established the relationship between isothermal temperatures and cyclization kinetics parameters, commercial stabilization process applies stepwise temperatures and various stresses throughout stabilization zones. While it has been shown that results from isothermal conditions cannot be obviously compared to non-isothermal process,[19, 37] it is of interests to establish the relationships between cyclization kinetics and applied tensions at non-isothermal heating processes in the current study.

To confirm the feasibility of monitoring reaction kinetics through chemical shrinkage under different heating rates, Fitzer et al. reported an thermocalorimetry analogy where higher heating rates could shift the peak of PAN chemical shrinkage derivative curve to higher temperatures and thus allow the application of Kissinger method. Here the maximum of PAN cyclization-induced shrinking rate, or the peak of PAN shrinkage derivative curve due to cyclization, was regarded as an analogy to exothermic peak of cyclization from DSC. As the TMA cyclization peak locations were in clear shifts toward higher temperatures with higher heating rates, this allows the applications of both the Kissinger method and Ozawa method to calculate the reaction kinetics with applied tensions. The fiber strain curves along with the strain derivative curves with respective to temperatures from TMA under a stress of 4 MPa are shown in Figure **3.5**. During the TMA experiments, two faster-shrinkage zones were observed from the strain curves. When

taking the strain derivatives curves with respect to temperatures for PAN (Figure **3.5**c) and PAN/SWL fibers (Figure **3.5**d), all strain derivative curves exhibited two peaks: one located below 125 °C due to entropic relaxation, and the other one located above 225 °C due to PAN cyclization. To further investigate the effect of tension on fibers during non-isothermal process, loading tensions of 0.2, 2, 4, 5.5, 7.5, 10, and 20 MPa were applied to all fibers. At least two trials were conducted in each case, to ensure reproducibility.

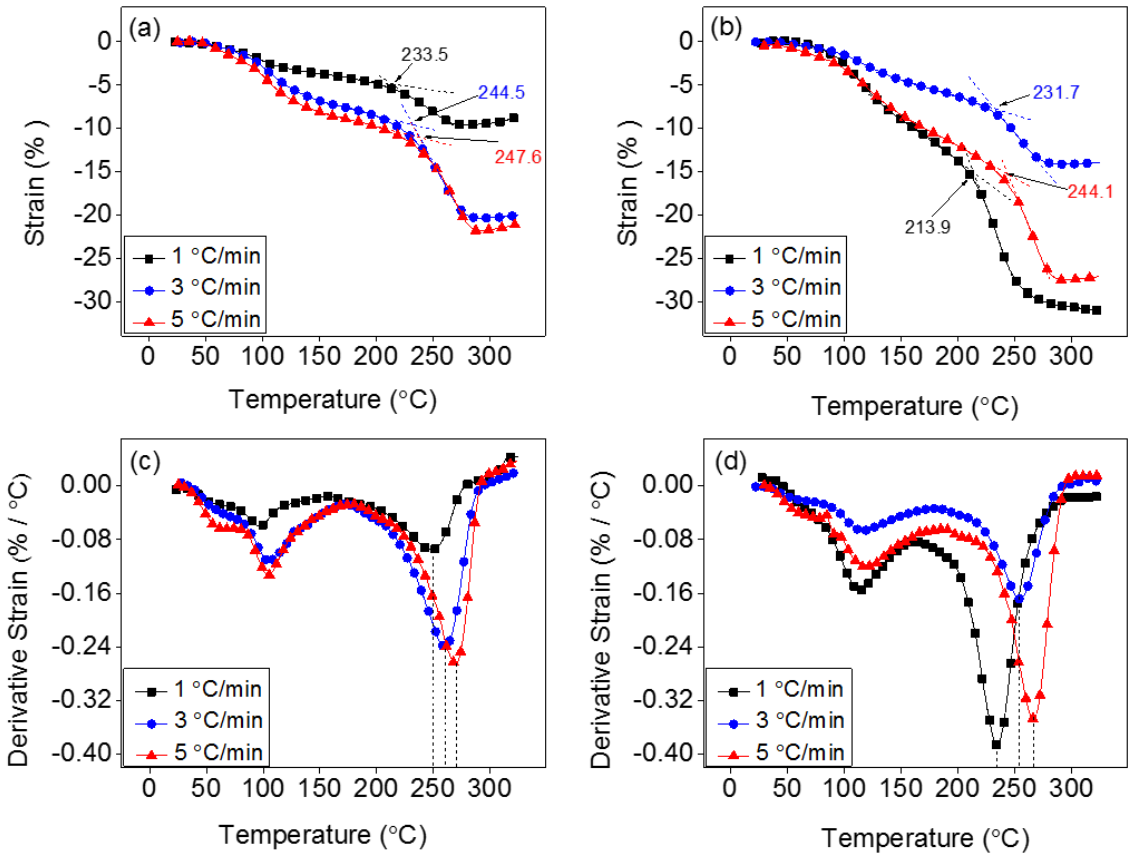

Figure 3.5. TMA results of strain for (a) PAN fiber, and (b) PAN/SWL fiber, with marked onset temperatures and the derivative of the strain with respect to temperature for (c) PAN, and (d) PAN/SWL. All fibers were heated to 325 °C continuously at indicated heating rates.

In this study, PAN fiber often broke, when applied stress was more than 7.5 MPa in nitrogen, but the same fiber survived when applied with more than 20 MPa stress in air. On the other hand, when heating under nitrogen, PAN/SWL fiber could survive with a loading stress of up to 20 MPa. This further confirms that the incorporation of lignin promotes PAN stabilization reactions that help it endure higher tension. TMA peak temperatures (T_p) from derivative curves of PAN and PAN/SWL fibers under various stresses and heating rates are summarized in Table 3.4. Under all stresses and heating rates, PAN/SWL fiber consistently showed lower T_p and lower onset temperatures than PAN fiber. This was also observed from previous TMA studies of copolymer PAN and PAN/lignin fiber. This suggested that lignin, similar to co-monomers for PAN, can promote PAN cyclization.[49]

Table 3.4. Strain derivative peak temperatures of Fibers at various applied tensions

	PAN strain derivative peak temp. (°C) at various heating rates			PAN/SWL strain derivative peak temp. (°C) at various heating rates		
Tension (MPa)	1 (°C/min)	3 (°C/min)	5 (°C/min)	1 (°C/min)	3 (°C/min)	5 (°C/min)
0.2	240.2	257.6	265.1	232.7	252.3	259.0
2	242.1	261.5	268.6	234.4	253.0	262.0
4	250.0	259.9	270.0	235.0	254.8	262.9
5.5	244.1	261.8	272.0	237.3	255.9	264.1
7.5	247.9	264.1	275.7	238.8	257.3	266.7
10	-	-	-	239.4	260.8	268.2
20	-	-	-	243.7	263.6	272.6

Activation energy by Kissinger method and the calculated reaction kinetics from TMA are shown as Figure 3.6 and provided in Table 3.5, respectively. In Figure 3.6a and Figure 3.6b, linear fitting lines for activation energies were obtained by the Kissinger method. This linear relationship between $d(\frac{1}{T_p})$ and $d(ln\frac{\varphi}{T_p^2})$ indicated a proper analogy

between the chemical shrinkage to the thermo-calorimetry of cyclization reaction. When PAN/SWL fiber consistently shows lower activation energies than PAN fiber at corresponding conditions, interesting effect of loading tensions on cyclization activation energies was observed from Figure 3.6c. Under increasing loading stresses, PAN fiber at 4 MPa exhibited an exceptionally high activation energy of 181.5 kJ/mol. On the other hand, PAN/SWL fiber shows a noticeable activation energy jump of 128.5 kJ/mol at 5.5 MPa under identical conditions, suggesting that cyclization behavior can be altered with the presence of lignin. To further investigate this phenomenon, reaction rate constants from TMA of both fibers at various applied tensions at 250 °C, 265°C, and 280 °C were plotted as Figure **3.7**. At 250 °C (Figure **3.7**a), PAN/SWL fiber exhibits higher calculated reaction rate constants than PAN fiber under all applied tensions. Both PAN and PAN/SWL fibers show gradually decreased reaction rate constants at increasing tensions. Similar observations were reported from a previous study where PAN fibers, under a small load, were gradually heated to target temperatures followed by applications of various tensions in order to study the influence of tensions on PAN stabilization.[50-51] The study showed that when temperatures were high enough (210 − 230 °C) to vibtrate and rotate molecular chains rapidly into favorable positions to initiate PAN cyclization without stretching, implementation of tensions under gradual heating in this stage can constrain molecular chains rearrangment and thus suppress cyclization initiation . While TMA in the current study were all performed under continuous, non-isothermal heating process started with various applied tensions, this effect is expected to be manifested at elevating temperatures. At 265 °C (Figure **3.7**b), both fibers exhibit increased reaction rates than at 250 °C, and PAN/SWL fiber continues to exhibit higher calculated reaction rate constants

than PAN fiber under all stresses while a subtle peak formation at 4 MPa of PAN fiber was observed. At 280 °C (Figure **3.7**c), reaction rate constants of PAN and PAN/SWL fibers are further increased. PAN/SWL generally shows higher reaction rates than PAN similar to previous cases. Interestingly, a significant peak reaction rate constant of PAN is observed at 4 MPa, implying that certain optimum tension can be identified to effectively promote PAN cyclization process. This observation is in agreement with previous PAN cyclization index studies,[50-51] where it was shown that a threshold tension/stretching of PAN molecules during stabilization is needed to effectively overcome the dipole - dipole interaction of nitrile groups and to provide necessary chain re-arrangement for cyclization. Further increase in tension/stretching disturbs cyclization.[51] This is the most likely explanation of the exceptionally high cyclization activation energy of PAN fiber at 4 MPa and the activation energy jump of PAN/SWL fiber at 5.5 MPa.

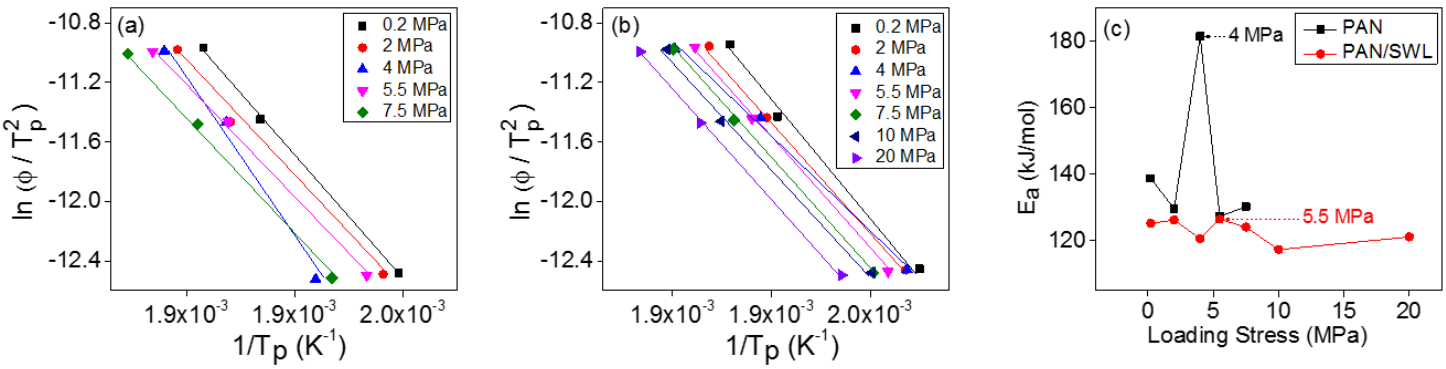

Figure 3.6. Plots for cyclization activation energy according to Kissinger method of (a) PAN, (b) PAN/SWL, and (c) cyclization activation energies at various loading tensions.

Table 3.5. Activation energies and reaction kinetics parameters for PAN and PAN/SWL fibers from TMA.

Tension	PAN				PAN/SWL			
	Kissinger Method		Ozawa Method		Kissinger Method		Ozawa Method	
(MPa)	E_a (kJ/mol)	A (s^{-1})	E_a (kJ/mol)	A (s^{-1})	E_a (kJ/mol)	A (s^{-1})	E_a (kJ/mol)	A (s^{-1})
0.2	138.7	8.4×10^{12}	140.2	1.2×10^{13}	125.3	5.0×10^{11}	127.3	8.1×10^{11}
2	129.7	8.5×10^{11}	131.7	1.3×10^{12}	126.3	5.6×10^{11}	128.3	9.1×10^{11}
4	181.5	1.0×10^{17}	181.0	9.4×10^{16}	122.9	1.4×10^{11}	125.1	2.4×10^{11}
5.5	127.4	4.1×10^{11}	129.5	6.7×10^{11}	127.5	6.5×10^{11}	128.5	9.2×10^{11}
7.5	130.3	6.5×10^{11}	132.3	1.0×10^{12}	124.1	2.6×10^{11}	126.3	4.4×10^{11}
10	-	-	-	-	117.3	4.8×10^{10}	119.9	8.8×10^{10}
20	-	-	-	-	121.2	9.7×10^{11}	123.6	1.7×10^{11}

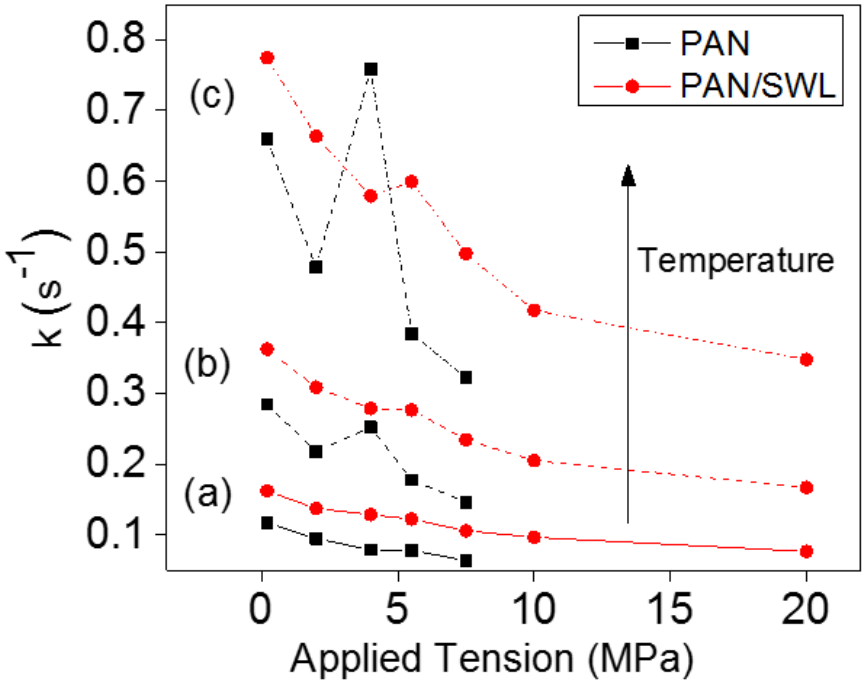

Figure 3.7. Cyclization reaction rate constants of PAN and PAN/SWL fibers at (a) 250 °C, (b) 265 °C, and (c) 280 °C under constant heating rate of 5°C/min and various loading tensions. Reaction rate constants were calculated from the corresponding cyclization peak temperatures of strain derivative curves and activation energies from TMA.

While the observations in the current study confirms the effect of optimal tension to promote PAN cyclization in a non-isothermal process, note that PAN/SWL reaction rate constant at 280 °C (Figure **3.7**c) shows an small peak at 5.5 MPa which is similar to the small peak of PAN fiber at 4 MPa at 265 °C (Figure **3.7**b) and corresponds to the PAN/SWL activation energy jump at 5.5 MPa from TMA. This raises the interest to investigate if the effect of optimal tension on cyclization can also be seen from PAN/SWL fiber. Calculated cyclization reaction rate constants of PAN/SWL fibers at various tensions and temperatures from 265 − 350 °C are shown in Figure **3.8**. At increasing temperatures, clear peak development of PAN/SWL cyclization rate constants at 5.5 MPa is shown. The higher tension of 5.5 MPa for PAN/SWL fiber (Figure **3.8**) than 4 MPa for PAN fiber (Figure **3.7**c) can be understood in the light of the literature results, where it was reported that increased crosslinking in PAN fiber will cause an upshift in optimum stress for cyclization . In the current study, both the significantly lower PAN/SWL crosslinking activation energy from DSC and the upshift of optimum stress to promote cyclization confirms that lignin incorporation promotes PAN crosslinking during stabilization. It is not clear, as to why the optimum stress effect of PAN/SWL on cyclization does not change as drastically as it does for PAN fiber. Nonetheless, the effect is observed in both cases, and the effect in PAN/SWL is more subdued than in PAN. However, the delayed appearance of PAN/SWL activation energy jump and peak cyclization rate constant from 4 MPa to 5.5 MPa, as well as the lower magnitude of the activation energy peak suggests that PAN molecules in PAN/SWL fiber are less sensitive to stress as compare to control PAN. Higher optimum tension required for PAN/SWL fiber implies that lignin in fiber contributes to

load sharing, so that overall higher tension is needed (increase from 4 to 5.5 MPa) in the composite fiber to effectively rearrange nitrile groups.

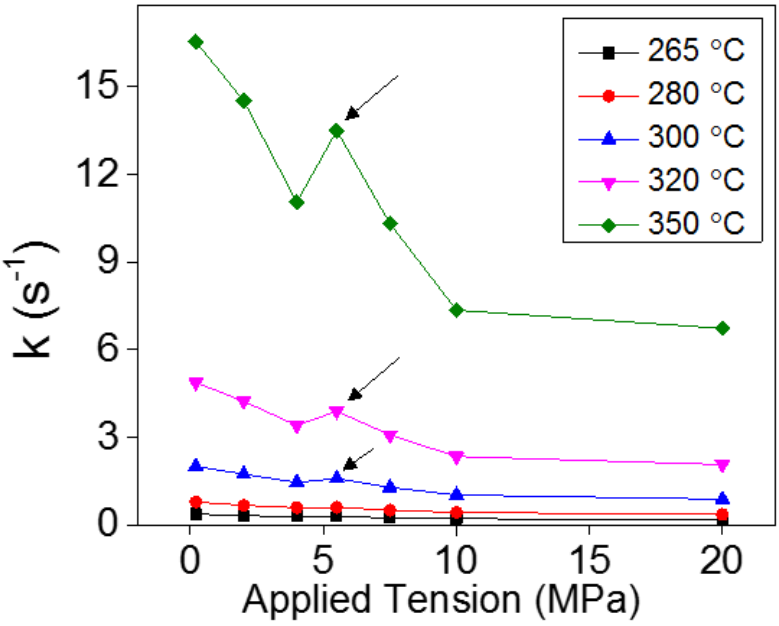

Figure 3.8. Cyclization reaction rate constants of PAN/SWL fiber calculated at various temperatures and applied tensions.

3.4 CONCLUSIONS

Composite fiber comprised of polyacrylonitrile and renewable biomaterial lignin was succsfully fabricated. With the incorporation of lignin, PAN/SWL precursor fiber shows improved tensile modulus, tensile strength, and toughness, as compared to the PAN fiber processed at the same draw ratio. The enhanced mechanical properties along with a suppressed β_c relaxation than PAN fiber suggest the antiplasticization effect of lignin on PAN. Stabilization reaction kinetics of oxidation, cyclization, and crosslinking were calculated according to Kissinger method and Ozawa method for PAN and PAN/SWL fibers by DSC analysis. PAN fibers exhibited activation energies for cyclization, oxidation,

and crosslinking reaction as 181.3 kJ/mol, 87.7 kJ/mol, and 127.0 kJ/mol, respectively. By comparison, PAN/SWL showed lower corresponding activation energies of 163.7 kJ/mol, 77.4 kJ/mol, and 57.3 kJ/mol, which are equivalent to 10.6%, 11.7%, and 54.9% reductions in activation energies, respectively. Cyclization exothermic heat flows of PAN/SWL fibers were shown to be lower than PAN fiber. This implied that incorporation of lignin can potentially expedite the stabilization process of PAN-based carbon fibers and also alleviate local overheating during stabilization. A relationship between cyclization kinetics and applied tensions on fiber between 0.2 to 20 MPa during non-isothermal heating process was developed by TMA with an analogy between the chemical shrinkage and the thermocalorimetry of cyclization reaction. With the addition of lignin, PAN/SWL could endure loading tensions up to 20 MPa in nitrogen while PAN could suffer from possible breakages when tension was more than 7.5 MPa. This implied that higher tensions can be applied on PAN/SWL than PAN fibers during stabilization. Calculated cyclization activation energies of PAN/SWL were shown to be lower than the ones for PAN fiber at all stresses. These observations along with lower crosslinking activation energy and higher reaction rate constants of PAN/SWL fiber confirmed that lignin can promote crosslinking during stabilization process. With the observations on how lignin incorporation can lower activation energies in PAN cyclization, oxidation, and crosslinking reactions and enhance reaction rate constants, this study serves to demonstrate how lignin can potentially reduce the production time and energy consumption for stabilization process of PAN-based carbon fiber manufacturing.

3.5 REFERENCES

[1]. Liu, Y.; Kumar, S., Recent Progress in Fabrication, Structure, and Properties of Carbon Fibers. *Polymer Reviews* **2012,** *52* (3-4), 234-258.

[2]. Ragauskas, A. J.; Beckham, G. T.; Biddy, M. J.; Chandra, R.; Chen, F.; Davis, M. F.; Davison, B. H.; Dixon, R. A.; Gilna, P.; Keller, M.; Langan, P.; Naskar, A. K.; Saddler, J. N.; Tschaplinski, T. J.; Tuskan, G. A.; Wyman, C. E., Lignin Valorization: Improving Lignin Processing in the Biorefinery. *Science* **2014,** *344* (6185).

[3]. Baker, D. A.; Rials, T. G., Recent Advances in Low-Cost Carbon Fiber Manufacture from Lignin. *Journal of Applied Polymer Science* **2013,** *130* (2), 713-728.

[4]. Kadla, J. F.; Kubo, S.; Venditti, R. A.; Gilbert, R. D.; Compere, A. L.; Griffith, W., Lignin-based Carbon Fibers for Composite Fiber Applications. *Carbon* **2002,** (15), 2913.

[5]. Frank, E.; Hermanutz, F.; Buchmeiser, M. R., Carbon Fibers: Precursors, Manufacturing, and Properties. *Macromolecular Materials and Engineering* **2012,** *297* (6), 493-501.

[6]. Otani, S.; Fukuoka, Y.; Igarashi, B.; Sasaki, K., Method for Producing Carbonized Lignin Fiber. U.S. Patents 3461082: **1969**.

[7]. Fukuoka, Y., Carbon fiber made from lignin (kayacarbon). *Japan Chemical Quarterly* **1969,** *5* (3), 63-66.

[8]. Zhang, M.; Ogale, A. A., Carbon fibers from dry-spinning of acetylated softwood kraft lignin. *Carbon* **2014,** *69*, 626-629.

[9]. Sudo, K.; Shimizu, K., A New Carbon Fiber from Lignin. *Journal of Applied Polymer Science* **1992,** *44* (1), 127-134.

[10]. Kubo, S.; Kadla, J. F., Lignin-based Carbon Fibers: Effect of Synthetic Polymer Blending on Fiber Properties. *Journal of Polymers & the Environment* **2005,** *13* (2), 97-105.

[11]. Eckert, R. C.; Abdullah, Z., Carbon fibers from kraft softwood lignin. U.S. Patents 7,678,358 B2: **2010**.

[12]. Ragauskas, A. J.; Williams, C. K.; Davison, B. H.; Britovsek, G.; Cairney, J.; Eckert, C. A.; Frederick, W. J.; Hallett, J. P.; Leak, D. J.; Liotta, C. L.; Mielenz, J.

R.; Murphy, R.; Templer, R.; Tschaplinski, T., The Path Forward for Biofuels and Biomaterials. *Science* **2006,** *311* (5760), 484-489.

[13]. Bissett, P. J.; Herriott, C. W., Lignin/Polyacrylonitrile-Containing Dopes, Fibers, and Methods of Making Same. U.S. Patents 2012/0003471: **2012**.

[14]. Maradur, S. P.; Kim, B. H.; Yang, K. S.; Kim, C. H.; Kim, S. Y.; Kim, W. C., Preparation of Carbon Fibers from a Lignin Copolymer with Polyacrylonitrile. *Synthetic Metals* **2012,** *162* (5-6), 453-459.

[15]. Sazanov, Y. N.; Kostycheva, D. M.; Fedorova, G. N.; Ugolkov, V. L.; Kulikova, E. M.; Gribanov, A. V., Composites of lignin and polyacrylonitrile as carbon precursors. *Russian Journal of Applied Chemistry* **2008,** *81* (7), 1220-1223.

[16]. Dong, X.; Lu, C.; Zhou, P.; Zhang, S.; Wang, L.; Li, D., Polyacrylonitrile/lignin Sulfonate Blend Fiber for Low-cost Carbon Fiber. *RSC Advances* **2015,** *5* (53), 42259-42265.

[17]. Husman, G. In *Development and Commercialization of a Novel Low-Cost Carbon Fiber*, Presentation at 2014 DOE Hydrogen and Fuel Cells Program and Vehicle Technologies Office Annual Merit Review and Peer Evaluation Meeting, **2014**.

[18]. Ding, R.; Wu, H.; Thunga, M.; Bowler, N.; Kessler, M. R., Processing and Characterization of Low-cost Electrospun Carbon Fibers from Organosolv Lignin/Polyacrylonitrile Blends. *Carbon* **2016,** *100*, 126-136.

[19]. Liu, H. C.; Chien, A. T.; Newcomb, B. A.; Liu, Y.; Kumar, S., Processing, Structure, and Properties of Lignin- and CNT-Incorporated Polyacrylonitrile-Based Carbon Fibers. *ACS Sustainable Chemistry & Engineering* **2015,** *3* (9), 1943-1954.

[20]. Husman, G. In *Development and Commercialization of a Novel Low-cost Carbon Fiber*, Presentation at 2012 DOE Hydrogen and Fuel Cells Program and Vehicle Technologies Program Annual Merit Review and Peer Evaluation Meeting, **2012**.

[21]. Sazanov, Y. N.; Fedorova, G. N.; Kulikova, E. M.; Kostycheva, D. M.; Novoselova, A. V.; Gribanov, A. V., Cocarbonization of polyacrylonitrile with lignin. *Russian Journal of Applied Chemistry* **2007,** *80* (4), 619-622.

[22]. Dodd, A. P.; Kadla, J. F.; Straus, S. K., Characterization of Fractions Obtained from Two Industrial Softwood Kraft Lignins. *ACS Sustainable Chemistry & Engineering* **2015,** *3* (1), 103-110.

[23]. Singh, R.; Singh, S.; Trimukhe, K. D.; Pandare, K. V.; Bastawade, K. B.; Gokhale, D. V.; Varma, A. J., Lignin–carbohydrate Complexes from Sugarcane Bagasse: Preparation, Purification, and Characterization. *Carbohydrate Polymers* **2005,** *62* (1), 57-66.

[24]. Sahoo, S.; Seydibeyoğlu, M. Ö.; Mohanty, A. K.; Misra, M., Characterization of Industrial Lignins for Their Utilization in Future Value Added Applications. *Biomass and Bioenergy* **2011,** *35* (10), 4230-4237.

[25]. Sawai, D.; Kanamoto, T.; Yamazaki, H.; Hisatani, K., Dynamic Mechanical Relaxations in Poly(acrylonitrile) with Different Stereoregularities. *Macromolecules* **2004,** *37* (8), 2839-2846.

[26]. Fischer, E. W.; Hellmann, G. P.; Spiess, H. W.; Hörth, F. J.; Ecarius, U.; Wehrle, M., Mechanical Properties, Molecular Motions and Density Fluctuations in Polymer-additive Mixtures. *Die Makromolekulare Chemie* **1985,** *12* (S12), 189-214.

[27]. Tiemblo, P.; Martinez, G.; Gómez-Elvira, J. M.; Millán, J., On a Novel Interpretation of PVC Antiplasticization Based on Some Local Chain Conformations. *Polymer Bulletin* **1994,** *32* (3), 353-359.

[28]. Vilics, T.; Schneider, H. A.; Manoviciu, V.; Manoviciu, I., A DMA Study of the Suppression of the β Transition in Slightly Plasticized PVC Blends. *Journal of Thermal Analysis* **1996,** *47* (4), 1141-1153.

[29]. Robeson, L. M.; Faucher, J. A., Secondary Loss Transitions in Antiplasticized Polymers. *Journal of Polymer Science Part B: Polymer Letters* **1969,** *7* (1), 35-40.

[30]. Kinjo, N.; Nakagawa, T., Antiplasticization in the Slightly Plasticized Poly(vinyl chloride). *Polym Journal* **1973,** *4* (2), 143-153.

[31]. Minus, M. L.; Kumar, S., The Processing, Properties, and Structure of Carbon Fibers. *JOM* **2005,** *57* (2), 52-58.

[32]. Dalton, S.; Heatley, F.; Budd, P. M., Thermal Stabilization of Polyacrylonitrile Fibres. *Polymer* **1999,** *40* (20), 5531-5543.

[33]. Schurz, J., Discoloration Effects in Acrylonitrile Polymers. *Journal of Polymer Science* **1958,** *28* (117), 438-439.

[34]. Watt, W.; Johnson, W., Mechanism of Oxidisation of Polyacrylonitrile Fibres. *Nature* **1975,** *257* (5523), 210-212.

[35]. Coleman, M. M.; Sivy, G. T., Fourier Transform IR Studies of the Degradation of Polyacrylonitrile Copolymers—I: Introduction and Comparative Rates of the Degradation of Three Copolymers Below 200°c and Under Reduced Pressure. *Carbon* **1981,** *19* (2), 123-126.

[36]. Gupta, A.; Harrison, I. R., New aspects in the oxidative stabilization of PAN-based carbon fibers. *Carbon* **1996,** *34* (11), 1427-1445.

[37]. Fitzer, E.; Frohs, W.; Heine, M., Optimization of Stabilization and Carbonization Treatment of PAN Fibres and Structural Characterization of the Resulting Carbon Fibres. *Carbon* **1986,** *24* (4), 387-395.

[38]. Fitzer, E.; Müller, D. J., The Influence of Oxygen on the Chemical Reactions During Stabilization of PAN as Carbon Fiber Precursor. *Carbon* **1975,** *13* (1), 63-69.

[39]. Liu, Y.; Chae, H. G.; Kumar, S., Gel-spun Carbon Nanotubes/Polyacrylonitrile Composite Fibers. Part II: Stabilization Reaction Kinetics and Effect of Gas Environment. *Carbon* **2011,** *49*, 4477-4486.

[40]. Mittal, J.; Bahl, O. P.; Mathur, R. B.; Sandle, N. K., IR Studies of PAN Fibres Thermally Stabilized at Elevated Temperatures. *Carbon* **1994,** *32* (6), 1133-1136.

[41]. Kissinger, H. E., Reaction Kinetics in Differential Thermal Analysis. *Analytical Chemistry* **1957,** *29* (11), 1702-1706.

[42]. Ozawa, T., A New Method of Analyzing Thermogravimetric Data. *Bulletin of the Chemical Society of Japan* **1965,** *38* (11), 1881-1886.

[43]. Nair, C. P. R.; Krishnan, K.; Ninan, K. N., Differential scanning calorimetric study on the Claisen rearrangement and thermal polymerisation of diallyl ether of bisphenols. *Thermochimica Acta* **2000,** *359* (1), 61-67.

[44]. Mukundan, T.; Bhanu, V. A.; Wiles, K. B.; Johnson, H.; Bortner, M.; Baird, D. G.; Naskar, A. K.; Ogale, A. A.; Edie, D. D.; McGrath, J. E., A Photocrosslinkable Melt Processible Acrylonitrile Terpolymer as Carbon Fiber Precursor. *Polymer* **2006,** *47* (11), 4163-4171.

[45]. Liu, Y.; Chae, H. G.; Kumar, S., Gel-spun Carbon Nanotubes/Polyacrylonitrile Composite Fibers. Part I: Effect of Carbon Nanotubes on Stabilization. *Carbon* **2011,** *49*, 4466-4476.

[46]. Liu, Y.; Chae, H. G.; Kumar, S., Gel-spun Carbon Nanotubes/Polyacrylonitrile Composite Fibers. Part III: Effect of Stabilization Conditions on Carbon Fiber Properties. *Carbon* **2011,** *49*, 4487-4496.

[47]. Simitzis, J.; Soulis, S., Correlation of chemical shrinkage of polyacrylonitrile fibres with kinetics of cyclization. *Polymer International* **2008,** *57* (1), 99-105.

[48]. Hou, Y.; Sun, T.; Wang, H.; Wu, D., A new method for the kinetic study of cyclization reaction during stabilization of polyacrylonitrile fibers. *Journal of Materials Science* **2008,** *43* (14), 4910-4914.

[49]. Wu, G.; Lu, C.; Ling, L.; Hao, A.; He, F., Influence of Tension on the Oxidative Stabilization Process of Polyacrylonitrile Fibers. *Journal of Applied Polymer Science* **2005,** *96* (4), 1029-1034.

[50]. Lian, F.; Liu, J.; Ma, Z.; Liang, J., Stretching-induced deformation of polyacrylonitrile chains both in quasicrystals and in amorphous regions during the in situ thermal modification of fibers prior to oxidative stabilization. *Carbon* **2012,** *50* (2), 488-499.

[51]. Liu, C.; Hu, L.; Lu, Y.; Zhao, W., Evolution of the crystalline structure and cyclization with changing tension during the stabilization of polyacrylonitrile fibers. *Journal of Applied Polymer Science* **2015,** *132* (27), 42182 (1-10).

CHAPTER 4

LIGNIN AND CNT INCORPORATED POLYACRYLONITRILE BASED CARBON FIBERS

4.1 INTRODUCTION

Carbon fibers have excellent mechanical properties and relatively low density and are therefore employed as reinforcing materials in aerospace structures, windmill blades, sport equipment and automotive applications. With its versatility, the carbon fiber demand has been growing steadily.[1-2] Today, polyacrylonitrile- (PAN) based fibers are the most dominant precursor of carbon fiber and the cost of PAN fibers contributes 30 to 50% to the carbon fiber cost.[3] Bio-macromolecules have been considered as alternative precursor fiber candidates. Early carbon fibers (in 1960s) were produced from cellulosic fibers such as Rayon. However, due to relatively low properties, rayon-based carbon fibers are no longer commercially manufactured. As the byproduct of the pulp and paper industry and also the second most abundant bio-macromolecule on earth, lignin has been proposed as a cost-effective alternative for carbon fiber precursor as a renewable feedstock.[4-5] However, mechanical properties of the lignin-based carbon fibers to-date are relatively low, as compared to the PAN-based carbon fibers.[6-9] Lignin fibers are typically processed by melt spinning, while PAN fibers are processed from solution.[5, 7] To integrate the advantages of good mechanical performance of PAN and the cost advantage of lignin, PAN/lignin blend fibers have been spun.[10-11] However, it has been reported that incorporating lignin into polymer composites could result in lower mechanical properties. Melt-extruded polyethylene and polypropylene with lignin (up to 30 wt. %) exhibited lower tensile

strength with increasing lignin content.[12] Melt-spun PLA/lignin fibers also showed decreasing tensile strength and modulus values when lignin was incorporated.[13] Industrial feasibility of solution-spun PAN/lignin carbon fiber production was investigated by Zoltek in partnership with Weyerhaeuser under a DOE funded program.[14-15] PAN/lignin precursor fibers with different lignin content (up to 45%), PAN molecular weights, and solution solid contents were reported.[14] Although carbon fibers up to 25 wt % lignin were in successful production to meet targeted properties, mechanical performance of composite carbon fibers were still lower than those reported for the control PAN carbon fibers due to increasing micro-voids in composite fibers with increasing lignin content.[14, 16] Possible causes of voids were attributed to low solution viscosities, type of lignin employed, and phase separation during coagulation.[5] Pores in PAN/lignin fiber were also observed in a more recent study as well.[17] Additionally, batch thermal oxidation studies suggested significant differences in stabilization process between PAN and PAN/lignin composite fibers.[14, 17] However, understanding of lignin interaction with polymers, and its conversion process to carbon is still limited.[18]

Carbon nanotubes (CNTs) have been known for influencing mechanical properties, thermal shrinkage, polymer orientation, crystal size, as well as thermal and electrical conductivity of both gel-spun PAN precursors and carbon fibers.[19-24] In 2011, Baker et al. reported melt-spun lignin/CNT fibers.[25] Although no mechanical properties were originally provided, in a later study enhancements in tensile strength and tensile modulus for both precursors and carbon fibers were reported with the addition CNTs.[5] However, absolute mechanical property values were not reported. More recently, Teng et al. reported electrospun softwood kraft lignin/CNT/poly(ethylene oxide) (PEO), and lignin/PEO

composite fibers and their carbonized products.[26] Solids including 1 to 6 wt % of CNT were prepared in dimethylformamide and PEO (1 wt %) was added to improve spinnability. Tensile strength and modulus of lignin/CNT/PEO precursor were lower than that for the corresponding values for lignin/PEO products when CNT loading was more than 4 wt % and tensile strength and moduli of carbonized lignin/CNT/PEO were lower than lignin/PEO carbon fiber mats in all cases. Lower mechanical properties of carbon fiber mats with the addition of CNT were reported and attributed to poor interfacial interaction as seen from debonding between CNT and the surrounding matrix according to TEM images of thermally stabilized and carbonized products.[26] Teng et al. further reported that lignin from different treatments or fractionations could critically affect intermolecular interactions with CNTs in solution.[27] However, the interactions between lignin and CNT during fiber spinning and in the final fiber remain unclear and are of interest in the current study.

In this work, both PAN/lignin and PAN/lignin/CNT precursor systems and their carbon fibers utilizing a gel-spinning technique were presented. This study is an attempt to understand the PAN/lignin and PAN/lignin/CNT precursors and to investigate the effects of lignin on polymer fiber structure and thermal stabilization and carbonization behavior in order to fully understand PAN/lignin, and PAN/lignin/CNT systems for industrial practice. Processing parameters, structure and thermal characterization, and mechanical performance are reported, and the effects of lignin and CNT on the fiber structure, and precursor as well as carbon fiber fabrication process are discussed.

4.2 EXPERIMENTAL

4.2.1 Materials

Sulfur free, annual plant lignin powder (Protobind 2400) from soda pulping process was provided by GreenValue (*Media, PA*) and was selected for composite fiber processing based on previously reported favorable properties of the PAN/lignin blend films.[11, 28] Homo-polymer polyacrylonitrile (250,000 g/mol) was acquired from Exlan, Co. (*Japan*), and multi-wall carbon nanotubes with an average diameter of 21.0 ± 3.1 nm were purchased from CheapTubes.com (*Brattleboro, VT*).[22] DMAc was obtained from Sigma-Aldrich. Co. and used as received. As-received lignin powder (ash content ~1 %) was washed with diluted HCl and distilled water repeatedly until the ash content was lower than 0.3%. Washed lignin was then dried under vacuum at 60˚C overnight before use.

4.2.2 Solution Preparation

Three types of solutions (PAN, PAN/lignin, and PAN/lignin/CNT) were prepared for spinning. For PAN solution, 14 g PAN was dissolved in 100 mL DMAc at 80 ˚C. For PAN/lignin solution, 14 g PAN and 6 g lignin were mixed and then dissolved in DMAc at the same conditions. To prepare for the PAN/lignin/CNT composite solutions, total of three CNT batches were added separately into the PAN/lignin solution. Each CNT batch was prepared in DMAc at a concentration of 250 mg/300 mL under 24 hours of sonication (Cole-Parmer 8891R-DTH, 80 W, 43 kHz). PAN (17.5 g) and Lignin (7.5 g) solids were dissolved in 100 mL of DMAc at 80 ˚C before the CNT batches (Total solid of 0.75 g) were added. The weight ratio for PAN/lignin and PAN/lignin/CNT were 70:30 and 70:30:3, respectively. Excessive DMAc solvent from CNT batches were evaporated by vacuum distillation. All prepared solutions were maintained at 60˚C before spinning.

4.2.3 Fiber Spinning and Characterizations

Fibers were gel-spun through a spinnerette with a 200 μm diameter hole on a spinning system built by Hills, Inc. PAN and PAN/lignin/CNT fibers were spun at the spinning temperature of 85 ˚C, while PAN/lignin fiber was spun at 60˚C for better spinnability, as this fiber exhibited poor spinnability at 85 °C. Solid content of PAN, PAN/lignin (70/30 weight ratio), and PAN/lignin/CNT (70/30/3 weight ratio) for successful fiber spinning was 14, 20, and 25.75 g/dL for fiber spinning, respectively. Fiber spinning for PAN/lignin (70/30 weight ratio) was also attempted at a lower solid content of 14 g/dL, and that for PAN/lignin/CNT (70/30/3 weight ratio), was attempted at 14 g/dL and 20 g/dL concentrations and were not successful. Note that for the PAN/lignin blend, solid content for the fiber spinning was notably higher than that for the homo-polymer PAN, but the solution temperature at which the PAN/lignin blend fiber could be spun was lower than that for the PAN or the PAN/lignin/CNT blend. This was the first indication of the interactions between PAN/lignin, and PAN/lignin/CNT. As shown in the results and discussion section, spectroscopic (FTIR and Raman) as well as physio-mechanical (DSC, TMA, DMA) methods provide further evidence of interaction in these binary and ternary blends.

All fibers were spun into methanol coagulation bath maintaine at -50 ˚C with an air gap of ~ 3 cm. As-spun fibers were stored in a methanol bath at -30˚C for over 12 hours and subsequently drawn at room temperature followed by drawing in a glycerol bath at 165 ˚C. While maximum draw ratio of PAN fiber could reach over 20, maximum draw ratio of PAN/lignin fiber was 13. With the incorporation of CNT, the maximum draw ratio of PAN/lignin/CNT fiber was improved to 20. In this study, for a meaningful comparison

between the three types of fibers, draw ratio of 13 was selected for all fibers. Dynamic mechanical analysis was performed on the precursor fiber at 0.1 Hz, 1 Hz and 10 Hz frequencies using RSA III solids analyzer. 30-filament bundles were used for the test at 25.4 mm gauge length with a heating rate of 1 ˚C/min from 30 to 200 ˚C. Thermal shrinkage was studied via thermo-mechanical analyzer (TMA Q400, TA Instruments) at a stress of 10 MPa with a heating rate of 0.5 ˚C/min to 280 ˚C. Tensile properties were tested via FAVIMAT on single filaments at 25.4 mm gauge length. The strain rates for tensile testing for precursors and carbon fibers were 1 %/s and 0.1 %/s, respectively. For each trial, more than 15 samples were tested. Differential scanning calorimetry was conducted on the precursor fibers (TA Instrument Q200) in an oxidative environment of air flow of 50 mL/min, and at a heating rate of 5 ˚C/min. To study the fiber structure, WAXD patterns were obtained by Rigaku Micromax-002 and Rigaku IV++ detecting system with operating parameters of 45 kV, 0.65 mA and λ = 1.5418 Å. Diffraction patterns were analyzed using AreaMax V1.00 and MDI Jade 6.1. For each sample, peak analysis was performed more than once to exclude experimental errors. FTIR spectra of the precursor and stabilized fibers were collected on Spectrum One from Perkin Elmer with a resolution of 4 cm^{-1}. Tube furnace (Lindberg, 51668-HR, Blue M Electric) was used for fiber stabilization and carbonization. Raman spectra of carbon fibers were obtained using a 785 nm laser on a Raman microscope system from HORIBA Scientific. For Raman spectroscopy, carbon fibers were mounted onto paper tabs and fixed with cyanoacrylate adhesive at both ends. Raman spectra were taken with an objective of magnitude 100× at 5.6 mW laser power with an exposure time of 12 s in the VV mode, and the fiber samples were aligned parallel to the polarizer and analyzer. PeakFit software was used to analyze the acquired Raman

spectra with Gaussian-Lorentzian curve fitting. SEM images were collected using Zeiss Ultra 60 FE-SEM at accelerating voltage of 2 kV.

4.3 RESULTS AND DISCUSSIONS

4.3.1 Effects of lignin on polymer packing and orientation

The WAXD patterns of the as-spun fiber with draw ratio (DR) of 2 and precursor with total DR of 13 are shown as Figure 4.1 and Figure 4.2, respectively. The structural parameters of as-spun and drawn precursor fibers are given in Table 4.1. Lignin is completely amorphous and PAN has both amorphous and crystalline peaks in the X-ray diffraction. Compared to the PAN fiber, PAN/lignin fiber shows smaller crystal size and lower crystallinity. Studies have shown that the packing of PAN polymer chains changes from orthorhombic to hexagonal under drawing, which results in ratio of d-spacing of $2\theta \approx 17^\circ$ to d-spacing of $2\theta \approx 30^\circ$ ($d_{17^\circ}/d_{30^\circ}$) approaching to $\sqrt{3}$ (1.732).[29-32] At a draw ratio of 2, d-spacing of $2\theta \approx 17^\circ$ and d-spacing of $2\theta \approx 30^\circ$ of PAN fiber are 5.28 Å and 3.19 Å, respectively ($d_{17^\circ}/d_{30^\circ} = 1.656$). With the incorporation of lignin, PAN/lignin fiber shows d-spacings of 5.26 Å at $2\theta \approx 17^\circ$ and 3.22 Å at $2\theta \approx 30^\circ$. This yields $d_{17^\circ}/d_{30^\circ} = 1.635$ which deviates from the PAN hexagonal packing ratio of 1.732. While the fibers are further drawn to a draw ratio of 13, PAN fiber shows d-spacings at $2\theta \approx 17^\circ$ and $2\theta \approx 30^\circ$ to be 5.25 Å and 3.03 Å, respectively and leads to $d_{17^\circ}/d_{30^\circ}$ of 1.733. On the other hand, PAN/lignin fiber (draw ratio 13) shows smaller d-spacings of 5.22 Å and 3.02 Å, with $d_{17^\circ}/d_{30^\circ}$ of 1.726 which is lower than that of PAN fiber, and the expected value of 1.732 for hexagonal packing. This suggests that the presence of lignin molecules in the fiber influences the PAN packing.

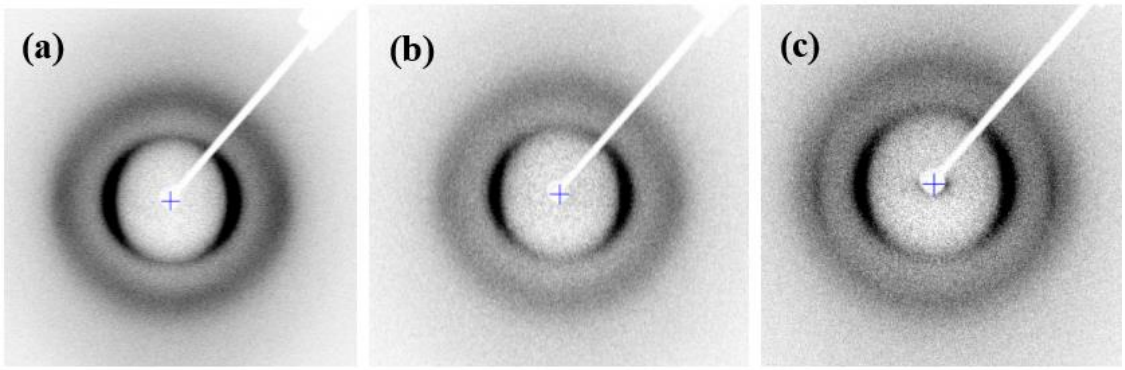

Figure 4.1. WAXD patterns of the as spun precursors (DR = 2) of (a) PAN, (b) PAN/lignin, and (c) PAN/lignin/CNT, respectively.

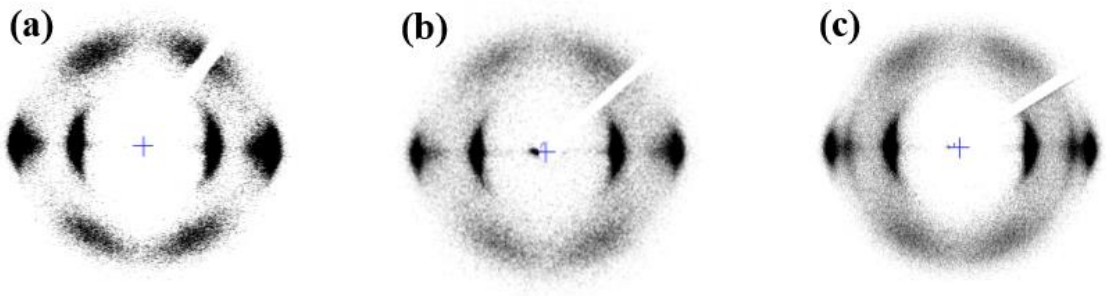

Figure 4.2. WAXD patterns of precursor fibers (DR = 13) of (a) PAN, (b) PAN/lignin, and (c) PAN/lignin/CNT, respectively.

Table 4.1. Structural parameters of PAN, and PAN/lignin/CNT precursors

Draw Ratio	PAN	PAN/lignin	PAN/lignin/CNT
Crystallinity[a] (%)	53	49	52
$L_{2\theta \approx 17^\circ}$ [b] (nm)	3.6	3.0	3.1
f_{PAN} [c]	0.57	0.55	0.54
d-spacing $_{2\theta \approx 17^\circ}$ (Å)	5.28	5.26	5.23
d-spacing $_{2\theta \approx 30^\circ}$ (Å)	3.19	3.22	3.19
$2\theta_{meridional}$ (˚)	39.65	39.86	39.43
$d_{17^\circ}/d_{30^\circ}$	1.656	1.635	1.640
Draw Ratio	PAN	PAN/lignin	PAN/lignin/CNT
Crystallinity[a] (%)	65	60	57
$L_{2\theta \approx 17^\circ}$ [b] (nm)	10.5	8.3	9.5
f_{PAN} [c]	0.88	0.86	0.85
d-spacing $_{2\theta \approx 17^\circ}$ (Å)	5.25	5.22	5.23
d-spacing $_{2\theta \approx 30^\circ}$ (Å)	3.03	3.02	3.02
$2\theta_{meridional}$ (˚)	39.25	39.35	39.13
$d_{17^\circ}/d_{30^\circ}$	1.733	1.726	1.728

[a] The crystallinity is only with respect to PAN crystal since lignin molecules are completely amorphous. [33]
[b] The crystal size of PAN at $2\theta \approx 17^\circ$.
[c] Herman's orientation factor of PAN, calculated from Azimuthal scan of PAN (2 0 0), (1 1 0) planes.

Meridional peak at $2\theta \approx 39^\circ$ refers to PAN (002) crystalline plane that is often used as an indicator of PAN polymer chain conformation and the periodic repeat distance along the fiber axis.[34-36] While the meridional peak location shifts toward lower 2θ values, PAN crystalline planes expand in meridional direction [34], which is analogous to more extended polymer chain along the fiber axis, i.e. PAN molecules transform from helical to planar zigzag conformation. In this work, PAN fiber shows a meridional peak at $2\theta = 39.25^\circ$ at a draw ratio of 13. When lignin is incorporated in the fiber, meridional peak location shifts to higher 2θ value of 39.35°, indicating a shorter PAN crystalline plane along fiber axis compared to PAN fiber. This result shows that lignin molecules also affect the periodicity development in meridional direction.

4.3.2 Effects of CNT on polymer packing and orientation

Previous studies show that CNT incorporation in PAN gel-spun fibers can promote PAN planar zigzag conformation.[37-38] In this study, similar effect was observed as merdional peak in PAN/lignin fiber at 39.35° shifted to 39.13° in the PAN/lignin/CNT fiber. This indicates that CNT can still promote planar zigzag conformation of PAN in the presence of lignin. Interestingly, when PAN/lignin/CNT fiber shows more extended (planar zigzag) conformation, PAN polymer orientation and d-spacing values at $2\theta \approx 17^{\circ}$ and $2\theta \approx 30^{\circ}$ in both draw ratio samples are reduced. The decreased d-spacings along with the lower PAN orientation suggest that PAN, lignin, and CNT might be more tightly packed when lignin molecules "squeeze" the PAN crystalline region against CNT in fiber and thus affect the PAN polymer orientation. Based on the experimental data, the proposed schematics of the molecular packing in the three fully drawn fibers are shown in Figure 4.3.

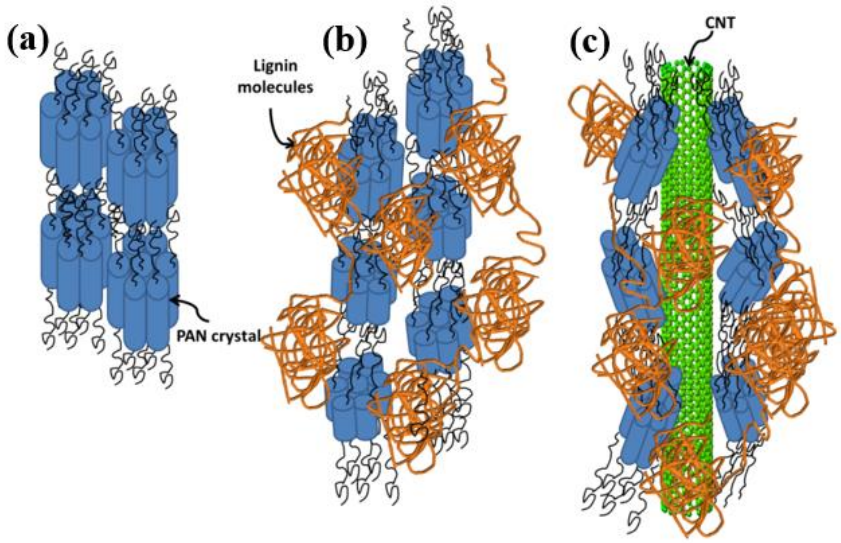

Figure 4.3. Schematics of (a) PAN, (b) PAN/lignin, showing a reduced PAN crystalline region, and (c) PAN/lignin/CNT, showing PAN crystal being squeezed by lignin and CNT.

4.3.3 Effects of lignin and CNT on mechanical properties of the composite fibers

The tensile properties of the precursor fibers (DR = 13) are reported in Table 4.2. PAN fiber shows higher tensile modulus than PAN/lignin and PAN/lignin/CNT fibers, owing to better PAN orientation in the former case. Elongation at break of PAN, PAN/lignin, and PAN/lignin/CNT fibers are 8.1%, 7.1%, and 8.7%, respectively. Results of dynamic mechanical analysis are shown in Figure 4.4. Among PAN, PAN/lignin and PAN/lignin/CNT fibers, PAN fiber exhibits the highest storage modulus. With the addition of CNT, PAN/lignin/CNT fiber shows higher storage modulus than PAN/lignin fiber over the entire temperature range. The peak of tan δ plot is referred to as β_c relaxation temperature that relates to the PAN polymer chain conformation in the paracrystalline region.[39] PAN precursor fiber shows tan δ peak at 80.3 ˚C while β_c relaxation in the PAN/lignin fiber shows higher tan δ magnitude, broader range and shifts to lower temperature (76.9˚C). The lower β_c transition temperature and broadened tan δ peak of PAN/lignin fiber, as compared to PAN fiber, imply that the molecular motion in PAN/lignin fiber is less restricted. In other words, there is more free volume created by the presence of lignin molecules in PAN. Higher tan δ magnitude also suggests that the PAN polymer in PAN/lignin fiber have more helical sequences as compared to the PAN fiber.[39] This is in agreement with the WAXD results discussed above. PAN/lignin/CNT fiber shows a lower tan δ magnitude, narrower temperature range for the peak, and a higher β_c relaxation temperature (81.4˚C) than PAN/lignin fiber. The lower-magnitude and narrowing tan δ peak suggest a more tightly packed structure between polymer and CNT that limits polymer mobility.[40-42]

Table 4.2. Mechanical properties of precursor fibers at DR = 13

Draw Ratio = 13	PAN	PAN/lignin	PAN/lignin/CNT
Diameter (μm)	17.5 ± 1	18.5 ± 2.5	17.1 ± 0.3
Tensile strength (MPa)	879 ± 65	742 ± 90	719 ± 45
Tensile modulus (GPa)	19.9 ± 0.4	17.2 ± 1	17.7 ± 0.5
Strain to failure (%)	8.1 ± 0.6	7.1 ± 0.6	8.7 ± 0.5

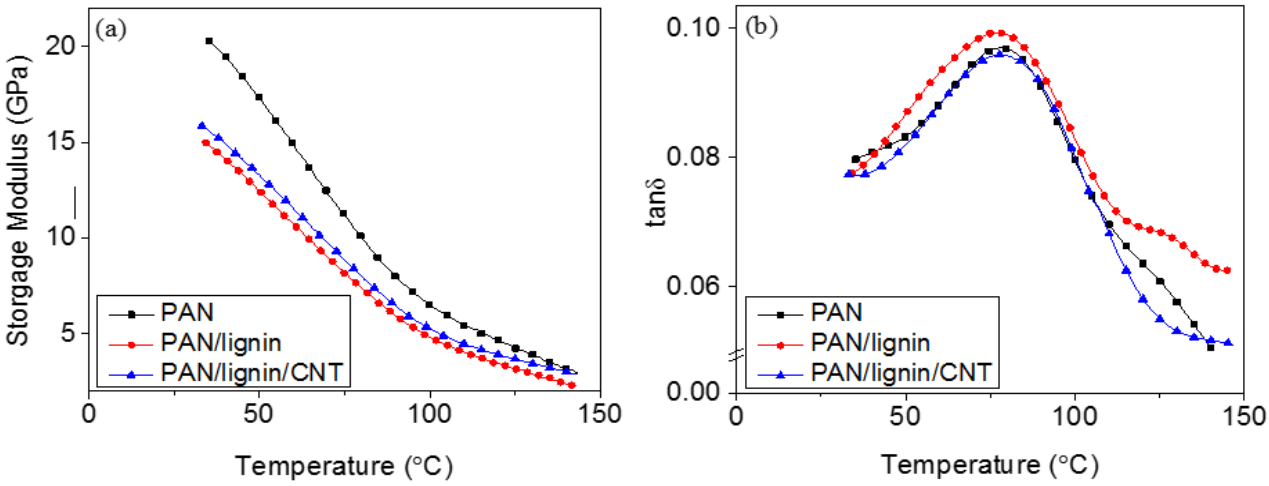

Figure 4.1. (a) Storage modulus and (b) tan δ plot v.s. temperature of precursor fibers (DR = 13) at 1 Hz.

Infrared spectra of lignin powder, as well as PAN and PAN/lignin fibers are reported in Figure 4.5a. In lignin, 1720 cm^{-1} and 1050 cm^{-1} peaks correspond to the ketone-like structure. The sharp peaks from 1426 to 1510 cm^{-1} and peak around 1600 cm^{-1} are due to C–C=C stretching in the aromatic rings, which are pervasive within monolignol units. The peaks from 1200 to 1050 cm^{-1} are attributed to the C–O stretching in lignin alcohols. For PAN fiber, peaks at 1374 cm^{-1}, 1453 cm^{-1} and 2940 cm^{-1} are assigned to CH_2 in the PAN backbone,[43] and the sharp peak at 2243 cm^{-1} belongs to the C≡N bond of PAN. For PAN/lignin composite fiber, C–O and C–C=C stretching for aromatic rings are still observed in the spectrum. However, peaks of the ketone-like structure at 1720 cm^{-1} and

1050 cm^{-1} are diminished significantly as compared to lignin spectra. This substantially

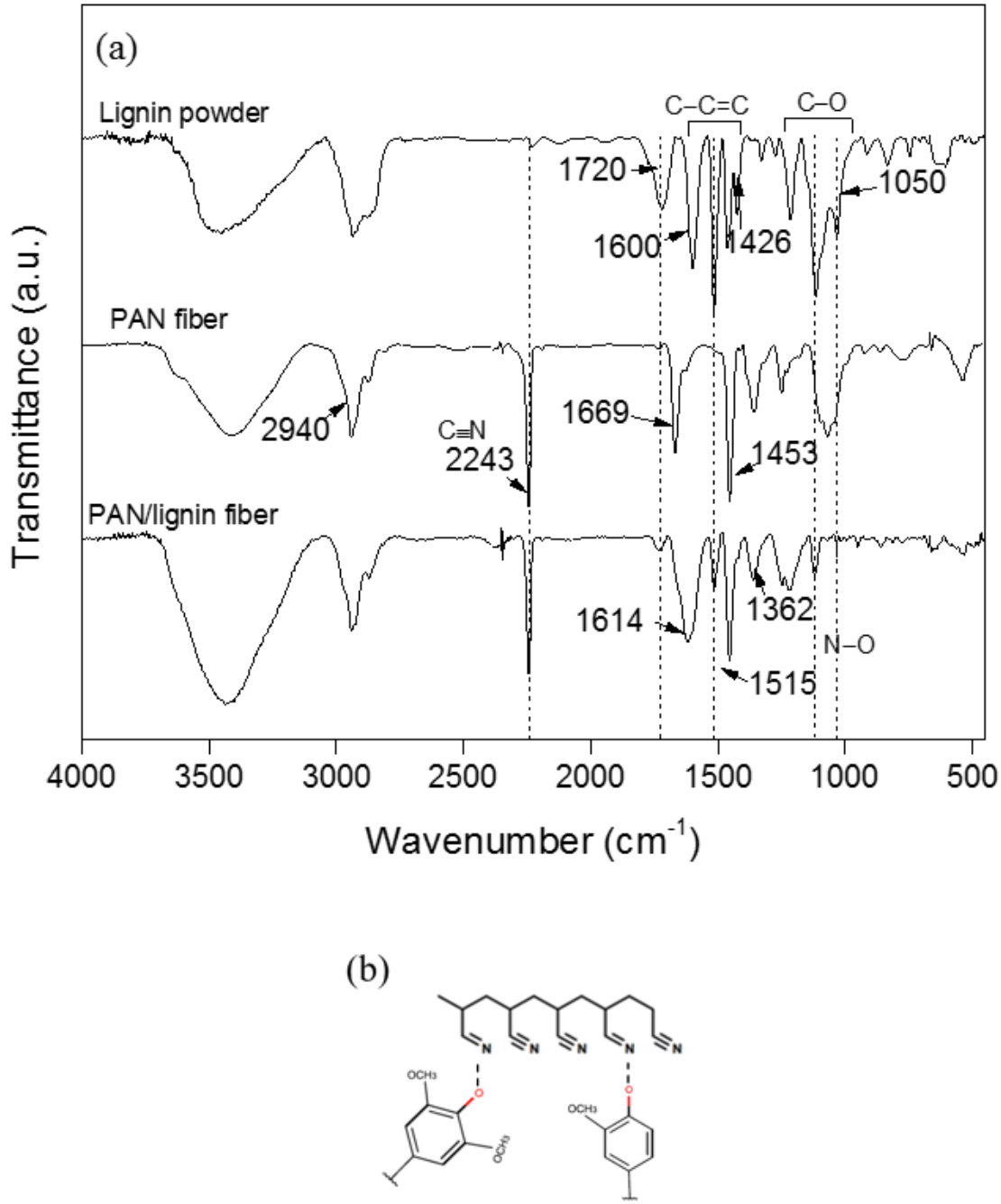

Figure 4.5. FTIR spectra (a) of lignin powder, PAN fiber, and PAN/lignin fiber (DR = 13), and (b) possible lignin/PAN interaction on nitrile group

decreased intensity for the lignin carbonyl peaks suggest this as the potential site for interaction with PAN nitrile group. The peaks at 1515 cm^{-1} and 1362 cm^{-1} in PAN/lignin fiber can be attributed to N–O stretching. Although these peaks were observed in previous PAN/lignin studies,[10-11] these peaks were not discussed. PAN/lignin fiber spectrum exhibited a slightly lower maginitude of C≡N peak at 2243 cm^{-1} as compared to the PAN fiber, and can be attributed to the reduced number of C≡N bonds in the blend fiber as compared to the control PAN fiber. The potential interaction between PAN and lignin is shown in Figure 4.5, suggesting that some of the C≡N peaks gets converted to C=N and form N–O bond. The broadening of the peak at 1614 cm^{-1} which can be attributed to the formation of C=N bond, resulting from PAN interaction with lignin. The appearancec of N–O peaks at 1515 and 1362 cm^{-1}, the diminishing of ketone peaks at 1720 cm^{-1} and 1050 cm^{-1}, and somewhat lower C≡N peak magnitude at 2243 cm^{-1}, along with broadening of the 1614 cm^{-1} peak are thought to be the essential hints of PAN/lignin bonding formation at PAN nitrile sites (Figure 4.5b).

4.3.4 Effects of lignin and CNT on stabilization behavior of composite fibers

DSC analysis is performed on the precursor fibers in air environment, and the thermograms of the precursor fibers are shown in Figure 4.6. All precursor fibers are heated from 50 to 350 ˚C at a heating rate of 5 ˚C/min. Exothermic peaks are observed during stabilization and the heat of stabilization values are listed in Table 4.3. According to the DSC thermograms, all fibers show a single exothermic peak, which are formed by multiple stabilization reactions and free radical cyclization reaction.[44] DSC curve of PAN fiber shows higher heat flow peak magnitude compared to PAN/lignin DSC curve. This suggests

that lignin can avoid excessive heat eruption during PAN stabilization, which is similar to the effect of acid-containing co-monomers on PAN fibers.[45-46] Additionally, both PAN/lignin and PAN/lignin/CNT fibers show broader exothermic peaks as compared to PAN fibers. These observations suggest that lignin can potentially expedite the PAN fiber stabilization process.

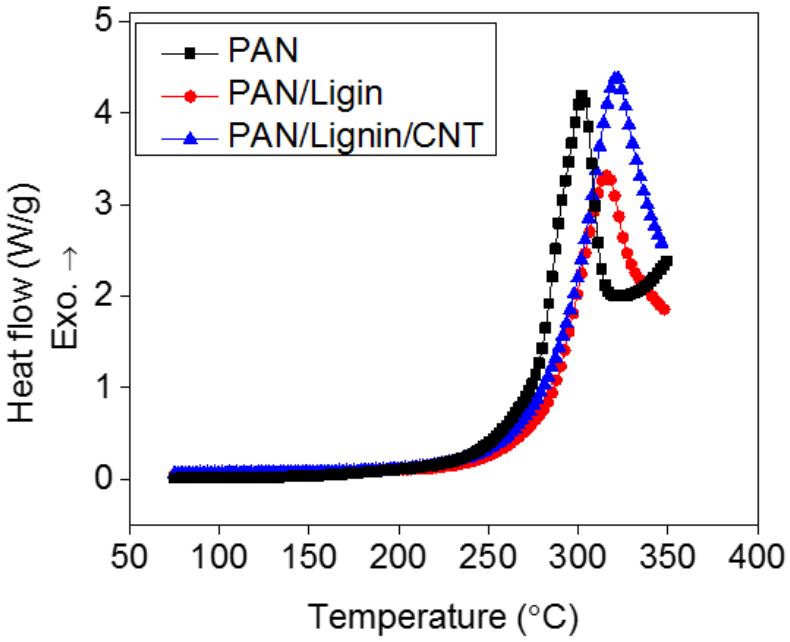

Figure 4.6. DSC thermograms for PAN fiber, PAN/lignin fiber, and (c) PAN/lignin/CNT fiber (All DR = 13) at a heating rate of 5˚C/min with air purging rate of 50 mL/min.

Table 4.3. DSC results of precursor fibers

Precursor Fibers	$\Delta H_{stabilization}$ (J/g)	FWHM (˚C)
PAN	942	17.3
PAN/lignin	748	24.7
PAN/lignin/CNT	1189	25.2

Fiber shrinkage during the stabilization reactions is monitored through TMA under an applied stress of 10 MPa at a heating rate of 0.5 ˚C/min, from room temperature to 280 ˚C, followed by holding at 280 ˚C for 150 min. The temperature profile and fiber strains during heating are shown in Figure 4.7. Under these conditions, the ultimate thermal shrinkage of PAN, PAN/lignin, and PAN/lignin/CNT fibers are 20.3%, 21.2% and 13.0%, respectively. This data unequivocally shows that the presence of CNTs significantly reduces thermal shrinkage during stabilization. Previous studies show that the fiber shrinkage can be due to entropic relaxation (100 – 175 ˚C range) which allows oriented amorphous polymer phase to recoil and due to chemical reaction (at above 175 ˚C) resulting from ladder structure formation.[38, 47] The current TMA data shows that PAN/lignin fiber shows earlier onset of polymer recoiling than PAN fiber. This suggests that the incorporation of lignin can promote the entropic relaxation of polymer. PAN/lignin/CNT fiber, on the other hand, shows a much slower onset for entropic relaxation than the other two fibers. Previous studies have shown that the presence of CNTs can reduce thermal shrinkage in PAN.[38, 40] This agrees with the current observations. Chemical reaction stage (above 175 ˚C) in Figure 4.7 corresponds to the cyclization of PAN molecules.[48] TMA results show that PAN/lignin fiber has earlier onset of the reaction than PAN and PAN/lignin/CNT fibers. Interestingly, this result correlates with the heat of stabilization ($\Delta H_{stabilization}$) observed from the DSC, where PAN/lignin fiber exhibits lower $\Delta H_{stabilization}$ than PAN fiber and PAN/lignin/CNT fiber. These findings imply that the incorporation of lignin can potentially promote the PAN cyclization during stabilization process, while the incorporation of CNT appears to delay this process.

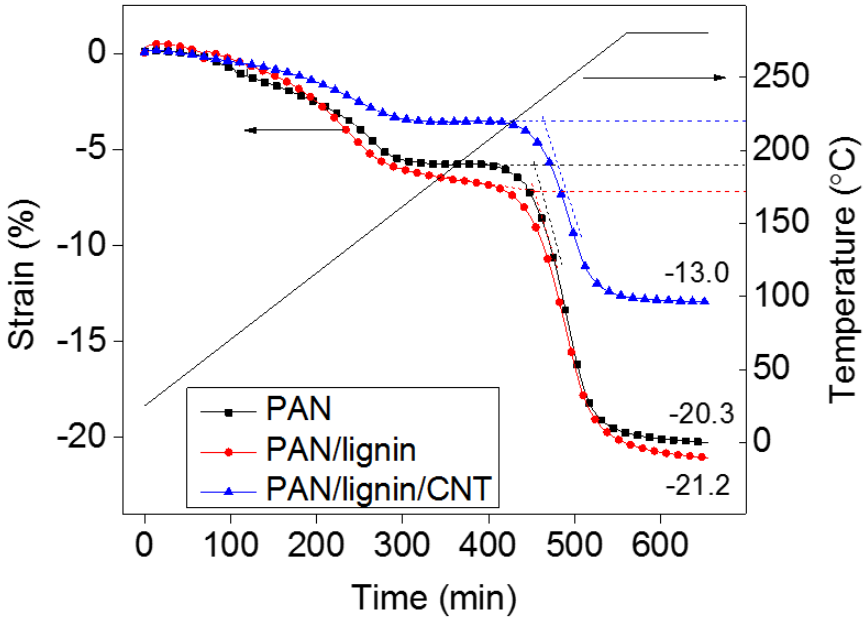

Figure 4.7. Strains of fiber during TMA with corresponding temperature profile.

4.3.5 Fiber stabilization and carbonization

Precursor fibers are stabilized under a stress of 22 MPa in the oxidative environment using a tube furnace. The fiber stabilization temperature profile is shown in Figure 4.8. During stabilization, PAN is known to undergo cyclization, oxidation and dehydrogenation.[45, 48-50] Stabilization for lignin is generally considered to be initiated by the homolytic cleavage of alkyl-aryl ether linkage and leads to further lignin units rearrangment and crosslinking.[51-54] FTIR spectra of stabilized PAN and PAN/lignin fibers are shown in Figure 4.9. After oxidative stabilization, PAN fiber shows diminishing C≡N structure at 2244 cm^{-1}.[55] Additionally, the appearance of peak shoulders at 1691 cm^{-1} and 1738 cm^{-1} corrspond to the C=O stretching of carbonyls. Stabilized PAN/lignin fiber shows clear 1050 cm^{-1} – 1200 cm^{-1} peaks, which are due to C–O stretching with possible overlap with C–N peak. Similar to stabilized PAN fiber, peak at 1740 cm^{-1} is assigned to the C=O

stretching in carbonyls for stabilized PAN/lignin fiber.[52] A new peak is observed ~1870 cm^{-1} in the stabilized PAN/lignin fiber. Previous XPS studies used this peak to identify anhydride linkage formation from the crosslinking of stabilized lignins.[52-53] Addtiontionally, small peaks between 2860 – 2970 cm^{-1} in the stabilized PAN/lignin fiber spectra represent C–H stretching from aromatic and aliphatic carbons, which are attributed to lignin units after stabilization.[52] The differences between stabilized PAN and PAN/lignin fiber spectra show the evidence of both PAN and lignin stabilization reactions.

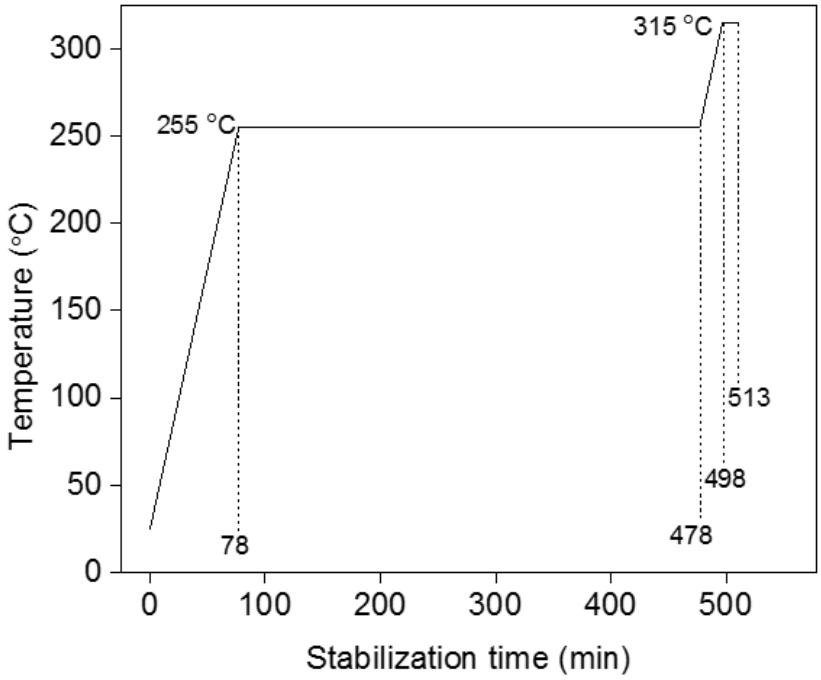

Figure 4.8. Stabilization temperature profile showing temperature stages and residence time with constant heating rate of 3 °C per minute. Air flow rate is 50 standard cubic feet per hour (SCFH).

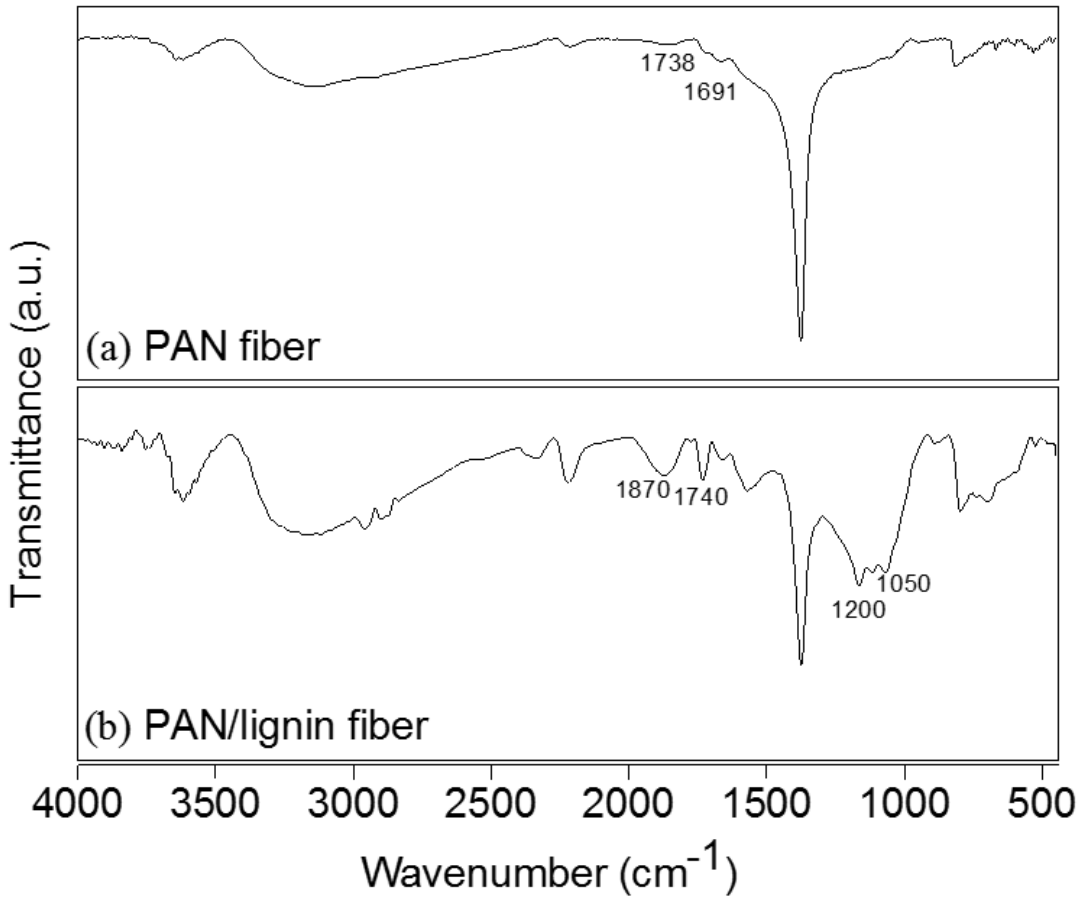

Figure 4.9. FTIR spectra of (a) PAN and (b) PAN/lignin fibers stabilized under conditions described by Figure 4.8.

Integrated WAXD scans of precursor, stabilized, and carbon fibers along with the WAXD patterns of the stabilized and carbon fibers are shown in Figure 4.10. All integrated scans of precursor fibers show a distinct PAN peak at $2\theta \approx 17°$ which diminishes upon stabilization. The peak at $2\theta \approx 26^{\circ}$ in stabilized and carbonized fibers is due to the formation of laddered polymer structure and carbon structure, respectively. Structural parameters of stabilized fibers are shown in Table 4.4. CNT incorporated stabilized fiber shows relatively large crystal size (1.4 nm v.s. 1.1 nm and 1.0 nm in PAN and PAN/lignin based fibers, respectively) corresponding to the $2\theta \approx 26^{\circ}$ peak, suggesting that CNTs promote the

development of the cyclized ladder structure in the vicinity of CNT. Compared with PAN stabilized fiber, PAN/lignin shows slightly lower crystal size corresponding to the peak at $2\theta \approx 43°$, indicating that the formation of cyclized ladder structure along the fiber axis might be disturbed by the incorporation of lignin. In addition to larger crystal sizes, stabilized fiber containing CNT has smaller ladder structure d-spacing of 3.40 Å, as compared to 3.43 Å and 3.48 Å in PAN and PAN/lignin fibers, respectively. Similar observations are found in previous studies on PAN/CNT fibers.[56-57]

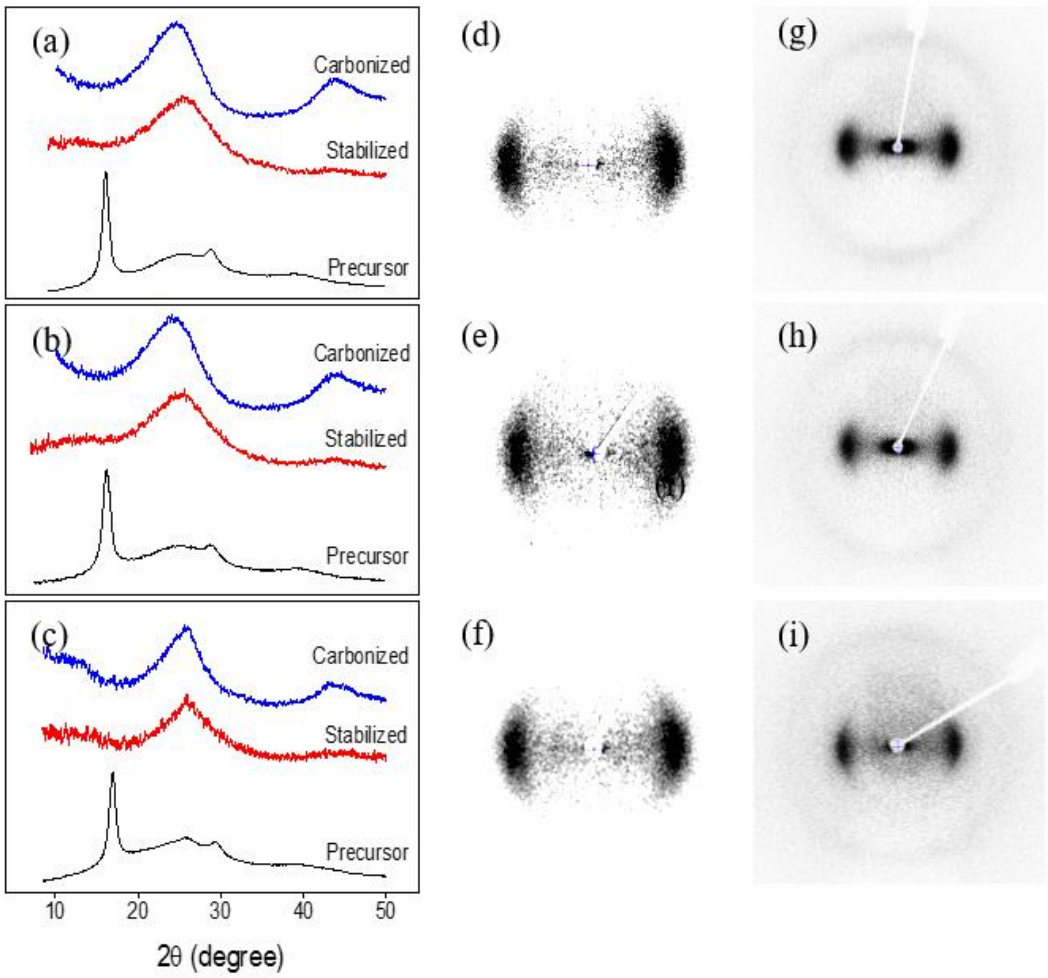

Figure 4.10. Integrated scans of precursor, stabilized fibers and carbon fibers for (a) PAN, (b) PAN/lignin and (c) PAN/lignin/CNT fibers with the corresponding WAXD patterns of stabilized (d) PAN, (e) PAN/lignin and (f) PAN/lignin/CNT fibers and carbonized (at 1000 ° C) (g) PAN, (h) PAN/lignin, and (i) PAN/lignin/CNT fibers.

Table 4.4. Structural parameters of stabilized fibers

Stabilized Fibers	PAN	PAN/lignin	PAN/lignin/CNT
$L_{2\theta \approx 26^\circ}$ [a] (nm)	1.1	1.0	1.4
$L_{2\theta \approx 43^\circ}$ [b] (nm)	1.4	1.2	1.6
f_{ladder} [c]	0.66	0.65	0.65
d-spacing ($2\theta \approx 26^\circ$) (Å)	3.43	3.48	3.40

[a] The crystal size of ladder structure at $2\theta \approx 26^\circ$.
[b] The crystal size from meridional scan at $2\theta \approx 43^\circ$.
[c] Orientation of ladder structure of stabilized fibers.

Stabilized fibers are carbonized under inert environment at a constant heating rate of 5 °C/min to 1,000°C and 1,100°C. No fusing of stabilized or carbonized fibers is observed, indicating proper heating rate is applied during each process for lignin incorporated fibers.[9, 58] After carbonization, the ladder structure from stabilization is then transformed into turbostratic carbon structure.[57] SEM images of the carbon fiber cross sections are shown in Figure 4.11. Under the identical stabilization and carbonization conditions, PAN and PAN/lignin carbon fibers show minimal voids in the fiber cross-sections, while the PAN/lignin/CNT carbon fiber exhibits more observable voids which would be detrimental for mechanical properties. The void formation caused by CNT was not noted in previous PAN/CNT batch processed carbon fiber studies.[19, 38, 48, 57, 59] However, in a recent PAN/CNT carbon fiber study, void formation was noted, and the presence of these voids was attributed to non-uniform CNT length, and CNT bundling.[24] The structural parameters and mechanical properties of carbonized fibers are summarized in Table 4.5. At both carbonization temperatures (1,000 °C and 1,100 °C), PAN/lignin/CNT fibers show relatively lower orientation as compared to PAN and PAN/lignin fibers, this can result from lower PAN orientations in CNT containing precursor fibers. The lower orientation along with the more voids in PAN/lignin/CNT carbon fiber results in lower tensile properties,[60]

as compared to the PAN and PAN/lignin fibers. All carbon fibers show improvements in tensile strength and tensile modulus with simultaneous increase of crystal size for (10) plane with increasing carbonization temperatures. When carbonized at 1,000 °C, PAN carbon fiber shows tensile strength, tensile modulus, and elongation at break of 1.54 GPa, 193 GPa, and 0.83%, respectively. When carbonized at 1100 °C, tensile modulus of PAN fiber is increased to 223 GPa, with a slightly decreased elongation at break of 0.70% and a relatively unchanged tensile strength of 1.60 GPa. Carbonized at 1,000 °C with identical conditions, PAN/lignin fiber shows comparable tensile modulus (194 GPa) but lower tensile strength (1.37 GPa) and elongation at break (0.72%). Interestingly, when carbonized at 1,100 °C, PAN/lignin carbon fiber exhibits noticeable improvement in tensile strength (1.72 GPa) and tensile modulus (230 GPa), while elongation at break remains intact (0.80%). To determine the statistical significance of the comparison between carbon fiber properties, a p-value test at the confidence limit of 95% was performed on the data sets of carbon fiber mechanical performance using the JMP™ 13 software. Results of the statistical significance are summarized in APPENDIX C.

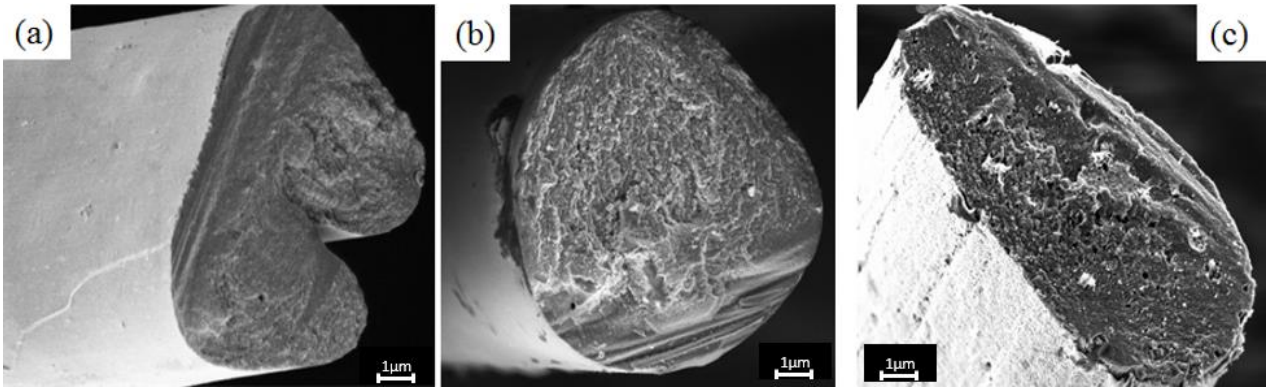

Figure 4.11. SEM images of carbon fiber cross sections of (a) PAN, (b) PAN/lignin, and (c) PAN/lignin/CNT carbonized at 1100 °C

Raman spectra of carbon fibers are shown in Figure 4.12. Raman D-band (at ~1340 cm^{-1}) is attributed to the structural disorder and G-band (at ~1560 cm^{-1}) is assigned to the graphitic planes. FWHM of both D and G bands along with the intensity ratio are normally used to characterize carbon materials[61-65] and to understand the carbonization mechanism of wood materials.[66-67] For example, amorphization trajectory can also be used to analyze carbonization behaviors by describing the transformation of neat graphite to nano-crystalline graphite, and further to sp^3 amorphous carbon. As carbon transforms along this

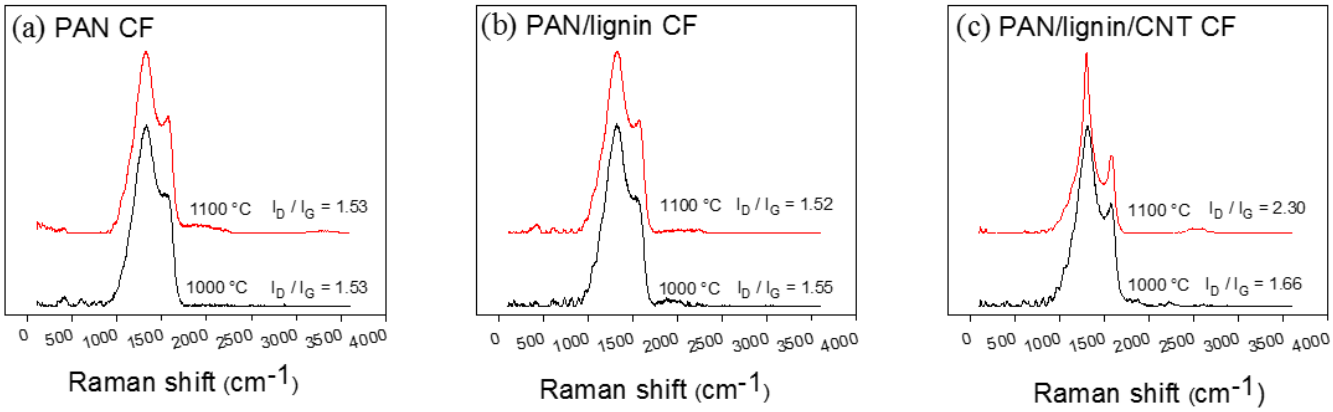

Figure 4.12. Raman spectra of fibers (a) PAN, (b) PAN/lignin and (c) PAN/lignin/CNT carbonized at 1000°C and 1100°C.

amorphization trajectory, I_D/I_G will first increase due to defects in the graphite structure, and then decrease during nano-crystalline graphite formation. This is followed by a further decrease in I_D/I_G owing to the formation of amorphous carbon.[62-63] In Raman spectroscopy studies on carbon materials, Tuinstra-Koenig law was often employed to estimate crystal size by correlation with intensity ratio I_D/I_G.[68] However, studies have shown that Tuinstra-Koenig correlation is not applicable when crystal sizes were below 2 nm, as it resulted in significant discrepancies.[69-70] In this study, we note that the crystal sizes obtained from

WAXD in Table 4.5 were mostly below 2 nm. Therefore Raman spectral features in the current study have not been used for crystal size determination. Raman spectroscopy and amorphization trajectory were used to study the electrospun kraft lignin and PAN fibrous materials carbonized at 600, 800 and 1,000 °C by Dallmeyer et al.[71] While PAN is considered as a semi-crystalline material, carbonization between 600 and 1,000 °C induces the nano-crystalline carbon formation that yields decreasing I_D/I_G values with increasing carbonization temperature. Lignin, in contrast, started with much more amorphous state, can transform to nano-crystalline graphite from nucleation and growth of disordered aromatic rings. PAN and lignin were then reported to undergo distinct stages of carbonization between 600 to 1,000 °C.[71]

When carbonized at 1,000 °C, all carbon fibers show obvious D-band peaks. PAN and PAN/lignin carbon fibers show G-band peaks as shoulders while PAN/lignin/CNT exhibits a more resolved G-band peak (Figure 4.12). When carbonization temperature is increased to 1100°C, further developments in the graphitic G-band for all the fibers are observed. Surprisingly, although G-band peaks seem to be more significant when carbonized at 1100°C, PAN and PAN/lignin carbon fibers show no significant changes in I_D/I_G values (Figure 4.12 a, b) while PAN/lignin/CNT fiber shows noticeably increased intensity peak ratio from 1.66 to 2.30 in going from 1,000 to 1,100 °C (Figure 4.12c). This implies that the incorporation of CNT might induce the transformation from amorphous carbon to nano-crystalline graphite when carbonized from 1,000 to 1,100 °C, as the development of D-peak can indicate the ordering of amorphous carbons.[63]

Table 4.5. Structural parameters and tensile properties of carbon fibers

Carbon Fiber Structural Parameters						
Carbonize Temp (°C)	1000 °C			1100 °C		
Carbon Fiber	PAN	PAN/lignin	PAN/lignin/CNT	PAN	PAN/lignin	PAN/lignin/CNT
L002[a] (nm)	1.3	1.3	1.6	1.3	1.4	1.8
L10[b] (nm)	1.5	1.5	1.7	2.3	2.0	1.9
f_{002}[c]	0.80	0.78	0.75	0.81	0.80	0.77
Z[d]	34.4	34.9	35.5	32.7	32.8	33.2
d-spacing $_{(002)}$ (Å)	3.48	3.53	3.51	3.51	3.52	3.49
Carbon Fiber Tensile Properties						
Diameter (μm)	10.5 ± 0.6	11.0 ± 1.1	9.0 ± 0.3	11.0 ± 0.7	11.0 ± 1.1	8.8 ± 0.3
Strength (GPa)	1.54 ± 0.6	1.37 ± 0.2	1.29 ± 0.2	1.60 ± 0.3	1.72 ± 0.2	1.40 ± 0.2
Modulus (GPa)	193 ± 12	194 ± 8	181 ± 5	223 ± 4	230 ± 7	200 ± 7
Elong. at break (%)	0.83 ± 0.2	0.72 ± 0.1	0.72 ± 0.1	0.70 ± 0.1	0.80 ± 0.1	0.71 ± 0.1

[a] The crystal size of (002) plane.
[b] The crystal size of (10) plane.
[c] Orientation of (002) structure of carbon fibers.
[d] Full width half maximum (FWHM) (in degree) from azimuthal scans of (002) planes.
* Modulus values have not been corrected for instrumental compliance.

The D and G band FWHM of the carbon fibers are shown in Figure 4.13 and Figure 4.14, respectively. In general, D-band FWHM of carbonized wood components are reported to decrease with increasing carbonization temperatures, indicating the ordering of polyaromatic carbons and the breakage of crosslinking between aliphatic carbons and small aromatic carbons.[67, 71] For the lignin incorporated carbon fibers in this work, a similar trend is observed (Figure 4.13). Both PAN/lignin and PAN/lignin/CNT fibers show noticeable decrease in D-band FWHM, when carbonization temperature is increased. However, D-band FWHM of PAN fiber does not exhibit significant change. This suggests that when incorporating lignin into PAN, re-ordering of polyaromatic stacks still occurs at elevated carbonization temperautres. Although both PAN/lignin and PAN/lignin/CNT fibers show narrowing D-band FWHM, PAN/lignin/CNT exhibits more significant change than the PAN/lignin fiber, suggesting that the presence of CNT promotes further reordering of the disordered aromatic rings in the carbon fiber.

G-band FWHM is often employed to characterize carbon crystallites. Narrower G-band FWHM implies more ordered structure of carbon crystallites.[65-66, 72] Although G-band FWHM of carbon materials is expected to decrease at higher carbonization temperatures, Dallmeyer et al. reproted an increasing G-band FWHM when lignin is carbonized from 600 to 1,000 °C. This might be ascribed to the increase in non-aromatic conjugated structure during polyaromatics reordering.[71] In Figure 4.14, PAN carbon fiber shows a decrease in G-band FWHM from 1,000 °C to 1,100°C which can be attributed to more refined structure at increased carbonization temperatures.[73] In contrast, G-band FWHM of PAN/lignin carbon fiber stays relatively unchanged when carbonization temperature is increased from 1,000 to 1,100°C. This unchanged G-band FWHM of PAN/lignin suggests

that the breaking of crosslinking between the aliphatic and aromiatic carbons discussed above can offset the ordering of PAN crystalline carbons. This indicates that the carbon crystallite refining and polyaromatic ordering are ongoing simultaneously in this temperature range. Interestingly, PAN/lignin/CNT shows a significant narrowing for both the G and D band FWHM in going from 1,000 to 1,100 °C. This finding agrees with the reported crystallites ordering during carbonization when CNTs are embedded in the PAN nanofibers, where the G-band FWHM is found to decrease with increasing CNT concentration.[56]

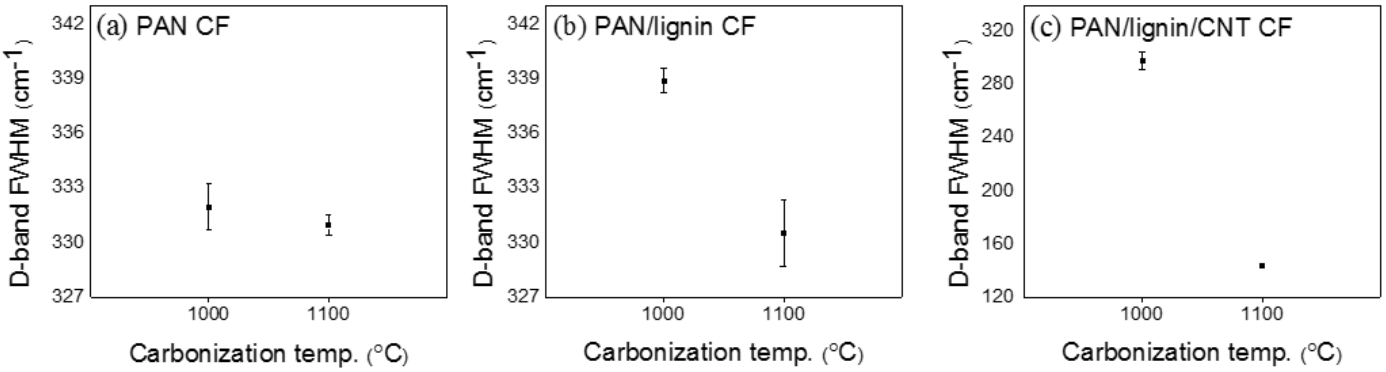

Figure 4.13. D-band FWHM when carbonized from 1000°C to 1100 °C for (a) PAN, (b) PAN/lignin and (c) PAN/lignin/CNT.

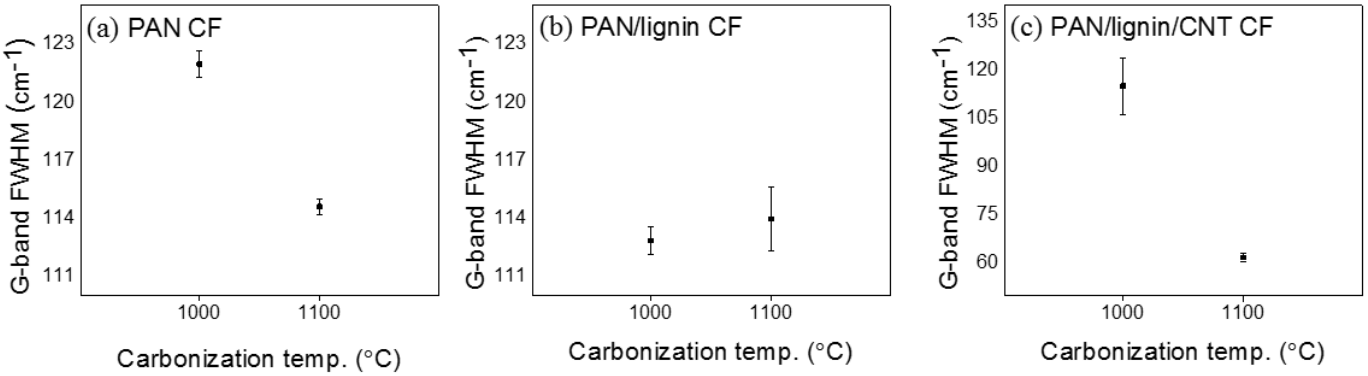

Figure 4.14. G-band FWHM when carbonized from 1000°C to 1100 °C for (a) PAN, (b) PAN/lignin and (c) PAN/lignin/CNT.

4.4 DISCUSSIONS AND CONCLUDING REMARKS

PAN, PAN/lignin (70/30 weight ratio), and PAN/lignin/CNT (70/30/3 weight ratio) precursor fibers have been successfully manufactured through gel-spinning. It is noted that while PAN fiber could be spun at concentration of 14 g/dL, PAN/lignin, and PAN/lignin/CNT fibers could be spun at a concentration of 20, and 25.75 g/dL, respectively. These significant differences in the spinning concentrations, along with differences in the spinning temperatures (as discussed in the experimental section) provided first evidence of interaction between these binary and ternary blend systems in DMAc. Subsequent studies on the precusrsor and carbon fibers provided further evidence of PAN/lignin, and PAN/lignin/CNT interaction by spectroscopic (FTIR and Raman) and physio-mechanical methods (WAXD, DMA, DSC, TMA). These studies show that the incorporation of lignin affects PAN polymer chain packing, as well as the fiber stabilization and carbonization behavior. FTIR spectra shows the evidence of specific interaction between lignin and PAN. DSC studies show that as compared to PAN, PAN/lignin fiber exhibits a broader exothermic peak of lower magnitude, while TMA exhbited earlier onset of PAN cyclization. These studies suggest that lignin promotes PAN stabilization. In the presence of CNT, thermal shrinkage of the fiber is significantly reduced during stabilization. Conversion process of the precursor fibers to carbon fibers have been studied and carbon fiber fabrication of all fibers is successfully achieved under identical conditions. Void free carbon fibers have been made from gel-spun PAN/lignin precursor fibers, while other studies reported in the literature to-date based on solution-spun PAN/lignin fibers all show significant voids in the final carbon fiber.[14, 16-17, 74] This comparison, shows the

advantage of the gel-spinning technique for making void free carbon fibers from PAN/lignin blend.

When carbonized at 1,100 °C under identical conditions, the mechanical properties of PAN/lignin carbon fiber are comparable to that of the PAN carbon fiber. By comparison, other studies in the literature to-date show lower properties for the carbon fibers from PAN/lignin than from PAN. Therefore, it has been clearly demonstarted that by the gel-spinning process, lignin can be incorporated into PAN-based carbon fibers without compromising mechanical properties. Mechanical properties of the PAN/lignin carbon fiber in the current study already exceeds U. S. Department of Energy target mechanical properties for automotive composites (DOE traget tensile strength is 1.72 GPa, and the target tensile modulus is 172 GPa). The properties achieved in the current study will be further improved for the following reasons: (a) highest tensile strength carbon fibers are processed at a temperature in the range of 1,400 to 1,600 °C,[2, 75] while the carbonization in the current study was only carried out at a maximum temperature of 1,100 °C. (b) Fiber modulus almost linearly increases with increasing carbonization temperature.[2] (c) High strength and high modulus carbon fibers are always processed on continuous stabilization and carbonization lines, where fiber tension can be controlled to different levels in stepwise temperature zones, and carbonization time in the high temperature range (500 to 1,600 °C range) can be limited to few minutes. Therefore, when the gel-spun PAN/lignin fiber is carbonized on a continuous stabilization and carbonization line, where temperature and tension can be controlled in various stabilization and carbonization temperature zones, significant further improvements in tensile strength and modulus can be expected. While comparing the mechanical properties of the PAN/lignin carbon fibers in the current stduy

to that of the Zoletk study, it should be noted that the fibers in the current study were processed in batch mode at a maximum temperature of 1,100 °C (due to temperature limitation of the furnace). In the Zoltek study, carbonization temperature was not reported. However, based on the known parameters for achieving high strength carbon fibers, we presume that Zoltek fibers would have been carbonized somewhere in the 1,400 to 1,600 °C temperature range. We also note that the modulus in the current study has not been corrected for instrumental compliance, and with this correction, the carbon fiber modulus in the current study will be about 5-7% higher than the values given in Table 4.5.[76]

Continuous stabilization and carbonization of gel-spun PAN fiber has resulted in a new milestone in developing high strength and high modulus carbon fibers, where average tensile strength and tensile modulus based on standard test protocols were in the range of 5.5 to 5.8 GPa, and in the range of 350 to 380 GPa, respectively.[77] At short gauge length tensile strength of gel-spun PAN-based carbon fiber was as high as 12 GPa.[77] This is a record tensile strength for a PAN-based carbon fiber at any gauge length. Thus considering that there is no loss in the mechanical properties of the gel-spun PAN/lignin based carbon fiber in the current study as compared to the gel-spun PAN-based carbon fiber, it can be expected that PAN/lignin based carbon fiber can compete in properties with the best in class PAN-based carbon fibers with appropriate materials and process optimization.

In addition, due to significantly lower cost of lignin as compared to PAN, PAN/lignin based fibers will have lower cost than PAN-based carbon fibers along with higher production rate from the acclerated stabilization process with the incorporation of lignin. Lignin being a bio-renewable product, PAN/lignin based carbon fibers will be more sustainable than PAN-based carbon fiber, as PAN is currently derived from petroleum. In

addition, due to the three diemnsional nature of the lignin molecule, PAN/lignin based carbon fibers are expected to have good compressive strength. This is in contrast to the pitch-based carbon fibers, where pitch leads to highly graphitic two dimension structure, and hence low compressive strength.[2, 78]

With the incorporation of lignin, CNT, or both, carbonization behavior of PAN is altered. When carbonization temperature increases, PAN shows narrowing G-band FWHM corresponding to lower structural disorder and a relatively unchaged D-band FWHM. PAN/lignin shows no significant change in G-band FWHM but a noticeably narrowing D-FWHM that is attributed to aliphatic and aromatic carbons re-ordering. PAN/lignin/CNT carbon fiber shows significant reduction of both G and D band FWHM, as compared to the PAN/lignin carbon fiber. This suggests that the presence of CNT can induce both structural re-ordering of PAN and aliphatic/aromatic carbon reodering during carbonization. Despite the enhanced order/crystal size, somewhat lower mechnical properties of PAN/lignin/CNT based carbon fibers, as compared to PAN and PAN/lignin based carbon fibers can be attributed to the presence of voids in the former fiber. The CNT diameter used in the current study, at 21.0 ± 3.1 nm, was significanly larger than the CNT diameter used in our previous studies, where CNT diameter was in the range of 1 to 12 nm.[19, 24, 57, 79-80] The large CNT diameter in the current study may at least be partially responsible for the lower tensile strength of the PAN/lignin/CNT based carbon fiber. On the other hand, the lower tensile modulus of the PAN/lignin/CNT based carbon fiber as compared to the PAN and PAN/lignin based carbon fibers was a result of lower graphitic plane orientation in the former fiber (Table 4.5). Consequently, the question is, is there an advantage of the addition of CNT in PAN/lignin for making carbon fiber. In yet another recent study on PAN/CNT

fiber, it has been shown that the addition of 0.5 to 1 wt% CNT in PAN, results in about 25% increase in axial electrical conductivity and upto 100% increase in thermal conductivity of the PAN-based carbon fiber.[24] Similarly PAN/lignin based carbon fibers with enhanced electrical and thermal conductivities can be produced with the addition of CNT. Exact influence on mechanical properties, as well as on electrical and thermal conductivity of the PAN/lignin/CNT based carbon will depend on CNT length, diameter, perfection, as well as on CNT dispersion in the matrix. Interaction of CNT has been shown on PAN previously,[19, 24, 40, 59, 80] and on the PAN/lignin blend in this study. Similarly, PAN/lignin fibers can also be processed with the addition of graphene nano-ribbons, as well as graphene oxide nano-ribbons.[81]

4.5 REFERENCES

[1]. Huang, X. S., Fabrication and Properties of Carbon Fibers. *MATERIALS* **2009,** *2* (4), 2369-2403.

[2]. Minus, M. L.; Kumar, S., The Processing, Properties, and Structure of Carbon Fibers. *JOM* **2005,** *57* (2), 52-58.

[3]. Liu, Y.; Kumar, S., Recent Progress in Fabrication, Structure, and Properties of Carbon Fibers. *Polymer Reviews* **2012,** *52* (3-4), 234-258.

[4]. Calvo-Flores, F. G.; Dobado, J. A., Lignin as Renewable Raw Material. *ChemSusChem* **2010,** *3* (11), 1227-1235.

[5]. Baker, D. A.; Rials, T. G., Recent Advances in Low-Cost Carbon Fiber Manufacture from Lignin. *Journal of Applied Polymer Science* **2013,** *130* (2), 713-728.

[6]. Sudo, K.; Shimizu, K., A New Carbon Fiber from Lignin. *Journal of Applied Polymer Science* **1992,** *44* (1), 127-134.

[7]. Frank, E.; Hermanutz, F.; Buchmeiser, M. R., Carbon Fibers: Precursors, Manufacturing, and Properties. *Macromolecular Materials and Engineering* **2012,** *297* (6), 493-501.

[8]. Kubo, S.; Kadla, J. F., Lignin-based Carbon Fibers: Effect of Synthetic Polymer Blending on Fiber Properties. *Journal of Polymers & the Environment* **2005,** *13* (2), 97-105.

[9]. Kadla, J. F.; Kubo, S.; Venditti, R. A.; Gilbert, R. D.; Compere, A. L.; Griffith, W., Lignin-based Carbon Fibers for Composite Fiber Applications. *Carbon* **2002,** (15), 2913.

[10]. Maradur, S. P.; Kim, B. H.; Yang, K. S.; Kim, C. H.; Kim, S. Y.; Kim, W. C., Preparation of Carbon Fibers from a Lignin Copolymer with Polyacrylonitrile. *Synthetic Metals* **2012,** *162* (5-6), 453-459.

[11]. Seydibeyoğlu, M. Ö., A Novel Partially Biobased PAN-Lignin Blend as a Potential Carbon Fiber Precursor. *Journal of Biomedicine and Biotechnology* **2012,** *2012*, 1-8.

[12]. Alexy, P.; Košíková, B.; Podstránska, G., The Effect of Blending Lignin with Polyethylene and Polypropylene on Physical Properties. *Polymer* **2000,** *41* (13), 4901-4908.

[13]. Thunga, M.; Chen, K.; Grewell, D.; Kessler, M. R., Bio-renewable Precursor Fibers from Lignin/Polylactide Blends for Conversion to Carbon Fibers. *Carbon* **2014,** *68*, 159-166.

[14]. Husman, G. In *Development and Commercialization of a Novel Low-cost Carbon Fiber*, Presentation at 2012 DOE Hydrogen and Fuel Cells Program and Vehicle Technologies Program Annual Merit Review and Peer Evaluation Meeting, **2012**.

[15]. Bissett, P. J.; Herriott, C. W., Lignin/Polyacrylonitrile-Containing Dopes, Fibers, and Methods of Making Same. U.S. Patents 2012/0003471: **2012**.

[16]. Husman, G. In *Development and Commercialization of a Novel Low-Cost Carbon Fiber*, Presentation at 2014 DOE Hydrogen and Fuel Cells Program and Vehicle Technologies Office Annual Merit Review and Peer Evaluation Meeting, **2014**.

[17]. Dong, X.; Lu, C.; Zhou, P.; Zhang, S.; Wang, L.; Li, D., Polyacrylonitrile/lignin Sulfonate Blend Fiber for Low-cost Carbon Fiber. *RSC Advances* **2015,** *5* (53), 42259-42265.

[18]. Ragauskas, A. J.; Beckham, G. T.; Biddy, M. J.; Chandra, R.; Chen, F.; Davis, M. F.; Davison, B. H.; Dixon, R. A.; Gilna, P.; Keller, M.; Langan, P.; Naskar, A. K.; Saddler, J. N.; Tschaplinski, T. J.; Tuskan, G. A.; Wyman, C. E., Lignin Valorization: Improving Lignin Processing in the Biorefinery. *Science* **2014,** *344* (6185).

[19]. Chae, H. G.; Choi, Y. H.; Minus, M. L.; Kumar, S., Carbon Nanotube Reinforced Small Diameter Polyacrylonitrile Based Carbon Fiber. *Composites Science and Technology* **2009,** *69* (3-4), 406-413.

[20]. Chae, H. G.; Kumar, S., Making Strong Fibers. *Science* **2008,** (5865), 908.

[21]. Chae, H. G. Polyacrylonitrile/Carbon Nanotube Composite Fibers: Reinforcement Efficiency and Carbonization Studies. Ph.D Thesis. Georgia Institute of Technology, Atlanta, GA, **2008**.

[22]. Chien, A.; Gulgunje, P. V.; Chae, H. G.; Joshi, A. S.; Moon, J.; Feng, B.; Peterson, G. P.; Kumar, S., Functional polymer–polymer/carbon nanotube bi-component fibers. *Polymer* **2013,** *54* (22), 6210-6217.

[23]. Liu, Y.; Kumar, S., Polymer/Carbon Nanotube Nano Composite Fibers–A Review. *ACS Applied Materials & Interfaces* **2014,** *6* (9), 6069-6087.

[24]. Newcomb, B. A.; Giannuzzi, L. A.; Lyons, K. M.; Gulgunje, P. V.; Gupta, K.; Liu, Y.; Kamath, M. G.; McDonald, K.; Moon, J.; Feng, B.; Peterson, G. P.; Chae, H. G.; Kumar, S., High Resolution Transmission Electron Microscopy Study on Polyacrylonitrile/Carbon Nanotube Based Carbon Fibers and the Effect of Structure Development on the Thermal and Electrical Conductivities. *Carbon* **2015,** *93*, 502-514.

[25]. Baker, F. S.; Baker, D. A.; Menchhofer, P. A. Carbon Nanotube (CNT)-Enhanced Precursor for Carbon Fiber Production and Method of Making a CNT-enhanced Continous Lignin Fiber. US 2011/0285049 A1, **2011**.

[26]. Teng, N.; Dallmeyer, I.; Kadla, J. F., Incorporation of Multiwalled Carbon Nanotubes into Electrospun Softwood Kraft Lignin-Based Fibers. *Journal of Wood Chemistry and Technology* **2013,** *33* (4), 299-316.

[27]. Teng, N.; Dallmeyer, I.; Kadla, J. F., Effect of Softwood Kraft Lignin Fractionation on the Dispersion of Multiwalled Carbon Nanotubes. *Industrial & Engineering Chemistry Research* **2013,** *52* (19), 6311-6317.

[28]. Sahoo, S.; Seydibeyoğlu, M. Ö.; Mohanty, A. K.; Misra, M., Characterization of Industrial Lignins for Their Utilization in Future Value Added Applications. *Biomass and Bioenergy* **2011,** *35* (10), 4230-4237.

[29]. Allen, R. A.; Ward, I. M.; Bashir, Z., The Variation of the d-Spacings with Stress in the Hexagonal Polymorph of Polyacrylonitrile. *Polymer* **1994,** *35* (19), 4035-4040.

[30]. Bashir, Z., A Critical Review of the Stabilisation of Polyacrylonitrile. *Carbon* **1991,** *29* (8), 1081-1090.

[31]. Bashir, Z., Co-crystallization of Solvents with Polymers: the X-ray Diffraction Behavior of Solvent-containing and Solvent-free Polyacrylonitrile. *Journal of Polymer Science, Part B: Polymer Physics* **1994,** *32* (6), 1115-1128.

[32]. Sokół, M.; Grobelny, J.; Turska, E., Investigation of Structural Changes of Polyacrylonitrile on Swelling. Wide-Angle X-ray Scattering Study. *Polymer* **1987,** *28* (5), 843-846.

[33]. Vainio, U.; Serimaa, R.; Maximova, N.; Laine, J.; Stenius, P.; Hortling, B.; Simola, L. K.; Gravitis, J., Morphology of Dry Lignins and Size and Shape of Dissolved Kraft Lignin Particles by X-ray Scattering. *Langmuir* **2004,** *20* (22), 9736-9744.

[34]. Gong, Y.; Du, R.; Mo, G.; Xing, X.; Lü, C.; Wu, Z., In-situ Microstructural Changes of Polyacrylonitrile Based Fibers with Stretching Deformation. *Polymer* **2014,** *55* (16), 4270-4280.

[35]. Sawai, D.; Yamane, A.; Kameda, T.; Kanamoto, T.; Ito, M.; Yamazaki, H.; Hisatani, K., Uniaxial Drawing of Isotactic Poly(acrylonitrile): Development of Oriented Structure and Tensile Properties. *Macromolecules* **1999,** *32* (17), 5622-5630.

[36]. Yamane, A.; Sawai, D.; Kameda, T.; Kanamoto, T.; Ito, M.; Porter, R. S., Development of High Ductility and Tensile Properties upon Two-Stage Draw of Ultrahigh Molecular Weight Poly(acrylonitrile). *Macromolecules* **1997,** *30* (14), 4170-4178.

[37]. Wang, W.; Murthy, N. S.; Chae, H. G.; Kumar, S., Structural Changes During Deformation in Carbon Nanotube-reinforced Polyacrylonitrile Fibers. *Polymer* **2008,** *49* (8), 2133-2145.

[38]. Liu, Y.; Chae, H. G.; Kumar, S., Gel-spun Carbon Nanotubes/Polyacrylonitrile Composite Fibers. Part I: Effect of Carbon Nanotubes on Stabilization. *Carbon* **2011,** *49*, 4466-4476.

[39]. Sawai, D.; Kanamoto, T.; Yamazaki, H.; Hisatani, K., Dynamic Mechanical Relaxations in Poly(acrylonitrile) with Different Stereoregularities. *Macromolecules* **2004,** *37* (8), 2839-2846.

[40]. Chae, H. G.; Sreekumar, T. V.; Uchida, T.; Kumar, S., A Comparison of Reinforcement Efficiency of Various Types of Carbon Nanotubes in Polyacrylonitrile Fiber. *Polymer* **2005,** *46* (24), 10925-10935.

[41]. Arrighi, V.; McEwen, I. J.; Qian, H.; Serrano Prieto, M. B., The Glass Transition and Interfacial Layer in Styrene-butadiene Rubber Containing Silica Nanofiller. *Polymer* **2003,** *44* (20), 6259-6266.

[42]. Rizzo, P.; Guerra, G.; Auriemma, F., Thermal Transitions of Polyacrylonitrile Fibers. *Macromolecules* **1996,** *29* (5), 1830-1832.

[43]. Devasia, R.; Nair, C. P. R.; Sadhana, R.; Babu, N. S.; Ninan, K. N., Fourier Transform Infrared and Wide-angle X-ray Diffraction Studies of the Thermal Cyclization Reactions of High-molar-mass Poly(acrylonitrile-co-itaconic acid). *Journal of Applied Polymer Science* **2006,** *100* (4), 3055-3062.

[44]. Ouyang, Q.; Cheng, L.; Wang, H.; Li, K., Mechanism and Kinetics of the Stabilization Reactions of Itaconic Acid-modified Polyacrylonitrile. *Polymer Degradation & Stability* **2008,** *93* (8), 1415-1421.

[45]. Fitzer, E.; Müller, D. J., The Influence of Oxygen on the Chemical Reactions During Stabilization of PAN as Carbon Fiber Precursor. *Carbon* **1975,** *13* (1), 63-69.

[46]. Rangarajan, P.; Bhanu, V. A.; Godshall, D.; Wilkes, G. L.; McGrath, J. E.; Baird, D. G., Dynamic Oscillatory Shear Properties of Potentially Melt Processable High Acrylonitrile Terpolymers. *Polymer* **2002,** *43* (9), 2699-2709.

[47]. Fitzer, E.; Frohs, W.; Heine, M., Optimization of Stabilization and Carbonization Treatment of PAN Fibres and Structural Characterization of the Resulting Carbon Fibres. *Carbon* **1986,** *24* (4), 387-395.

[48]. Liu, Y.; Chae, H. G.; Kumar, S., Gel-spun Carbon Nanotubes/Polyacrylonitrile Composite Fibers. Part II: Stabilization Reaction Kinetics and Effect of Gas Environment. *Carbon* **2011,** *49*, 4477-4486.

[49]. Schurz, J., Discoloration Effects in Acrylonitrile Polymers. *Journal of Polymer Science* **1958,** *28* (117), 438-439.

[50]. Watt, W.; Johnson, W., Mechanism of Oxidisation of Polyacrylonitrile Fibres. *Nature* **1975,** *257* (5523), 210-212.

[51]. Nimz, H., A New Type of Rearrangement in the Lignin Field. *Angewandte Chemie International Edition in English* **1966,** *5* (9), 843-843.

[52]. Braun, J. L.; Holtman, K. M.; Kadla, J. F., Lignin-based Carbon Fibers: Oxidative Thermostabilization of Kraft Lignin. *Carbon* **2006,** (2), 385.

[53]. Brodin, I.; Ernstsson, M.; Gellerstedt, G.; Sjöholm, E., Oxidative Stabilisation of Kraft Lignin for Carbon Fibre Production. *Holzforschung: International Journal of the Biology, Chemistry, Physics, & Technology of Wood* **2012,** *66* (2), 141-147.

[54]. Foston, M.; Nunnery, G. A.; Meng, X.; Sun, Q.; Baker, F. S.; Ragauskas, A., NMR a critical tool to study the production of carbon fiber from lignin. *Carbon* **2013,** *52* (0), 65-73.

[55]. Shimada, I.; Takahagi, T.; Fukuhara, M.; Morita, K.; Ishitani, A., FT-IR Study of the Stabilization Reaction of Polyacrylonitrile in the Production of Carbon Fibers. *Journal of Polymer Science Part A: Polymer Chemistry* **1986,** *24* (8), 1989-1995.

[56]. Prilutsky, S.; Zussman, E.; Cohen, Y., The Effect of Embedded Carbon Nanotubes on the Morphological Evolution During the Carbonization of Poly(acrylonitrile) Nanofibers. *Nanotechnology* **2008,** *19* (165603), 1-9.

[57]. Chae, H. G.; Minus, M. L.; Rasheed, A.; Kumar, S., Stabilization and Carbonization of Gel Spun Polyacrylonitrile/Single wall Carbon Nanotube Composite Fibers. *Polymer* **2007,** *48* (13), 3781-3789.

[58]. Kubo, S.; Uraki, Y.; Sano, Y., Preparation of Carbon Fibers from Softwood Lignin by Atmospheric Acetic Acid Pulping. *Carbon* **1998,** *36* (7–8), 1119-1124.

[59]. Liu, Y.; Chae, H. G.; Kumar, S., Gel-spun Carbon Nanotubes/Polyacrylonitrile Composite Fibers. Part III: Effect of Stabilization Conditions on Carbon Fiber Properties. *Carbon* **2011,** *49*, 4487-4496.

[60]. Fischer, L.; Ruland, W., The influence of graphitization on the mechanical properties of carbon fibers. *Colloid & Polymer Sci* **1980,** *258* (8), 917-922.

[61]. Ferrari, A. C., Raman Spectroscopy of Graphene and Graphite: Disorder, Electron-phonon Coupling, Doping and Nonadiabatic Effects. *Solid State Communications* **2007,** *143* (1), 47-57.

[62]. Ferrari, A. C.; Robertson, J., Resonant Raman Spectroscopy of Disordered, Amorphous, and Diamondlike Carbon. *Physical Review B (Condensed Matter and Materials Physics)* **2001,** *64* (7), 075414/1-13.

[63]. Ferrari, A. C.; Robertson, J., Interpretation of Raman Spectra of Disordered and Amorphous Carbon. *Physical Review B (Condensed Matter)* **2000,** *61* (20), 14095-14107.

[64]. Cuesta, A.; Dhamelincourt, P.; Laureyns, J.; Martínez-Alonso, A.; Tascón, J. M. D., Raman Microprobe Studies on Carbon Materials. *Carbon* **1994,** *32* (8), 1523-1532.

[65]. Katagiri, G.; Ishida, H.; Ishitani, A., Raman Spectra of Graphite Edge Planes. *Carbon* **1988,** *26* (4), 565-571.

[66]. Ishimaru, K.; Hata, T.; Bronsveld, P.; Imamura, Y., Microstructural Study of Carbonized Wood After Cell Wall Sectioning. *Journal of Materials Science* **2007,** *42* (8), 2662-2668.

[67]. Ishimaru, K.; Hata, T.; Bronsveld, P. M., D.; Imamura, Y., Spectroscopic Analysis of Carbonization Behavior of Wood, Cellulose and Lignin. *Journal of Materials Science* **2007,** *42* (1), 122-129.

[68]. Tuinstra, F.; Koenig, J. L., Raman Spectrum of Graphite. *The Journal of Chemical Physics* **1970,** *53* (3), 1126-1130.

[69]. Mallet-Ladeira, P.; Puech, P.; Toulouse, C.; Cazayous, M.; Ratel-Ramond, N.; Weisbecker, P.; Vignoles, G. L.; Monthioux, M., A Raman study to obtain crystallite size of carbon materials: A better alternative to the Tuinstra–Koenig law. *Carbon* **2014,** *80*, 629-639.

[70]. Zickler, G. A.; Smarsly, B.; Gierlinger, N.; Peterlik, H.; Paris, O., A Reconsideration of the Relationship Between the Crystallite Size La of Carbons Determined by X-ray Diffraction and Raman Spectroscopy. *Carbon* **2006,** *44* (15), 3239-3246.

[71]. Dallmeyer, I.; Lin, L. T.; Li, Y.; Ko, F.; Kadla, J. F., Preparation and Characterization of Interconnected, Kraft Lignin-Based Carbon Fibrous Materials by Electrospinning. *Macromolecular Materials and Engineering* **2013,** *298* (5), 540-551.

[72]. Ferrari, A. C. R., J., Raman Spectroscopy of Amorphous, Nanostructured, Diamond–like Carbon, and Nanodiamond. *Philosophical Transactions of the Royal Society of London. Series A: Mathematical, Physical and Engineering Sciences* **2004,** *362* (1824), 2477-2512.

[73]. Rodríguez-Mirasol, J.; Cordero, T.; Rodríguez, J. J., High-temperature Carbons from Kraft Lignin. *Carbon* **1996,** *34* (1), 43-52.

[74]. Husman, G. In *Development and Commercialization of a Novel Low-Cost Carbon Fiber*, 2013 DOE Hydrogen and Fuel Cells Program and Vehicle Technologies Program Annual Merit Review and Peer Evaluation Meeting, **2013**.

[75]. Rahaman, M. S. A.; Ismail, A. F.; Mustafa, A., A review of heat treatment on polyacrylonitrile fiber. *Polymer Degradation and Stability* **2007,** *92* (8), 1421-1432.

[76]. Lyons, K. M.; Newcomb, B. A.; McDonald, K. J.; Chae, H. G.; Kumar, S., Development of Single Filament Testing Procedure for Polyacrylonitrile Precursor and Polyacrylonitrile-based Carbon Fibers. *Journal of Composite Materials* **2014**, 1-10.

[77]. Chae, H. G.; Newcomb, B. A.; Gulgunje, P. V.; Liu, Y.; Gupta, K. K.; Kamath, M. G.; Lyons, K. M.; Ghoshal, S.; Pramanik, C.; Giannuzzi, L.; Şahin, K.; Chasiotis, I.; Kumar, S., High Strength and High Modulus Carbon Fibers. *Carbon* **2015,** *93*, 81-87.

[78]. Kumar, S.; Anderson, D. P.; Crasto, A. S., Carbon Fibre Compressive Strength and Its Dependence on Structure and Morphology. *Journal of Materials Science* **1993,** *28* (2), 423-439.

[79]. Şahin, K.; Fasanella, N. A.; Chasiotis, I.; Lyons, K. M.; Newcomb, B. A.; Kamath, M. G.; Chae, H. G.; Kumar, S., High Strength Micron Size Carbon Fibers From Polyacrylonitrile–Carbon Nanotube Precursors. *Carbon* **2014,** (0).

[80]. Newcomb, B. A.; Chae, H. G.; Gulgunje, P. V.; Gupta, K.; Liu, Y.; Tsentalovich, D. E.; Pasquali, M.; Kumar, S., Stress transfer in polyacrylonitrile/carbon nanotube composite fibers. *Polymer* **2014,** *55* (11), 2734-2743.

[81]. Chien, A. T.; Liu, H. C.; Newcomb, B. A.; Xiang, C.; Tour, J. M.; Kumar, S., Polyacrylonitrile Fibers Containing Graphene Oxide Nanoribbons. *ACS Applied Materials & Interfaces* **2015,** *7* (9), 5281-5288.

CHAPTER 5

GEL-SPUN POLYACRYLONITRILE, POLYACRYLONITRILE/LIGNIN BI-COMPONENT CARBON FIBERS

5.1 INTRODUCTION

Carbon fibers, exhibiting superior specific strength and modulus, have attracted great attention as reinforcing material in aerospace, sporting goods, premium automotive, and structural applications.[3-5] Currently, high performance carbon fibers are predominantly manufactured from petroleum-derived polymer, polyacrylonitrile (PAN). Owing to the high production cost, carbon fiber remains a specialty product and the use of carbon fiber in broader applications is still limited. To produce low-cost carbon fibers, cost-effective alternatives for carbon fiber precursor materials are needed.[4, 6] As a carbon fiber precursor candidate since 1960s, lignin has a high carbon yield with a low production cost compared to PAN. In addition, lignin is one the most abundant biopolymers on earth.[4, 7-8] Yet no pure lignin-based carbon fibers to date have been reported to meet the low-cost carbon fiber mechanical performance standard (1.72 GPa tensile strength, 172 GPa tensile modulus) set by the U.S. Department of Energy. As an alternative approach to fabricate low-cost carbon fibers enabled by the use of lignin, recent studies have focused on the blend processing of PAN with lignin or lignin sulfonate.[2, 9-12] Some of these studies have reported porous structure,[2, 11, 13] and reduced mechanical performance of the resultant carbon fibers with the incorporation of lignin.[1, 13] To address these issues, a study of gel-spun PAN/lignin blend (annual plant lignin, 30 wt%) carbon fiber has shown that lignin incorporation does not cause pores in the fiber structure nor yield reduced mechanical properties when

compared to PAN carbon fiber under identical fabrication process (e.g., draw ratio and the processing conditions of stabilization and carbonization.)[10] Yet the maximum draw ratio of the gel-spun PAN/lignin blend fiber was relatively low compared to that of PAN control fiber. While fibers manufactured at higher draw ratio can render smaller diameter to reduce number of defects per unit volume in fiber structure and thus lead to improved tensile strength of resultant carbon fibers,[5, 14-15] processing improvement to enhance drawability and to reduce the diameter of PAN/lignin blend is highly desired to fully realize the mechanical performance of PAN/lignin carbon fibers.

Developed around 1940s, bi-component fiber spinning is a versatile technique that enables the fiber processing with two distinct spinning dopes that can each impart specific properties.[16-19] Although bi-component spinning was originally proposed for melt processing, previous studies have shown that bi-component technique can be applied in gel-spinning process to enhance maximum draw ratio of high carbon nanotubes (CNT) loading fibers or fabricate small diameter (~ 1 μm) PAN/CNT carbon fibers.[20-21] In the current study, bi-component fibers with PAN and PAN/lignin components with the respective sheath-core geometry are fabricated by gel-spinning process. While high lignin loading (> 30 wt%) can be incorporated in PAN/lignin blend core component to enhance the PAN-based carbon fiber renewability, the PAN sheath can provide protection and endurance to the fiber towards higher draw ratio to reduce defects and fiber diameter for better mechanical performance of the derived carbon fiber. Processing, structure, thermal characterization of the PAN fiber and bi-component fibers along with the mechanical performance of precursor fiber and carbon fiber are reported herein.

5.2 EXPERIMENTAL

5.2.1 Materials and Processing

Polyacrylonitrile (PAN) copolymer with methacrylic acid (PAN-co-MAA, 96/4) with a viscosity average molecular weight of 247,000 g/mol was obtained from Exlan, Co. (*Osaka, Japan*) and the annual plant lignin (APL) powder Protobind 2400 was provided by GreenValue (Media, PA). Organic solvent dimethyformamide (DMF) was purchased from Sigma-Aldrich and distilled before use. For PAN solution, PAN solids were added into DMF in a glass reactor with a solid content of 15 g/dL at room temperature, followed by eight hours of stirring before being slowly heated to 80 °C in silicone oil bath. The solution is then maintained at 80 °C for five hours under constant stirring at 200 rpm before collection. For PAN/APL solution, APL solids were first dissolved and maintained in DMF at a solid content of 9 g/dL at 40 °C in an orbital shaker (MaxQ 4450, Thermo Scientific.) at 180 rpm for eight hours. The APL solution was then transferred to glass reactor with subsequent addition of PAN polymer at a solid content of 15 g/dL. This yields 37.5 wt% lignin incorporation (9 g/dL) with respect to total solid content of PAN/APL solution (24 g/dL). Similar to the PAN solution, PAN/APL solution first undergoes an eight-hour stirring at room temperature and a slow heating process in silicone oil bath to 80 °C, followed by a five-hour stirring process at 200 rpm before collection. All collected solutions were maintained in oven 60 °C for three hours before use. PAN sheath, PAN/APL core bi-component composite fibers were spun using a spinning unit manufactured by Hills, Inc (Melbourne, FL). PAN solution and PAN/APL solution were maintained at 60 °C in solution barrel reservoirs before being co-extruded through a single-hole spinnerette (diameter of 200 μm) maintained at 75 °C. Schematic of spinning setup is shown in Figure

5.1a. The extrudate was then passed through a 25-mm air gap and a methanol gelation bath maintained at -50 °C to form as-spun fiber collected at a spin draw ratio (SDR) of 1 and 2. After immersion in a methanol bath at -30 °C for twelve hours to ensure gelation, the as-spun fibers were then drawn in ambient condition (CDR) and subsequently drawn in a hot glycerol oil bath (HDR) maintained at 165 °C. Total draw ratio (TDR) of drawn fibers were calculated as SDR × CDR × HDR.

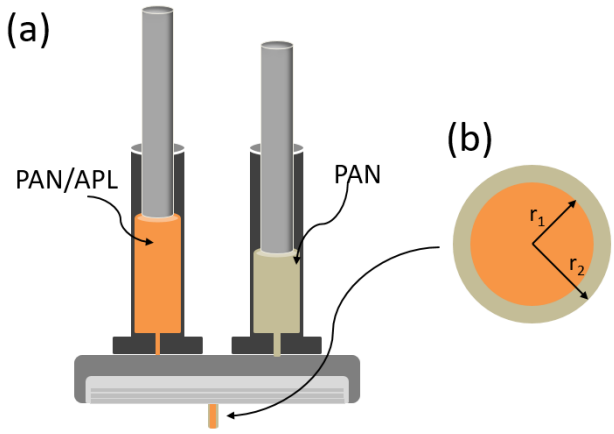

Figure 5.1. Schematics of (a) bi-component fiber spinning apparatus, and (b) sheath-core bi-component fiber geometry.

5.2.2 Characterization

For bi-component fiber manufacturing, solution flow rates are used to control the radius ratio between the overall fiber and the core component. Optical microscope was used to obtain cross section images of as-spun and drawn fiber, in which the sheath and core component radii ratios were calculated according to component areas in the fiber cross section, analyzed by software ImageJ. Microscope samples were prepared by embedding fiber bundles in epoxy followed by sectioning embedded samples to 10–15 μm thickness

using a microtome (Leica RM2255). Illustration of overall fiber radius, r_2 with respect to core radius r_1 is shown in Figure 5.1b. Tensile properties of precursor fiber are analyzed by FAVIMAT (Textechno H. Stein GmbH & Co. KG) on single filaments at a gauge length of 25.4 mm and a strain rate of 1%/s. More than 25 trials were conducted for each sample. Wide angle X-ray diffraction (WAXD) of fiber bundles are investigated on Rigaku Micromax-002 and Rigaku IV++ detecting systems with operating parameters of 0.65 mA, 45 kV, and $\lambda = 1.5418$ Å. WAXD patterns were then analyzed by software AreaMax V1.00 and MDI Jade 9.0. Dynamic mechanical analysis (DMA) of fibers was conducted on 25-filament fiber bundles at a frequency of 1 Hz using RSA III solids analyzer (Rheometric Scientific Co.) at a heating rate of 1 °C/min from 30 °C to 170 °C. Thermo-mechanical analyzer (TMA Q400, TA Instruments) was used to study the stress-temperature evolution in fibers under iso-strain mode. Differential scanning calorimetry (DSC; TA Instruments Q100) was conducted on all fibers in oxidative environment with an air flow of 50 mL/min and a heating rate of 5 °C/min from 30 °C to 400 °C. Scanning electron microscopy (SEM) was performed on a Zeiss Ultra 60 FE-SEM with an accelerating voltage of 3 kV. Raman spectra of carbon fibers were obtained in VV mode using a HORIBA Scientific Raman microscope system (Xplora, $\lambda = 785$ nm) at a laser power (10% power) of 5.6 mW with a 100x objective. Analysis of the Raman spectra was done by PeakFit software with Gaussian-Lorentzian curve fitting of D-band and G-band peaks.

5.3 RESULTS AND DISCUSSION

5.3.1 Precursor fiber processing and properties

Optical micrographs of the as-spun bi-component fibers (DR = 2) are shown in

Figure 5.2. When the sheath (PAN solution) and core (PAN/APL solution) components were extruded with low flow rate (0.4 cc/min each), the ratio between effective outer fiber radius to that of core radius (r_2/r_1) is ~1.10. When increase the sheath/core component flow rates to 0.5 cc/min and 0.6 cc/min (for both component), r_2/r_1 is then increased to ~1.25 and ~1.52, respectively. The fiber spinning flow rates, maximum draw ratios of control PAN fiber and bi-component fibers along the r_2/r_1 value and the derived overall lignin content of bi-component fibers are summarized in Table 5.1. Fabricated under the identical processing conditions, maximum draw ratio of 28 was achieved on single-component PAN fiber. With the most incorporation of lignin, the maximum draw ratio of BF-A fiber (Table 5.1, $r_2/r_1 \approx 1.10$) was then reduced to 16. This reduction in maximum draw ratio with the presence of lignin in PAN fiber agrees with our previous study of homopolymer PAN/APL blend, where 30 wt% APL loading can decrease the maximum fiber draw ratio from ≥ 20 to 13.[8] In the current investigation, when r_2/r_1 increases from ~1.1 to ~1.25 and ~1.52, the maximum draw ratio of bi-component fibers was improved from 16 to 18 and 20, respectively. This observation indicates that PAN sheath supports the integrity of PAN/APL core component during fiber drawing stage to achieve better fiber drawability.

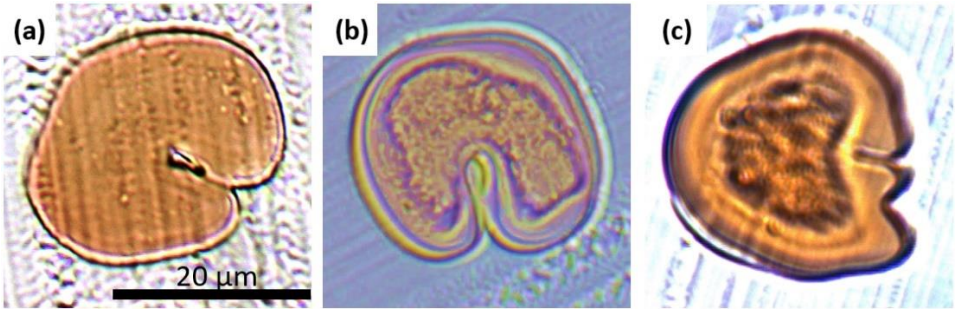

Figure 5.2. Optical micrographs of as-spun bi-component fiber cross sections of (a) BF-A (r_2/r_1 = 1.10), (b) BF-B (r_2/r_1 = 1.25), and (c) BF-C (r_2/r_1 = 1.52) fibers. Scale bar applies to all three images.

Table 5.1. Fiber spinning flow rate, fiber maximum draw ratio and derived diameter ratio

Fiber sample	PAN fiber	Bi-component fiber (BF)		
		BF-A_2	BF-B_2	BF-C_2
Flow rates (PAN : PAN/APL, cc/min)	1 : -	0.4 : 0.4	0.5: 0.5	0.6 : 0.6
Maximum draw ratio (DR)	28	15	17	20
r_2/r_1 of as-spun fiber, $_{DR=2}$	-	~1.10	~1.25	~1.52
Overall APL incorporation* (wt.%)	-	~31	~24	~16

*Calculated based on r_2/r_1

Structural parameters and mechanical properties of the fibers at a draw ratio of 10 are listed in Table 5.2. PAN fibers and bi-component fibers at various draw ratio are shown as PAN_{DR}, BF-A_{DR}, BF-B_{DR}, and BF-C_{DR}, respectively. At the same time, bi-component fibers exhibit lower crystallinity, PAN crystal size, and PAN crystal orientation compared to PAN control fiber at a draw ratio of 10. The lowered crystallinity, crystal size, and PAN crystal orientation imply that the presence of lignin affects PAN crystal ordering. Unsurprisingly, when compare the mechanical performance of PAN control fiber with bi-component fibers (Table 5.2) at draw ratio of 10, bi-component fibers consistently exhibit decreasing tensile strength and tensile modulus with increasing size of core component (decreasing r_2/r_1). These observations of the structural parameters and mechanical performance agrees with our previous report of homo-PAN/APL blend fibers at a maximum draw ratio of 13.[10] Optical microscopy images of the drawn PAN_{20} fiber, and bi-component fibers at the corresponding maximum draw ratio BF-A_{16}, BF-B_{18}, and BF-C_{20} cross section are shown in Figure 5.3. PAN_{20} fiber cross section exhibits a bean-like shape (Figure 5.3a). Interestingly, while the as-spun bi-component fibers all display a similar bean-like cross section (Figure 5.3), drawn bi-component fibers show various cross section shapes depending on the size of core component in fiber cross section. With increasing r_2/r_1 values, BF-A_{16}, BF-B_{18}, and BF-C_{20} are shown with cross sections of

irregular, bean-like, and polygon-like shapes, respectively. In addition, voids are observed in the draw fibers cross sections, where void content increases with increasing r_2/r_1 values of BF-B_{18} (Figure 5.3c, g) and BF-C_{20} fibers (Figure 5.3d, h) but not observed in PAN_{20} (PAN single component cross section) fiber, BF-A_{16} fiber (PAN/APL predominant cross section), nor the as-spun precursor fibers. These observations suggest that the during drawing processes (e.g., ambient and hot drawing stages), the PAN (sheath) and PAN/APL (core) components can experience non-uniform deformation and thus render the variant cross-sectional shapes depending on the r_2/r_1 value. Structural parameters and mechanical properties of PAN_{20} and the bi-component fibers BF-A_{16}, BF-B_{18}, and BF-C_{20} are summarized in Table 5.3. Despite the voids presented in BF-B_{18} and BF-C_{20} fibers, all bi-component fibers at the maximum draw ratios exhibit marginally improved tensile properties compared to PAN fiber at a draw ratio of 20 (PAN_{20}). P-value tests at a confidence limit of 95% was performed on the fiber tensile data using the JMP™ 13 software to determine the statistical significance of the comparison of precursor fiber properties (APPENDIX D.1). Similar structural parameters (e.g., PAN crystal size, crystallinity, and orientation) are observed among all fibers except for a slightly lower PAN crystal size of BF-A_{16} fiber. This suggests that under sufficient drawing (higher draw ratio), APL incorporation in blend does not affect the PAN crystal ordering or alignment.

Table 5.2. Fiber (total draw ratio = 10) mechanical properties and structural parameters

Fiber sample (SDR × CDR × HDR = 1 × 2 × 5)	PAN_{10} fiber	Bi-component fiber (BF)		
		BF-A_{10}	BF-B_{10}	BF-C_{10}
Effective diameter (μm)	19.8 ± 0.8	20.9 ± 0.6	20.6 ± 1.1	20.0 ± 1.6
Tensile strength (MPa)	759 ± 1.0	546 ± 42	591 ± 61	655 ± 103
Tensile modulus (GPa)	15.9 ± 0.5	12.7 ± 0.5	13.3 ± 0.9	14.0 ± 1.0
X_c[a] (%)	46	42	41	44
X_s[b] (nm)	9.8	9.3	9.1	9.4
f_{PAN}[c]	0.82	0.78	0.81	0.81

[a] PAN crystallinity.
[b] PAN crystallite size, calculated from PAN (2 0 0, 1 1 0) peak by Scherrer equation.
[c] Herman's orientation of PAN. Calculated from azimuthal scan of PAN (2 0 0), (1 1 0) planes.

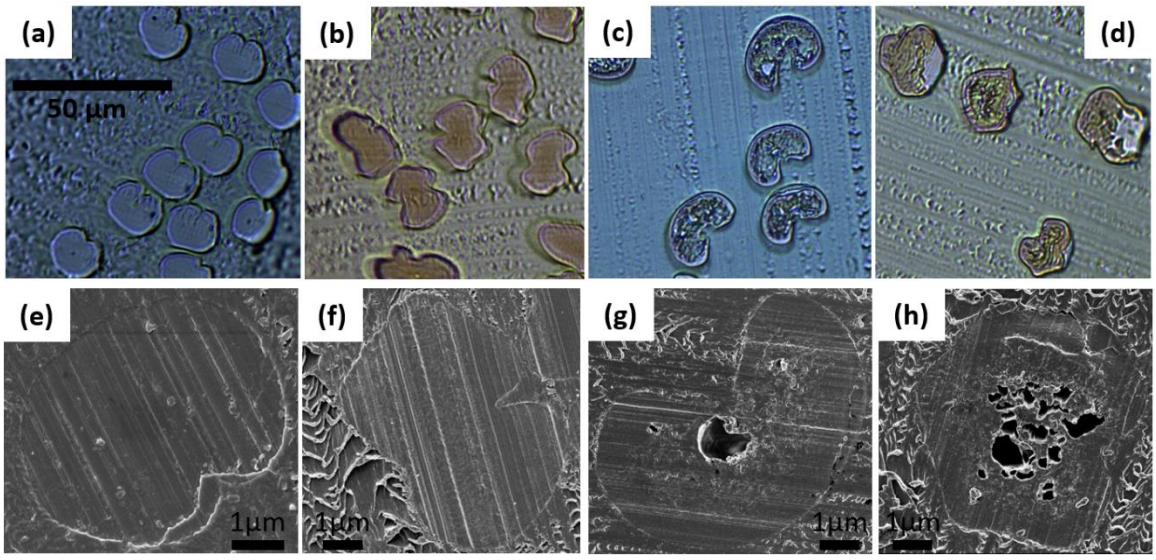

Figure 5.3. Optical microscopy images of (a) PAN_{20}, (b) BF-A_{16}, (c) BF-B_{18}, and (d) BF-C_{20} fiber cross sections, and the SEM images of (e) PAN_{20}, (f) BF-A_{16}, (g) BF-B_{18}, and (h) BF-C_{20} fibers cross sections. The scale bar in (a) applies to optical microscopy images (b), (c), and (d).

Table 5.3. Fibers (various draw ratios) mechanical properties and structural parameters

Fiber sample (SDR = 2, CDR = 1.5)	PAN_{20} fiber	Bi-component fiber (BF)		
		BF-A_{16}*	BF-B_{18}*	BF-C_{20}*
Effective diameter (µm)	14.4 ± 0.3	16.5 ± 0.8	15.8 ± 0.7	14.5 ± 0.8
Tensile strength (MPa)	753 ± 32	843 ± 64	849 ± 53	800 ± 59
Tensile modulus (GPa)	16.0 ± 0.3	17.3 ± 0.6	16.7 ± 0.6	17.8 ± 0.6
X_c[a] (%)	65	65	65	65
X_s[b] (nm)	10.6	9.9	10.8	10.6
f_{PAN}[c]	0.86	0.85	0.85	0.84

[a] PAN crystallinity.
[b] PAN crystallite size, calculated from PAN (2 0 0, 1 1 0) peak by Scherrer equation.
[c] Herman's orientation of PAN. Calculated from azimuthal scan of PAN (2 0 0), (1 1 0) planes.
[*] Maximum draw ratio.

To investigate the effect of PAN/APL core on dynamic mechanical performance of the fibers, storage moduli and tan δ values from DMA at 1 Hz of all fibers at the same draw ratio of 10 are shown in Figure 5.4. While all fibers display decreasing storage moduli with increasing temperature, PAN_{10} fiber exhibits higher storage modulus than all bi-component fibers over entire temperature range. Meanwhile, bi-component fiber storage moduli are

shown to reduce with decreasing r_2/r_1 (increasing APL incorporation in fiber cross section), which is consistent with the tensile moduli of DR=10 bi-component fibers determined from tensile testing. PAN tan δ peak around 90 °C (Figure 5.4b) is referred as the βc transition which describes the PAN molecular motion of helical sequences in the paracrystalline regions.[22-24] With the increasing APL incorporation (BF-A_{10} > BF-B_{10} > BF-C_{10}) in core component, bi-component fibers show increasing tan δ magnitudes and broadened widths compared to that of PAN fibers. The broadened tan δ peaks suggest that PAN molecular motions in the paracrystalline are less restricted, and the increasing tan δ magnitudes imply that PAN polymer chains might exhibit higher helical sequence and less planar zig-zag conformations with the presence of the APL in fiber.[10, 24]

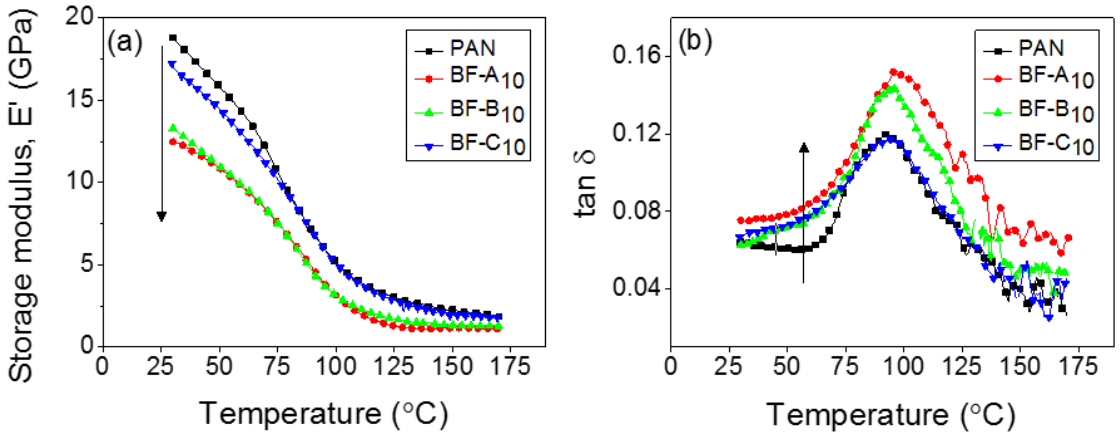

Figure 5.4. (a) Storage moduli, and (b) tan δ of PAN fiber and bi-component fibers from DMA at 1 Hz. Arrow direction indicates increasing lignin incorporation in the fiber cross section (decreasing r_2/r_1).

While WAXD and DMA results indicate that lignin incorporation affects the PAN structure in fibers, for bi-component fiber where the PAN sheath and PAN/APL core undergo simultaneous heat treatment and tension loading during carbon fiber fabrication, it is important to monitor the thermo-mechanical response of the sheath/core components

during processing. The stress-temperature evolution of PAN and bi-component fibers under iso-strain mode is then investigated by TMA. A constant pre-strain of 0.3% was applied on all fibers on a 10-filament bundle sample before fibers are heated from 25 °C to 175 °C and then cooled down from to 50 °C at a heating rate of 5 °C/min in air. A total of three heating-cooling cycles is applied in each trial. The stress evolution of fibers obtained from TMA is shown in Figure 5.5. For PAN fiber, stress development from thermal shrinkage is observed during the initial heating scan starting above 70 °C which corresponds to the entropic relaxation of polymer chains (Figure 5.5a)

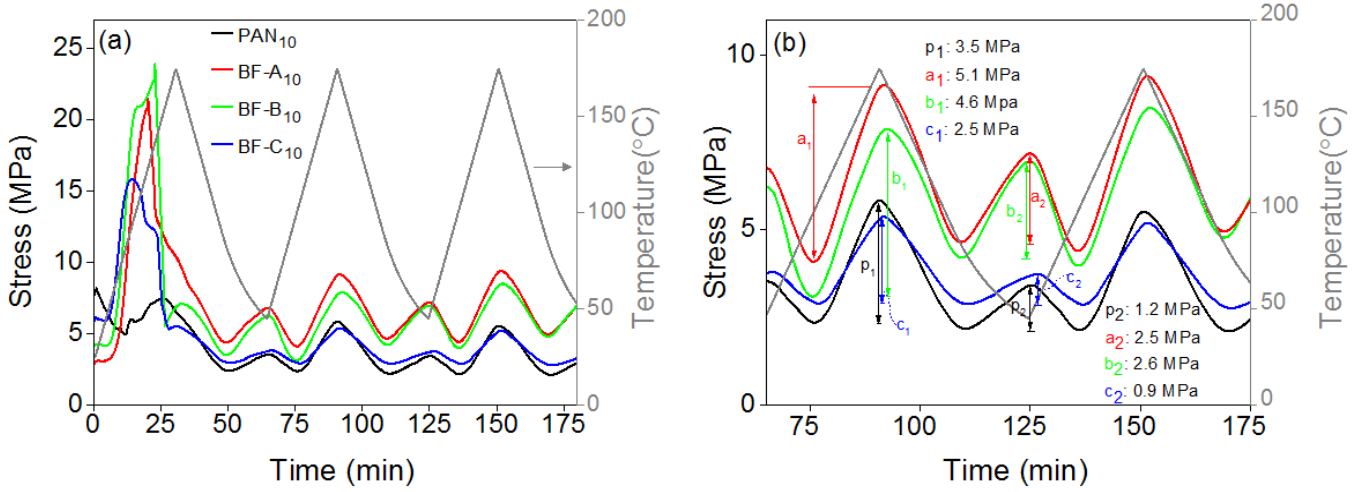

Figure 5.5. Stress development of PAN fiber and bi-component fibers under iso-strain mode (0.3 % pre-strain) from TMA (a), and the (b) stress-temperature evolutions of all fibers during the second and third heat scans.

When cooling is initiated after the initial heating scan, a reduction of stress is observed and thus renders a peak shrinkage stress around 7.5 MPa right before cooling process. Note that although the shrinkage stress peaks still form in the subsequent thermal scans, the magnitudes of shrinkage stress peak decrease in the second and the third heat treatment. This indicates an irreversible entropic relaxation process, attributed to the stretched

polymer chains recoil in the amorphous phase that results in permanent deformation during the first thermal scan.[25] With the incorporation of lignin in the core, bi-component fibers exhibit earlier onsets and significantly higher magnitude of entropic stress ranging from 15.8 – 22.9 MPa along with a more pronounced irreversible entropic relaxation when compared to PAN fiber. This suggests that APL incorporation promotes recoiling of stretched polymer chains in amorphous phase in the core component. Additionally, shoulder formation and broadening of entropic stress peaks are observed from bi-component fibers during stress evolution in the first heating scan, suggesting the sheath and core components may experience different entropic relaxation rates in the first heat scan. During the second or third heat scan, PAN_{10} fiber and bi-component fibers exhibit good thermal reversibility of shrinkage stresses upon heating and cooling, suggesting a more stable polymer structure. Unlike the shoulder formation during the first heat scan, no shoulders or multiple stress peaks were observed in the second and third heat scans, indicating the stress evolution rate gradients between the sheath/core components is now diminished, potentially due to crosslinking between the sheath and core component. Since PAN βc transition (~90 °C in the current study) is attributed to the molecular motions in the paracrystalline region, previous PAN iso-strain, thermo-mechanical study indicates that a minimum stress around PAN βc transition temperature can be used to distinguish PAN stress developments due to intrinsic thermal shrinkage/expansion (< 90 °C) or entropic stress (> 90 °C).[25] Stress-temperature evolutions of all fibers in the second and third scans are magnified and depicted in Figure 5.5b. Entropic stresses of PAN_{10}, BF-A_{10}, BF-B_{10}, BF-C_{10} fibers are denoted as p_1, a_1, b_1, and c_1 and the corresponding intrinsic thermal shrinkage stresses are symbolized as p_2, a_2, b_2, and c_2, respectively. For PAN fiber in the

second and third heat scan, the amplitude of entropic stress between 90 °C and 175 °C (p_1 in Figure 5.5b) is 3.5 MPa, and the magnitude of intrinsic thermal shrinkage stress (p_2) between 90 °C and 25 °C is 1.2 MPa. With the least lignin incorporation across the fiber cross section among bi-component fibers, BF-C_{10} ($r_2/r_1 \approx 1.52$) shows slightly decreased magnitude for both entropic stress (c_1: 2.5 MPa) and intrinsic thermal shrinkage stress (c_2: 0.9 MPa) compared to PAN fiber. With the increasing presence of lignin in the fiber cross section, BF-B_{10} ($r_2/r_1 \approx 1.25$) and BF-A_{10} ($r_2/r_1 \approx 1.10$) exhibit increasing entropic stresses (b_1: 4.6 MPa, a_1: 5.1 MPa) and intrinsic thermal shrinkage stresses (b_2: 2.6 MPa, a_2: 2.5 MPa) than those of PAN_{10} fiber. This result indicates that lignin incorporation in the PAN/APL component promotes both the intrinsic thermal shrinkage and the entropic force from the stretched polymer chains by inducing a more spring-like molecular structure.

To study the effect of PAN/APL core component on the PAN stabilization process, DSC thermograms of PAN_{10} fiber and bi-component fibers are shown in Figure 5.6. For PAN fiber, one major peak is observed around 263 °C along with subsequent subtle peak around 320 °C that can be attributed to the concurrent reactions of PAN cyclization, oxidation, and crosslinking reactions.[9, 26] With the incorporation of lignin in core component, bi-component fiber thermograms exhibit a broadening trend of the ~263 °C peak and an increasing evolution of the ~320 °C peak with increasing presence of lignin in the fiber cross section (decreasing r_2/r_1). In the current study, APL-containing fibers have exhibited increasing heat flow intensity than the single-component PAN_{10} (PAN-co-MAA) fibers. This is not observed in our previous observations on homopolymer PAN/APL blend and PAN-co-MAA/softwood lignin blend studies.[9-10] In addition, unlike the case of PAN fiber, the bi-component fiber heat flow intensity around ~320 °C has increased and even

surpassed the heat flow intensity of ~263 °C peak. Note that this phenomenon is more pronounced with the increasing radius of the core component (i.e. more lignin incorporation). This result which deviates from our previous observations on single-component homopolymer PAN/APL blend and PAN-co-MAA/softwood lignin blend studies[9-10] implies potential chemical interactions between the sheath/core components during thermal stabilization, and is also consistent to the previous TMA observation of potential crosslinking between the sheath/core component during heat treatment.

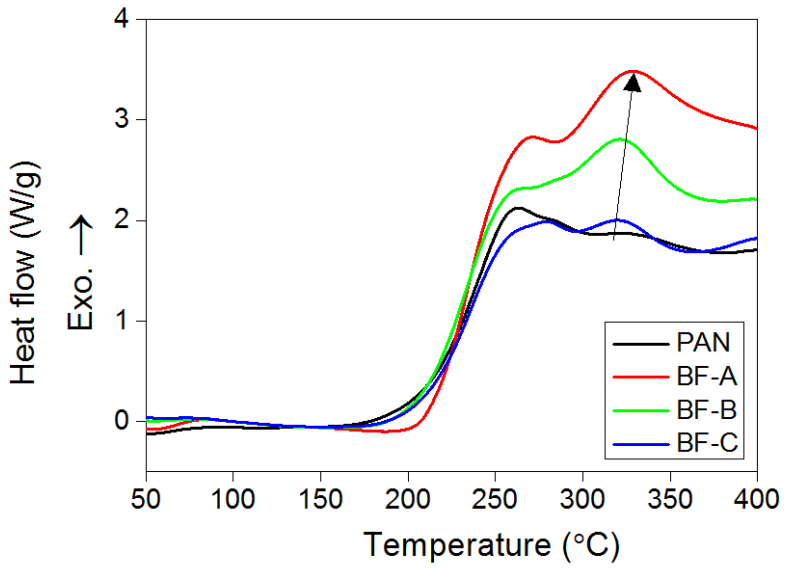

Figure 5.6. DSC thermograms of PAN fiber, and bi-component fibers in oxidative environment. (Air flow rate = 50 mL/min) Arrow direction indicates increasing lignin incorporation in the fiber cross section. (Decreasing r_2/r_1)

5.3.2 Carbon fibers

5.3.2.1 Thermal stabilization and carbon fiber morphology

Drawn fibers PAN_{20}, BF-A_{16}, and BF-C_{20} are stabilized by a batch process in oxidative environment at a constant air flow rate of 50 standard cubic feet per hour (SCFH) in a tube furnace manufactured by Micropyretics Heaters International (Cincinnati, OH). During the thermal stabilization process, a fixed heating rate (3 °C/min) and a two-stage (265 °C / 305 °C) heat treatment with various residence times was applied on fibers. Stabilized fibers then undergo carbonization process with a nitrogen flow rate of 75 SCFH and a fixed heating rate of 5 °C/min to 1,000 °C, 1,200 °C, and 1,300 °C, followed by a 10-minute isothermal residence time at the designated temperature to form carbon fibers. In both stabilization and carbonization process, a pre-stress calculated based on the precursor diameter is applied onto fiber bundles (typically 25-30 filaments) using weight assemblies by graphite or tungsten clamps and bolts. Total weight of each assembly installed on the precursor fibers is fixed during stabilization and carbonization process. Carbon fiber (carbonized at 1,000 °C) cross section SEM images of fibers PAN_{20}, BF-A_{16}, and BF-C_{20} are shown in Figure 5.7. Carbonized at 1,000 °C, PAN_{20}, and BF-A_{16}, carbon fibers show smooth fiber cross sections with no observable boundary between the sheath and core component of BF-A_{16} (Figure 5.7c). Interestingly, honeycomb-like, highly porous structure consists of carbon sheets along the fiber axis is observed in the core region of BF-C_{20} cross section (Figure 5.7d). It is also interesting that while voids in the core component is observable on the BF-C_{20} precursor fiber (Figure 5.3h), carbonized BF-C_{20} fiber exhibits

very distinct porous (honeycomb-like) morphology (Figure 5.7d) than the pores observed in the precursor fiber (Figure 5.3h).

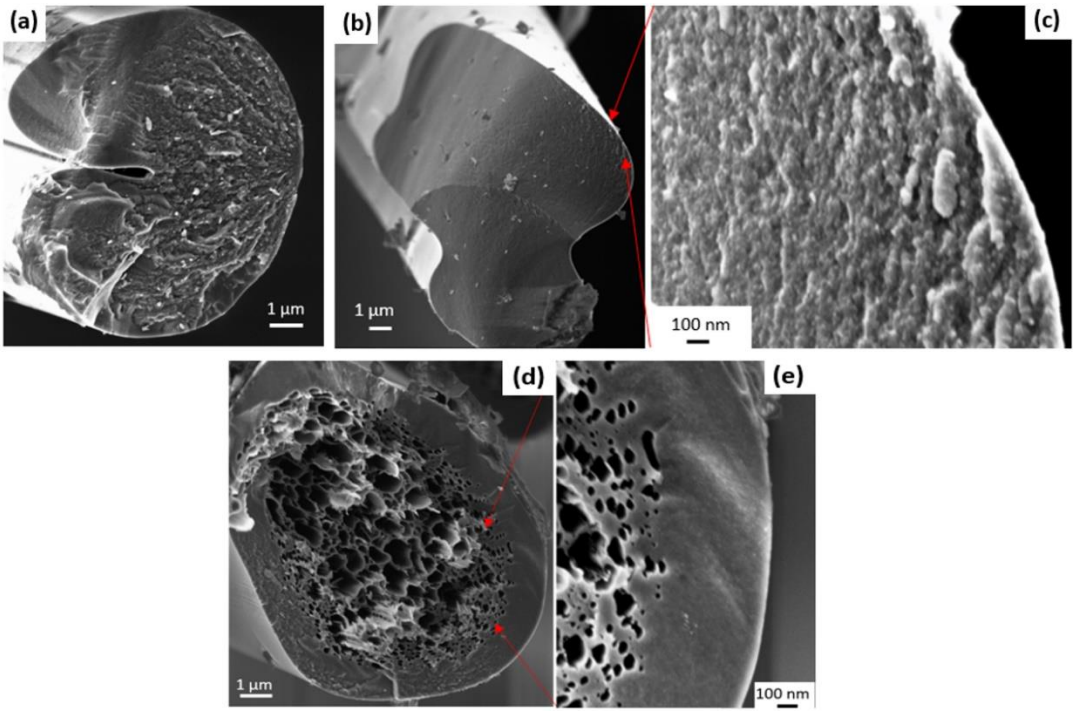

Figure 5.7. Carbon fiber (carbonized at 1000 °C) cross section images of PAN_{20} (a), BF-A_{16} (b), (c), and BF-C_{20} (d), (e).

Carbon fiber cross section SEM images of PAN_{20}, BF-A_{16}, and BF-C_{20} carbonized at 1200 °C and 1300 °C are shown in Figure 5.8. For PAN_{20} and BF-C_{20}, carbon fibers microstructures carbonized at 1200 °C and 1300 °C are similar to the carbon fiber microstructure carbonized at 1,000 °C (Figure 5.7). For BF-A_{16}, nano-scale particle-like microstructure emerges among the cross section of the fiber carbonized at 1,300 °C. (Figure 5.8e, h) While these nano-particles are not observed in the PAN_{20} and nor the porous BF-C_{20} carbon fibers, this suggests that PAN and APL in the core component of BF-A_{16} can

be forming distinct carbonaceous microstructure than PAN_{20} and BF-C_{20} carbon fibers. The SEM images of both BF-A_{16} precursor fibers and carbon fibers do not show a clear boundary of sheath and core component. (from Table 5.1). Using the image analysis software ImageJ, the cross-sectional porosity of BF-C_{20} carbon fiber at 1300 °C (Figure 5.8f) is approximately 24.2%. Example of porosity estimation is shown in APPENDIX D.2.

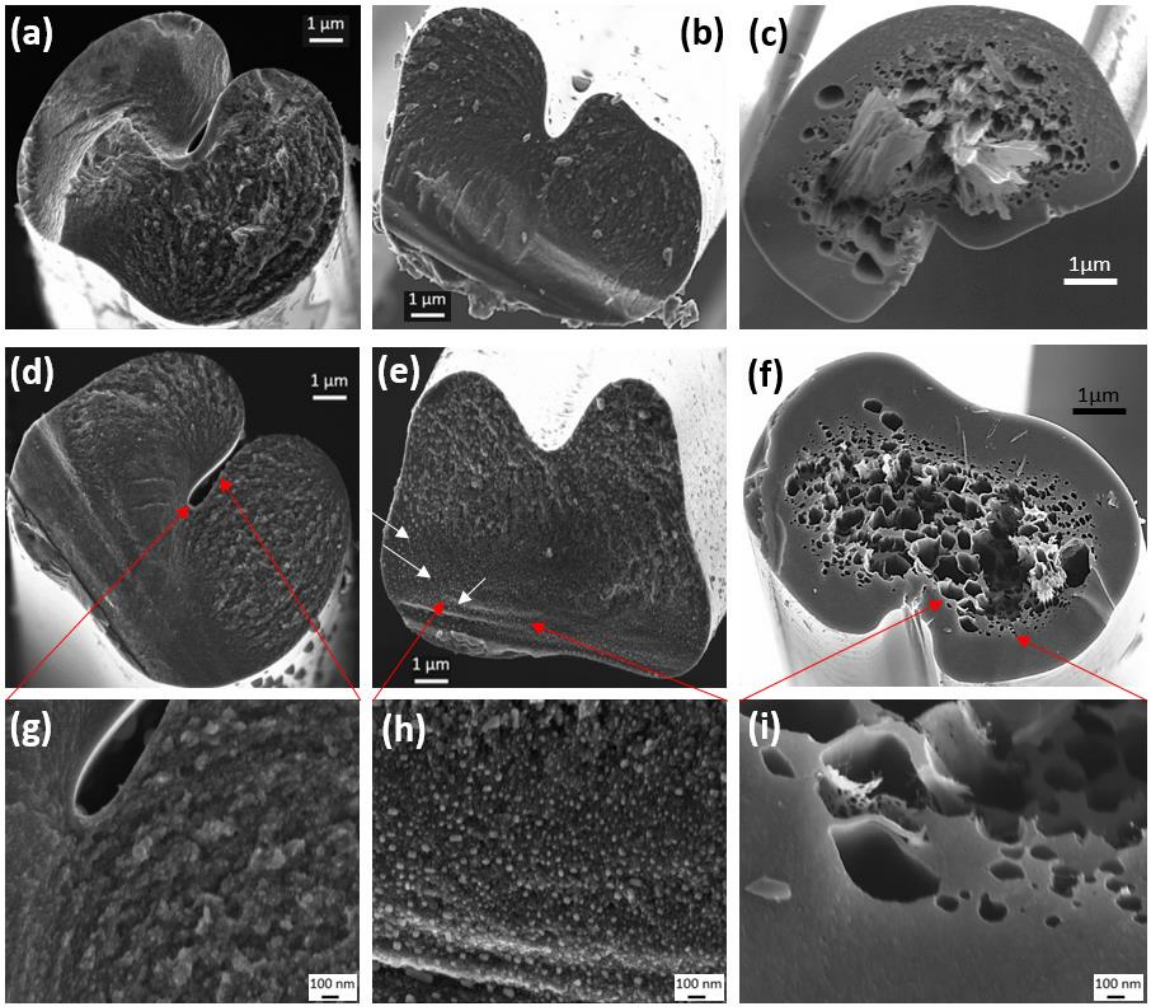

Figure 5.8. Carbon fiber cross section of (a) PAN_{20}, (b) BF-A_{16}, and (c) BF-C_{20} carbonized at 1200 °C, and (d) PAN_{20}, (e) BF-A_{16}, and (f) BF-C_{20} fibers carbonized at 1300 °C along with the magnified sections in (g), (h), and (i), respectively. White arrows on (e) indicates the emergence of the particle-like microstructure in (h).

5.3.2.2 Carbon fiber mechanical properties and structural parameters

When investigating the tensile properties of the carbon fibers, effective diameters of PAN_{20}, BF-A_{16} carbon fiber is determined from the single-filament linear density measurement, which was then used to evaluate the tensile strength, modulus, and elongation at break of each carbon fiber filament. For BF-C_{20} carbon fiber, the effective diameter is measured from the SEM micrographs of the carbon fibers using image-analysis software ImageJ. Due to the porous structure, BF-C_{20} tensile properties are measured by RSA-III solid analyzer (TA Instruments, Inc.)[27] For all carbon fiber tensile testing, a gauge length of 25.4 mm and a strain rate of 0.1%/s were used. Details of the fiber stabilization and carbonization and the tensile properties of the resultant carbon fibers are summarized in Table 5.4. For PAN_{20} and BF-A_{16} carbon fibers, increasing carbonization temperature from 1,000 °C to 1,300 °C enhances the PAN_{20} and BF-A_{16} carbon fiber tensile modulus from 233 ± 8 to 288 ± 9 GPa, and from 225 ± 6 to 274 ± 9 GPa, respectively. Between the carbonization temperature range of 1,000 °C and 1,300 °C, both PAN_{20} and BF-A_{16} carbon fibers exhibit the optimal tensile strength when carbonized at 1,200 °C, rendering a tensile strength of 2.47 ± 0.33 GPa, and 2.11 ± 0.30 GPa, respectively. Limited to the porous internal structure, BF-C_{20} carbon fiber (carbonized at 1300 °C) exhibits relatively low tensile strength and tensile modulus of 910 ± 240 MPa and 242 ± 15 GPa, respectively, when compared to the PAN_{20} and BF-A_{16} carbon fibers. P-value tests at a confidence limit of 95% was performed on the carbon fiber tensile data using the JMP™ 13 software to determine the statistical significance of the compared carbon fiber properties (APPENDIX D.1).

Table 5.4. Carbon fiber stabilization/carbonization conditions and tensile properties

Sample¤	Stabilization scheme† (°C – min -°C - min)	Applied tension‡ (MPa)	Carbonization temp. (°C)	Effective diam.(μm)	Strain at break (%)	Tensile strength (GPa)	Tensile modulus (GPa)
PAN_{20}-1	266-158-305-10	40*	1000	8.5 ± 0.2	0.99 ± 0.23	2.33 ± 0.58	241 ± 4
PAN_{20}-2	266-158-305-10	30	1000	8.9 ± 0.3	0.95 ± 0.12	2.13 ± 0.29	230 ± 4
PAN_{20}-3	266-170-305-10	30	1000	9.1 ± 0.4	1.01 ± 0.17	2.32 ± 0.43	233 ± 8
PAN_{20}-4	266-182-305-10	30	1000	9.0 ± 0.2	0.90 ± 0.18	2.01 ± 0.43	229 ± 7
PAN_{20}-5	266-170-305-10	30	1200	8.4 ± 0.2	0.90 ± 0.13	2.42 ± 0.37	276 ± 6
PAN_{20}-6	266-170-305-10	37	1200	8.3 ± 0.2	0.91 ± 0.11	2.47 ± 0.33	280 ± 4
PAN_{20}-7	266-170-305-10	30	1300	8.2 ± 0.2	0.79 ± 0.10	2.08 ± 0.29	288 ± 9
BF-A_{16}-1	266-230-305-10	22	1000	9.7 ± 0.6	0.76 ± 0.17	1.60 ± 0.37	211 ± 9
BF-A_{16}-2	266-230-305-10	30	1000	9.7 ± 0.5	0.75 ± 0.11	1.64 ± 0.23	225 ± 6
BF-A_{16}-3	266-255-305-10	22	1000	9.4 ± 0.6	0.84 ± 0.16	1.80 ± 0.36	216 ± 4
BF-A_{16}-4	266-255-305-10	30	1000	9.3 ± 0.6	0.78 ± 0.19	1.70 ± 0.43	220 ± 7
BF-A_{16}-5	266-255-305-10	27	1200	9.0 ± 0.5	0.79 ± 0.11	1.94 ± 0.23	254 ± 7
BF-A_{16}-6	266-255-305-10	30	1200	8.9 ± 0.6	0.84 ± 0.11	2.11 ± 0.30	260 ± 5
BF-A_{16}-7	266-255-305-10	30	1300	8.7 ± 0.7	0.71 ± 0.07	1.81 ± 0.25	274 ± 10
BF-C_{20}-1	266-170-305-10	22.5	1300	9.6 ± 0.6§	0.50 ± 0.06	0.91 ± 0.24	242 ± 25
Zoltek[8] PAN/Lignin (65/35)	N/A	-	-	-	0.76	1.68	201
Zoltek[11] PAN/Lignin (75/25)	N/A	-	-	-	1.0 ± 0.1	2.24 ± 0.34	217 ± 15

¤ PAN_{20}, BF-A_{16}, and BF-C_{20} carbon fibers are batched processed and tensile properties were reported without compliance correction. Zoltek carbon fiber are continuously processed.
† Stabilization and carbonization heating rates are 3 °C/min and 5 °C/min, respectively.
‡ Stress calculated according to precursor diameter.
§ About 24.2% cross-sectional porosity.
* fiber bundle broken when unload.

Carbon fiber structural parameters of PAN_{20} (trials PAN_{20}-4, 5, and 7), BF-A_{16} (trials BF-A_{16}-4, 6, and 7), and BF-C_{20} carbon fibers at 1,000 °C, 1,200 °C, and 1,300 °C are included in Table 5.5. For all carbon fibers, increasing carbonization temperature results in increasing crystal sizes ($L_{2\theta \approx 26^\circ}$ and $L_{2\theta \approx 43^\circ}$), and improved carbonized turbostratic plane orientation (f_{002}). Note that BF-C_{20} carbon fiber exhibits a significantly less orientated turbostratic carbon plane at 1,000 °C yet only a moderately lower orientation of the carbonized plane at 1,300 °C when compared to PAN_{20} and BF-A_{16} carbon fibers. This suggests that BF-C_{20} carbon fibers can undergo a more vigorous ordering process of turbostratic carbon plane than PAN_{20} and BF-A_{16} when carbonized at 1,200 and 1,300 °C. A possible explanation for the observation is that while the voids existence (and possible propagation) in BF-C_{20} fibers during lower temperature (1,000 °C) carbonization can be interfering the turbostratic structure formation along the fiber axis, the effect is less prominent towards the later carbonaceous structural reordering stage at increasing carbonization temperatures. Raman spectroscopy is a useful technique to characterize and interpret the structural features of various forms of carbons, e.g., ordered, graphite-like, carbon crystallites, and disordered, amorphous, diamond-like carbons.[28-30] Raman spectra collected on the carbon fibers listed in the Table 5.5. are shown in Figure 5.9, where the Raman D-band peak (~1360 cm^{-1}) is the disorder-induced peak due to the breathing mode of the sp^2 carbons.[31-32] The G-band peak (~1580 cm^{-1}), due to the bond stretching of sp^2 carbons in rings and chains, is a signature peak arises from an ordered, graphitic structure.[33] For PAN_{20}, BF-A_{16}, and BF-C_{20} carbon fibers, a more developed G-band peak is observed at increasing carbonization temperature, which agrees with the increasing size of carbon crystallites from the structural parameters (Table 5.5). Additionally, when carbonization

temperature is increased from 1,000 °C to 1,300 °C, all fibers exhibit a narrowing D-band FWHM (Figure 5.10a) that indicates a reordering process of poly-aromatic carbons. This narrowing D-band FWHM is especially pronounced for BF-C_{20} carbon fibers (Figure 5.10a), agrees with the previous discussion of more vigorous turbostratic carbon plane ordering process for BF-C_{20} carbon fibers carbonized at 1,200 °C to 1,300 °C. For G-band FWHM of carbon fibers (Figure 5.10b), PAN_{20}, and BF-A_{16} show a decreasing G-band FWHM when carbonization temperature is increased to 1,300 °C, indicating a more refined graphitic structure of the carbon fibers. As for BF-C_{20} carbon fibers, a relatively unchanged G-band FWHM is observed throughout the entire carbonization temperature range, implying that the porous morphology can be limiting the graphitic structure refining process within the temperature range.

Table 5.5. Carbon fiber structural parameters

Carbon fiber	PAN_{20}			BF-A_{16}			BF-C_{20}		
Carbonization temp.(°C)	1000	1200	1300	1000	1200	1300	1000	1200	1300
$L_{2\theta \approx 26°}$ [a] (nm)	1.4	1.6	1.8	1.3	1.7	1.8	1.2	1.5	1.7
$L_{2\theta \approx 43°}$ [b] (nm)	1.8	1.9	2.0	1.7	1.8	1.9	1.6	1.8	1.9
f_{002} [c]	0.68	0.78	0.81	0.68	0.76	0.81	0.63	0.73	0.78
Z_{002} [d] (deg)	30.08	27.46	26.15	30.04	28.49	27.17	32.95	29.68	28.33

[a] crystal size at $2\theta \approx 26°$, calculated according to Scherrer's equation with K= 0.9.
[b] crystal size at $2\theta \approx 43°$, calculated according to Scherrer's equation with K= 0.9.
[c] orientation factor of carbonized turbostratic (002) plane.
[d] full-width at half maximum (FWHM) from the azimuthal scan of the carbonized turbostratic (002) plane.

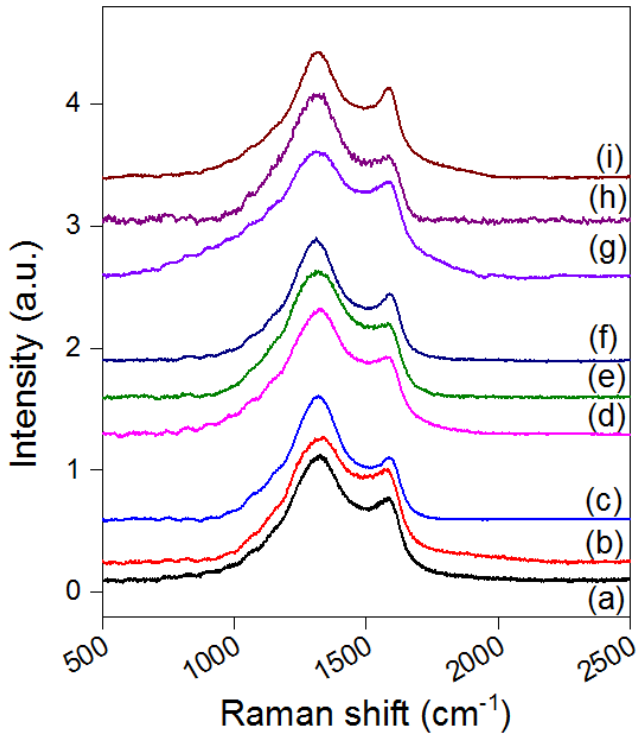

Figure 5.9. Raman spectra of PAN_{20} carbon fibers at 1000 °C (a), 1200 °C (b), 1300 °C (c), and BF-A_{16} carbon fibers at 1000 °C (d), 1200 °C (e), 1300 °C (f), and BF-C_{20} carbon fibers at 1000 °C (g), 1200 °C (g), 1300 °C (i). Spectra are normalized to D-band peak and upshifted for clarity.

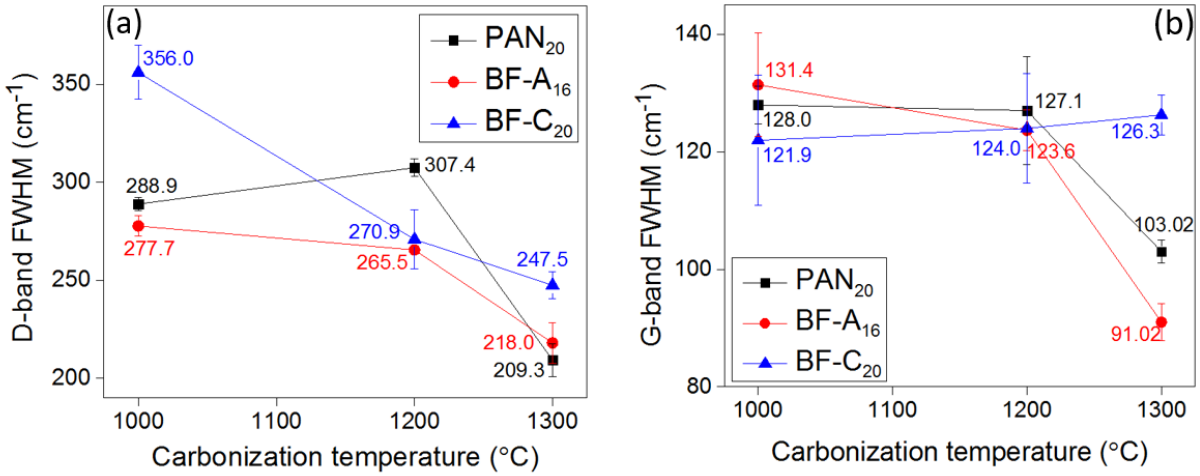

Figure 5.10. (a) D-band peak FWHM, and (b) G-band peak FWHM of carbon fibers carbonized at various temperatures.

5.4 CONCLUSIONS

In this study, the processing and properties of PAN sheath, PAN/APL core bi-component fibers and derived carbon fibers are reported. During the fiber spinning process, increasing flow rates of sheath : core components from 0.4 : 0.4, 0.5 : 0.5, to 0.6 : 0.6 c.c./min results in increasing ratios of overall fiber radius to core-component radius (r_2/r_1) of ~1.10 (BF-A fiber), ~1.25 (BF-B fiber), and ~1.52 (BF-C fiber), respectively. Fibers with higher r_2/r_1 values render higher drawability. At maximum draw ratio, BF-A_{16} (draw ratio 16), BF-B_{18} (draw ratio 18), and BF-C_{20} (draw ratio 20) fiber show comparable tensile properties to PAN_{20} fiber (draw ratio 20) though BF-B_{18} and BF-C_{20} fiber exhibit voids in the fiber cross sections. However, these voids are not observed in the BF-B and BF-C as-spun fibers. TMA results suggests that lignin induces a more spring-like molecular structure and promotes both the intrinsic thermal shrinkage and the entropic force from the stretched polymer chains. DSC and TMA analysis of the PAN and bi-component fibers suggest possible crosslinking between the sheath and core component. PAN_{20}, BF-A_{16}, and BF-C_{20} fibers are stabilized and carbonized by batch process at 1,000 to 1,300 °C. BF-A_{16} carbon fiber, with an effective lignin content ~31 wt.%, exhibits a tensile strength and a tensile modulus around 2.1 GPa, and 260 GPa, respectively, when carbonized at 1,200 °C. When carbonized at 1300 °C, the tensile modulus of BF-A_{16} carbon fiber is increased to 274 GPa. PAN_{20} carbon fiber exhibits respective tensile strength and modulus of 2.42 GPa and 276 GPa when carbonized at 1,200 °C, and the tensile modulus can be further increased to 288 GPa when carbonized at 1,300 °C. When carbonized at 1,300 °C, BF-C_{20} carbon fiber exhibits a tensile modulus around 242 GPa and a relatively low (0.91 GPa) tensile

strength due to the limitation of around 24.2% porosity in the fiber cross sections. This serves as a potential approach to fabricate low-density PAN/APL carbon fibers.

5.5 REFERENCES

[1]. Husman, G. In *Development and Commercialization of a Novel Low-Cost Carbon Fiber*, Presentation at 2014 DOE Hydrogen and Fuel Cells Program and Vehicle Technologies Office Annual Merit Review and Peer Evaluation Meeting, **2014**.

[2]. Husman, G. In *Development and Commercialization of a Novel Low-cost Carbon Fiber*, Presentation at 2012 DOE Hydrogen and Fuel Cells Program and Vehicle Technologies Program Annual Merit Review and Peer Evaluation Meeting, **2012**.

[3]. Chae, H. G.; Newcomb, B. A.; Gulgunje, P. V.; Liu, Y.; Gupta, K. K.; Kamath, M. G.; Lyons, K. M.; Ghoshal, S.; Pramanik, C.; Giannuzzi, L.; Şahin, K.; Chasiotis, I.; Kumar, S., High Strength and High Modulus Carbon Fibers. *Carbon* **2015,** *93*, 81-87.

[4]. Baker, D. A.; Rials, T. G., Recent Advances in Low-Cost Carbon Fiber Manufacture from Lignin. *Journal of Applied Polymer Science* **2013,** *130* (2), 713-728.

[5]. Liu, Y.; Kumar, S., Recent Progress in Fabrication, Structure, and Properties of Carbon Fibers. *Polymer Reviews* **2012,** *52* (3-4), 234-258.

[6]. Naskar, A. K.; Hunt, M. A.; Saito, T., Method for the preparation of carbon fiber from polyolefin fiber precursor, and carbon fibers made thereby. U.S. Patents 9096955: **2015**.

[7]. Ragauskas, A. J.; Beckham, G. T.; Biddy, M. J.; Chandra, R.; Chen, F.; Davis, M. F.; Davison, B. H.; Dixon, R. A.; Gilna, P.; Keller, M.; Langan, P.; Naskar, A. K.; Saddler, J. N.; Tschaplinski, T. J.; Tuskan, G. A.; Wyman, C. E., Lignin Valorization: Improving Lignin Processing in the Biorefinery. *Science* **2014,** *344* (6185).

[8]. Otani, S.; Fukuoka, Y.; Igarashi, B.; Sasaki, K., Method for Producing Carbonized Lignin Fiber. U.S. Patents 3461082: **1969**.

[9]. Liu, H. C.; Chien, A. T.; Newcomb, B. A.; Bakhtiary Davijani, A. A.; Kumar, S., Stabilization Kinetics of Gel Spun Polyacrylonitrile/lignin Blend Fiber. *Carbon* **2016,** *101*, 382-389.

[10]. Liu, H. C.; Chien, A. T.; Newcomb, B. A.; Liu, Y.; Kumar, S., Processing, Structure, and Properties of Lignin- and CNT-Incorporated Polyacrylonitrile-Based Carbon Fibers. *ACS Sustainable Chemistry & Engineering* **2015,** *3* (9), 1943-1954.

[11]. Dong, X.; Lu, C.; Zhou, P.; Zhang, S.; Wang, L.; Li, D., Polyacrylonitrile/lignin Sulfonate Blend Fiber for Low-cost Carbon Fiber. *RSC Advances* **2015,** *5* (53), 42259-42265.

[12]. Ding, R.; Wu, H.; Thunga, M.; Bowler, N.; Kessler, M. R., Processing and Characterization of Low-cost Electrospun Carbon Fibers from Organosolv Lignin/Polyacrylonitrile Blends. *Carbon* **2016,** *100*, 126-136.

[13]. Husman, G. In *Development and Commercialization of a Novel Low-Cost Carbon Fiber*, 2013 DOE Hydrogen and Fuel Cells Program and Vehicle Technologies Program Annual Merit Review and Peer Evaluation Meeting, **2013**.

[14]. Tagawa, T.; Miyata, T., Size Effect on Tensile Strength of Carbon Fibers. *Materials Science and Engineering: A* **1997,** *238* (2), 336-342.

[15]. Nicoll, A. R.; Perry, A. J., Diameter Dependence of Carbon Fibre Mechanical Properties. *Fibre Science and Technology* **1973,** *6* (2), 135-139.

[16]. Kikutani, T.; Radhakrishnan, J.; Arikawa, S.; Takaku, A.; Okui, N.; Jin, X.; Niwa, F.; Kudo, Y., High-speed Melt Spinning of Bicomponent Fibers: Mechanism of Fiber Structure Development in Poly(ethylene terephthalate)/Polypropylene System. *Journal of Applied Polymer Science* **1996,** *62* (11), 1913-1924.

[17]. Shi, X. Q.; Ito, H.; Kikutani, T., Structure Development and Properties of High-speed Melt spun Poly(butylene terephthalate)/Poly(butylene adipate-co-terephthalate) Bicomponent Fibers. *Polymer* **2006,** *47* (2), 611-616.

[18]. Radhakrishnan, J.; Ito, H.; Kikutani, T.; Okui, N., Enhancement of Fiber Structure Formation of a Liquid Crystalline Copolyester via Ultra-high Speed Bicomponent Spinning with Poly(ethylene terephthalate). *Polymer Engineering & Science* **1999,** *39* (1), 89-98.

[19]. Jeffries, R., *Bicomponent Fibres*. Merrow Publishing Company Limited: U.K., **1971**.

[20]. Chae, H. G.; Choi, Y. H.; Minus, M. L.; Kumar, S., Carbon Nanotube Reinforced Small Diameter Polyacrylonitrile Based Carbon Fiber. *Composites Science and Technology* **2009,** *69* (3-4), 406-413.

[21]. Chien, A.; Gulgunje, P. V.; Chae, H. G.; Joshi, A. S.; Moon, J.; Feng, B.; Peterson, G. P.; Kumar, S., Functional polymer–polymer/carbon nanotube bi-component fibers. *Polymer* **2013,** *54* (22), 6210-6217.

[22]. Chae, H. G.; Minus, M. L.; Kumar, S., Oriented and Exfoliated Single Wall Carbon Nanotubes in Polyacrylonitrile. *Polymer* **2006,** *47* (10), 3494-3504.

[23]. Liu, Y.; Choi, Y. H.; Chae, H. G.; Gulgunje, P. V.; Kumar, S., Temperature Dependent Tensile behavior of Gel-spun Polyacrylonitrile and Polyacrylonitrile/Carbon Nanotube Composite Fibers. *Polymer* **2013,** *54* (15), 4003-4009.

[24]. Sawai, D.; Kanamoto, T.; Yamazaki, H.; Hisatani, K., Dynamic Mechanical Relaxations in Poly(acrylonitrile) with Different Stereoregularities. *Macromolecules* **2004,** *37* (8), 2839-2846.

[25]. Liu, Y.; Chae, H. G.; Kumar, S., Gel-spun Carbon Nanotubes/Polyacrylonitrile Composite Fibers. Part I: Effect of Carbon Nanotubes on Stabilization. *Carbon* **2011,** *49*, 4466-4476.

[26]. Liu, Y.; Chae, H. G.; Kumar, S., Gel-spun Carbon Nanotubes/Polyacrylonitrile Composite Fibers. Part II: Stabilization Reaction Kinetics and Effect of Gas Environment. *Carbon* **2011,** *49*, 4477-4486.

[27]. Gulgunje, P. V.; Newcomb, B. A.; Gupta, K.; Chae, H. G.; Tsotsis, T. K.; Kumar, S., Low-density and High-modulus Carbon Fibers from Polyacrylonitrile with Honeycomb Structure. *Carbon* **2015,** *95*, 710-714.

[28]. Tanaka, F.; Okabe, T.; Okuda, H.; Ise, M.; Kinloch, I. A.; Mori, T.; Young, R. J., The effect of nanostructure upon the deformation micromechanics of carbon fibres. *Carbon* **2013,** *52*, 372-378.

[29]. Ferrari, A. C. R., J., Raman Spectroscopy of Amorphous, Nanostructured, Diamond–like Carbon, and Nanodiamond. *Philosophical Transactions of the Royal Society of London. Series A: Mathematical, Physical and Engineering Sciences* **2004,** *362* (1824), 2477-2512.

[30]. Ferrari, A. C., Raman Spectroscopy of Graphene and Graphite: Disorder, Electron-phonon Coupling, Doping and Nonadiabatic Effects. *Solid State Communications* **2007,** *143* (1), 47-57.

[31]. Ferrari, A. C.; Robertson, J., Resonant Raman Spectroscopy of Disordered, Amorphous, and Diamondlike Carbon. *Physical Review B (Condensed Matter and Materials Physics)* **2001,** *64* (7), 075414/1-13.

[32]. Heremans, J.; Rahim, I.; Dresselhaus, M. S., Thermal conductivity and Raman spectra of carbon fibers. *Physical Review B* **1985,** *32* (10), 6742-6747.

[33]. Ferrari, A. C.; Robertson, J., Interpretation of Raman Spectra of Disordered and Amorphous Carbon. *Physical Review B (Condensed Matter)* **2000,** *61* (20), 14095-14107.

CHAPTER 6

CONCLUSIONS AND RECOMMENDATIONS

6.1 CONCLUSIONS

This research systematically investigates on the lignin/polyacrylonitrile (PAN) blends in solution, the fiber structure, and during the thermal stabilization and carbonization process to valorize biorefinery waste lignin for its potential in the green manufacturing and renewability of carbon fibers.

This dynamic shear rheology study of PAN with lignin content up to 37.5 wt.% in solutions reports the potential boundary conditions for lignin incorporation and characterizes the interactions of PAN and lignin with respect to fiber processing. The miscibility of PAN and lignin in solutions are confirmed through a constant (temperature/composition independent) slope value of log G' versus log G" curves (Han plot) for solutions with lignin incorporation up to 37.5 wt% between a temperature range of -7 °C to 56 °C. Findings show that increasing the incorporation of lignin in PAN solution promotes a fluid-solid transition during the quenching process under an oscillatory shear frequency of 100 rad/s, suggesting that possibility that lignin promotes a coagulation mechanism during the fiber spinning process. In addition, lignin incorporation into PAN solution reduces solution viscosity, yield stress, relaxation time, and thermo-reversibility.

The rheology findings along with gel spinning technology have been successfully leveraged to address the un-favored porous structure of PAN/lignin blends reported in the literature. In the thermal stabilization process, a critical step in carbon fiber conversion,

lignin was shown to reduce PAN cyclization, oxidation, and crosslinking reaction activation energies and to increase the corresponding reaction rates, rendering a potential for reducing time and energy consumption during carbon fiber manufacturing.

Single-component, pore-free PAN/lignin and PAN/lignin/carbon nanotube (CNT)-blend fibers as well as PAN-sheath and PAN/lignin-core bi-component fiber are successfully processed (Chapter 3, 4, and 5). Overall, the presence of lignin in the spinning dope reduces the fiber maximum draw ratio and affects PAN polymer chain packing in the precursor fiber. With the presence of CNT, the PAN/lignin/CNT fiber exhibits a more tightly packed molecular structure with an improved crystalline structure than PAN/lignin fibers. Raman spectroscopy of PAN, PAN/lignin, and PAN/lignin/CNT carbon fibers indicates that the carbon fiber structure reordering process is altered by the incorporation of lignin, and the presence of CNT in PAN/lignin/CNT carbon fibers can promote structural reordering. Single-component PAN, PAN/lignin, and PAN/lignin/CNT carbon fibers exhibit a tensile strength of 1.60 GPa, 1.72 GPa, and 1.40 GPa, and a tensile modulus of 223 GPa, 230 GPa, and 220 GPa, respectively.

Since fibers fabricated with a higher draw ratio can render a smaller diameter to reduce the number of defects per unit volume in the fiber structure, the decrease in the maximum draw ratio limits improvements in derived carbon fiber mechanical properties. With the aid of bi-component fiber spinning, the PAN sheath provides more and more protection and endurance of fibers as it approaches higher draw ratios. With the incorporation of ≥ 30 wt.% of lignin, batch-processed PAN/lignin carbon fibers exhibit a tensile strength of 2.11 GPa and a tensile modulus of 260 GPa, exceeding the low-cost carbon fiber performance target (1.72 GPa, 172 GPa) set by the U.S. Department of Energy

and the best PAN/APL carbon fiber mechanical performance reported in the literature to date. At higher carbonization temperature (1300 °C), the PAN/lignin carbon fiber exhibits a tensile modulus value as high as 274 GPa. With proper processing parameters, the PAN sheath, and PAN/APL core bi-component carbon fibers with a porous core (translates to ~24% overall porosity) can be manufactured as an approach for low-density carbon fibers.

6.2 RECOMMENDATIONS FOR FUTURE STUDY

1. Results of the current study of PAN and PAN/lignin blends showed a reduction in maximum draw ratios for the lignin-containing fibers, which can be attributed to (1) a more aggravated liquid-solid transition during quenching that affects the gel-state processing window, and (2) a reduced thermo-reversibility of the lignin-containing dopes affecting the viscoelasticity of the fiber during the subsequent drawing stages. As the mechanical performance of the precursor fiber and the resultant carbon fiber depends on the molecular structure of the fiber, which rearranges during fiber processing stages, further instrumental investigation of optimal gel-state processing parameters (e.g., optimal air gap length, air gap temperature, and coagulation temperature/duration) of PAN/lignin systems that optimize the properties of PAN/lignin blend carbon fibers are recommended.
2. In the industrial carbon fiber manufacturing process, fibers undergo step-wise temperature zones with various applied tensions in continuous production. Previous PAN stabilization studies have reported the reaction kinetics at various stabilization temperatures and residence time; however, little success have been observed to address the relationship between applied tensions on fibers and the stabilization reaction

kinetics. In the current study of stabilization kinetics of PAN/lignin blend, a relationship between the reaction kinetics, thermo-calorimetry, and a reaction-specific (cyclization) chemical shrinkage is established. Since the relationship proposed in the current study can monitor the reaction kinetics in response to various applied tensions and temperatures in parallel to the thermo-calorimetry results, it is recommended that a future kinetic study account for this relationship in an examination of the optimal processing parameters in the industrial PAN carbon fiber manufacturing process.

3. Raman spectroscopy analysis of PAN and PAN/lignin carbon fibers (Chapter 4) indicated different polyaromatic reordering process of PAN and lignin during carbonization. In Chapter 5, the cross-sectional SEM images of the BF-A_{16} carbon fiber (effective lignin content ~31 wt.%) showed the emergence of a nanoscale, particle-like microstructure for fibers carbonized at 1,300 °C. Note that the nanoscale, particle-like microstructure is not observed in neither the PAN carbon fiber nor the BF-A_{16} fibers carbonized at 1,000 °C and 1,200 °C. These results suggest that the graphitic structures of PAN/lignin blends differ from those of PAN-based carbon fibers. Further TEM analysis, Raman spectroscopy mapping of the cross-sectional graphitic structures of PAN and PAN/lignin carbon fibers, and the potential graphitization studies of the PAN/lignin blends are recommended.

4. The study found that fiber cross-sectional shapes (i.e., cross-section circularity) are related to molecular structure, which can affect the turbostratic crystalline orientation and mechanical properties of the resultant carbon fibers. Chapters 4 and 5 reported bean-shaped cross sections of the PAN precursor and carbon fibers. However, the cross section of the single-component (Chapter 4) PAN/lignin (APL) blend fibers exhibited

better circularity than the PAN fiber. In addition, the cross-sectional shapes of bi-component PAN/lignin blends (Chapter 5) differed, depending the size of the PAN/lignin core component. These observations of various cross-sectional shapes of fibers suggest that lignin incorporation contributes to the diffusion and coagulation mechanisms during the fiber manufacturing process. To further optimize the PAN/lignin blend carbon fiber properties, a root-cause analysis of the varying cross-sectional shapes on PAN-sheath and PAN/lignin-core bi-component fibers are recommended.

5. To further create value-added applications for the lignin-derived renewable carbons, APPENDIX E presents a study titled “Lignin-Derived High Surface Area Carbon.” Using sacrificial polymers to fabricate polymer/liginn blend film, the study showed that resultant carbons exhibit appproximately four to five times as high surface area values as the control samples. Further optimization of the system is recommended.

APPENDIX A

COMMERCIAL CARBON FIBER MECHANICAL PROPERTIES

Table A.1. Mechanical properties of commercial PAN based carbon fiber

PAN based carbon fiber (Source, Product)		Tensile strength (GPa)	Tensile modulus (GPa)
Toray	T300	3.53	230
	T400H	4.41	250
	T700S	4.9	230
	T700G	4.9	240
	T1000	6.37	294
	T1100G	6.6	324
	M35J	4.71	344
	M40	2.74	392
	M40J	4.41	377
	M46J	4.21	436
	M50J	4.12	475
	M55J	4.02	540
	M60J	3.92	588
Hexel	IM6	5.72	279
	IM7	5.65	276
	IM9	6.14	304
	IM10	6.96	310
Cytec	Thornel T650/35	4.28	255
	Thornel T300	3.75	231
Mitsubishi pyrofil	HR 40	4.41	395
	HS 40	4.61	455
	MS 40	4.41	345
	TRH50	4.9	255
Zoltek	PX35	4.14	242

Table A.2. Mechanical properties of commercial pitch based carbon fiber

Pitch based carbon fiber (Source, Product)		Tensile strength (GPa)	Tensile modulus (GPa)
Cytec	P-25	1.56	172
	P-30	1.38	207
	P-55	1.38	414
	P-55S	1.72	415
	P-100S	2.41	758
	P120S	2.41	827
	K-800X	2.34	896
	K-1100	3.1	965
Mitsubishi Dialead	K63A12	2.6	790
	K13916	3.2	760
	K63712	2.6	640
	K13D2U	3.7	935
	K13C6U	3.6	900

APPENDIX B

FTIR SPECTRA AND FIBER FRACTURE IMAGE OF PAN AND PAN/SWL FIBERS

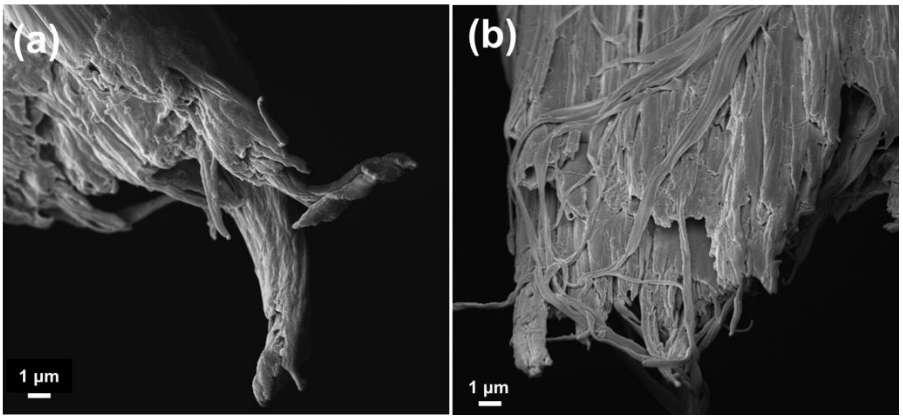

Figure B.1. Scanning electron micrographs of the fracture surface of (a) PAN fiber and (b) PAN/SWL fiber at draw ratio of 10.

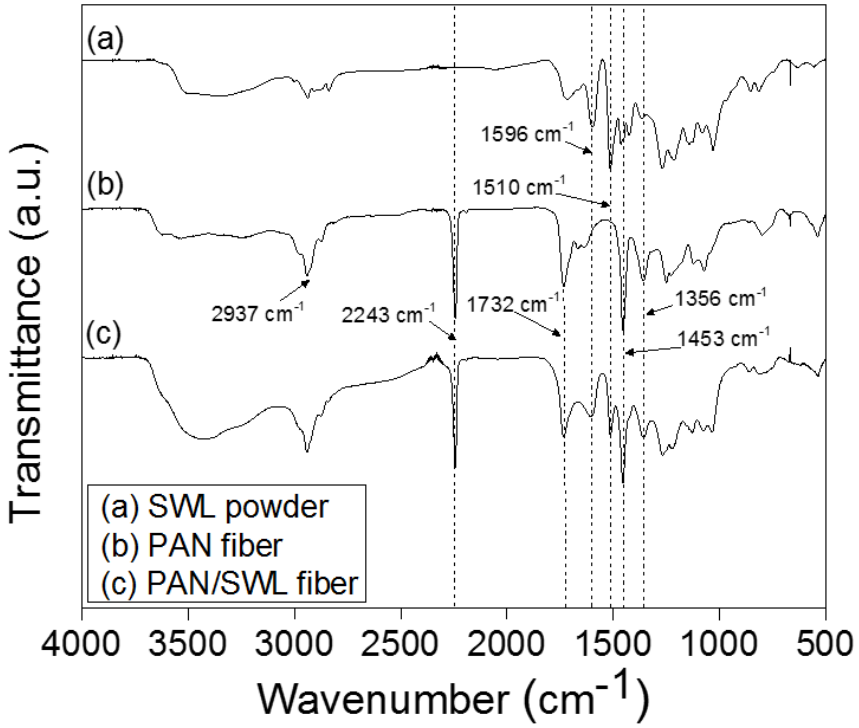

Figure B.2. Fourier transform infrared spectra of (a) softwood lignin (SWL) powder, (b) PAN fiber, and (c) PAN/SWL fiber.

In Chapter 2, the rheological characterization of annual plant lignin (APL) and PAN (with 4% MAA copolymer) suggests possible chemical interaction between PAN nitrile side chain and APL. In Chapter 4, this chemical interaction is observed by the FTIR analysis of the APL powder and PAN/APL blend fiber, where: (1) the ketone-like structure (1720 cm^{-1} and 1050 cm^{-1} peaks) from lignin diminishes when forming PAN/APL blend fibers, (2) N–O peaks at 1515 and 1362 cm^{-1} emerges in PAN/APL blends, and (3) decreased magnitude of C≡N peak (2243 cm^{-1}) accompanied by a broadening peak at 1614 cm^{-1} around C=N region. In this chapter, for softwood lignin (SWL) powder, the peaks at 1510 and 1596 cm^{-1} are assigned to the aromatic skeletal vibrations [1], and the peaks around 1268 and 1139 cm^{-1} are due to guaiacyl unit stretching with carbonyl groups in lignin structure [1, 2]. For PAN fiber (with 4% MAA copolymer), the sharp peak at 2243 cm^{-1} is assigned to the C≡N bond of polyacrylonitrile (PAN), and peaks at 1356, 1453, and 2937 cm^{-1} belong to the CH_2 in the PAN backbone [3]. It is possible that the aforementioned chemical interaction between lignin and the nitrile side chain can still occur in the PAN/SWL blend fiber. However, unlike the previous homopolymer PAN spectra, the MAA copolymer in PAN used in this study contributes to the peaks around 1720 cm^{-1}, which makes structural change of lignin hard to be observed. While characteristic peaks for both SWL powder and PAN fibers are present in the spectra, no conclusions regarding direct chemical interactions between PAN and SWL can be drawn in the current study.

REFERENCES

[1] Faix O. Classification of Lignins from Different Botanical Origins by FT-IR Spectroscopy. Holzforschung. 1991;45(s1):21-28.

[2] Boeriu CG, Bravo D, Gosselink RJA, van Dam JEG. Characterisation of structure-dependent functional properties of lignin with infrared spectroscopy. Industrial Crops and Products. 2004;20(2):205-218.

[3] Devasia R, Nair CPR, Sadhana R, Babu NS, Ninan KN. Fourier Transform Infrared and Wide-angle X-ray Diffraction Studies of the Thermal Cyclization Reactions of High-molar-mass Poly(acrylonitrile-co-itaconic acid). Journal of Applied Polymer Science. 2006;100(4):3055-3062.

APPENDIX C

STATISTICAL SIGNIFICANCE OF THE PROPERTIES

COMPARISON BETWEEN CARBON FIBERS

Table C.1. p-values for the statistical significance of comparison between carbon fiber properties

Carbon fiber sample (carbonized temperature)	p-value of tensile strength*	p-value of tensile modulus*	p-value of elongation at break*
PAN/lignin (1000 °C)	0.061	0.399	0.020
PAN/lignin/CNT (1000 °C)	0.319	0.093	0.294
PAN/lignin (1100 °C)	0.052	0.256	0.018
PAN/lignin/CNT (1100 °C)	0.014	< 0.0001	0.074

* with respect to the PAN carbon fiber at corresponding carbonization temperatures.
** A p-value < 0.05 indicates the difference between carbon fiber mechanical properties is significant.

For PAN/lignin fibers carbonized at 1000 °C and 1100 °C, the p-values of carbon fiber tensile strength and tensile modulus are consistently greater than 0.05, indicating that PAN/lignin carbon fibers exhibited comparable tensile strength and modulus values to the PAN fibers carbonized at the same temperatures.

APPENDIX D

PAN-SHEATH AND PAN/LIGNIN-CORE BI-COMPONENT FIBERS AND CARBON FIBERS

D.1 STATISTICAL SIGNIFICANCE OF THE PROPERTIES COMPARISON BETWEEN BI-COMPONENT FIBERS AND CARBON FIBERS

Table D.1. p-values for the statistical significance of comparison between fiber properties

Sample	p-value of tensile strength*	p-value of tensile modulus*	p-value of elongation at break*
BF-A_{16}	< 0.0001	< 0.0001	< 0.0001
BF-B_{18}	< 0.0001	< 0.0001	0.001
BF-C_{20}	0.0225	< 0.0001	< 0.0001

*With respective to PAN_{20} fiber.
**A p-value < 0.05 indicates the difference between carbon fiber mechanical properties is significant.

Table D.2. P-values for mechanical properties of bi-component carbon fibers

Carbon fiber sample (carbonized temperature)	p-value of tensile strength*	p-value of tensile modulus*	p-value of elongation at break*
BF-A_{16}-4 (1000 °C)	0.0005	< 0.0001	0.0014
BF-A_{16}-5 (1200 °C)	< 0.0001	< 0.0001	0.0124
BF-A_{16}-7 (1300 °C)	0.033	0.0053	0.0543

*With respect to PAN_{20}-3, PAN_{20}-6, and PAN_{20}-7, carbon fiber at corresponding carbonization temperatures.
** A p-value < 0.05 indicates the difference between carbon fiber mechanical properties is significant.

For BF-A_{16} fibers carbonized at 1000, 1200, and 1300 °C, the p-values of carbon fiber tensile strength and tensile modulus are consistently lower than 0.05, confirming the lower tensile strength and tensile modulus values compared to the corresponding PAN_{20} carbon fibers.

D.2. POROSITY CALCULATION

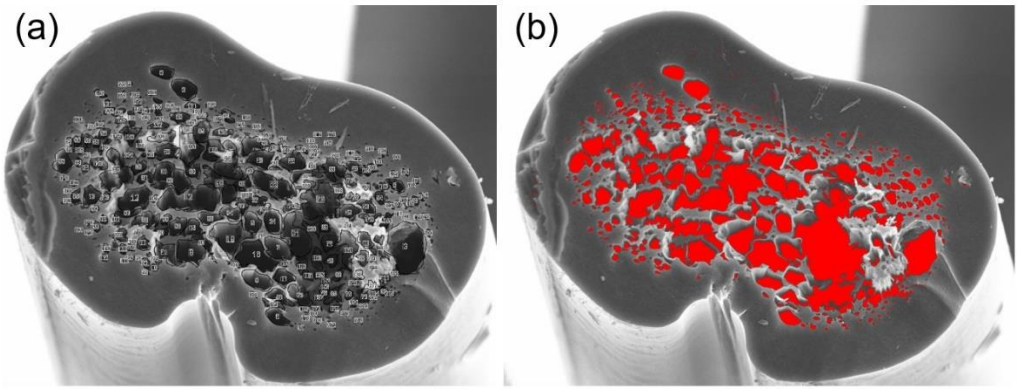

Figure D.1. SEM cross-sectional images of BF-C_{20} carbon fiber with (a) manual selection of the cross-sectional pores, and (b) software selection (red) of pores by ImageJ.

In the example presented by Figure D.1., manual selection and software selection of pores yields an overall cross-sectional porosity of 24.9% and 22.1%, respectively. In Chapter 5, an average between the manual and software selection over three different carbon fiber cross sections was used to estimate the overall porosity of the BF-C_{20} carbon fibers.

APPENDIX E

LIGNIN DERIVED HIGH SURFACE AREA CARBON

E.1 INTRODCUTION

High surface area carbon has versatile applications. It is used for water filtration, air purification, carbon capture, electrode materials in supercapacitors, fuel storage, reinforcement agent in rubber tires, and many other places. To create high specific surface area carbon (>1000 m^2/g), activation processes (with steam, strong acid, or base at elevated temperatures) are conventionally employed and can therefore lead to high production cost and hazardous byproducts. Recently, worldwide growing interests in next-generation biorefineries has called for investigations of biofuel, chemical, and value-added commodity products from lignocellulosic biomass. In this work, we propose a high surface area carbon material derived from biorefinery waste, lignin. With the addition of a sacrificial polymer to lignin as precursor materials, high surface area carbon from direct stabilization/carbonization without any activation process are shown comparable to some chemically activated carbonized lignin[1] and commercial activated carbons.

E.2 EXPERIMENTAL

E.2.1 Materials

Softwood kraft lignin (SWL, Indulin AT) powder was provided by MeadWestvaco (*Richmond, VA*), and the soda-pulped annual plant lignin (APL, Protobind 2400,) powder was acquired from GreenValue (*Media, PA*). To eliminate the ash content and metal impurities from manufacturing process, softwood lignin (SWL) and soda-pulped annual plant lignin (APL) were washed repeatedly by diluted HCl and deionized water upon receiving. SWL was subsequently washed with methanol in order to filtrate and collect the

insoluble fraction. After washes, lignins were then dried under vacuum at 60 °C before use. Dimethylformamide (DMF, ACS grade, 99.8% purity) and poly(methyl methacrylate) (PMMA) with average M_w of ~15,000, ~350,000, and ~996,000 g/mol were obtained from Sigma Aldrich and used as received.

E.2.2 Solution and Film Preparation

Two lignin solutions (SWL and APL) are prepared by dissolving lignin powders into DMF at a concentration of 30 mg/mL and three PMMA/DMF solutions (each with PMMA M_w of 15,000, 350,000, and 996,000 g/mol, respectively.) are prepared at the same concentration. Before further use, each solution was kept in the orbital shaker (MaxQ 4450, Thermo Scientific.) at 45 °C and a speed of 200 rpm for six hours to ensure dissolution. For PMMA/lignin composite solutions, various volumetric ratios of PMMA and lignin solution were added into a vial, which is subsequently kept in the orbital shaker at 45 °C and a speed of 200 rpm for three hours. For film casting, each solution was poured into a glass mold immediately upon removal from the shaker and placed into a vacuum oven maintained at 60 °C for twelve hours. During film formations, DMF was evaporated and subsequently distilled by a glass cold trap for solvent recovery. All samples were then gently scraped off and collected in vials before use.

E.2.3. Carbonization Process

In the current stage of the study, all samples are converted into carbons by thermogravimetric analysis (TGA, Q500 by TA Instruments). During each trial, around 30 mg of precursor materials are prepared to first undergo oxidative stabilization with a heating rate of 5 °C/min from room temperature to 280 °C, followed by a 5-hour isothermal residence process. Immediately after the isothermal residence, nitrogen stream will be

introduced to create an inert environment while the stabilized samples are heated from 280 °C to 900 °C at a heating rate of 10 °C/min followed by a 6-hour isothermal residence for carbonization. All carbonized samples are collected after cooling at room temperature.

E.2.4 Characterization

For surface area and pore size analysis, isothermal nitrogen gas adsorption study was carried out on various carbon samples using ASAP 2020 (Micromeritics Inc.) at 77 Kelvin. BET and BJH theories are used to obtain the specific surface area and pore size distribution, respectively.

E.3 RESULTS AND DISCUSSIONS

The surface area results (BET) of each sample along with the details of PMMA molecular weights, and lignin types and contents for film preparation are summarized in Table E.1. Trials 1 and 2 are pure lignin powders which undergo identical treatments with the rest of film samples prepared with PMMA of indicated molecular weights. According to the results, no clear trend is observed between the lignin type and the specific surface area of derived carbons (Trial 1 and 2). Upon the addition of low molecular weight (15 kg/mol) PMMA to lignin for film fabrication, the derived carbon surface area almost doubled (Trial 3 and 4). Interestingly, as the PMMA with higher molecular weight (350 kg/mol) is used for film preparations, higher specific surface area values can be achieved (Trial 5 and 6). In the current scope of the study, high surface area carbons (~1,000 m^2/g) can be fabricated from the carbonized films using PMMA with molecular weight of 996 kg/mol without chemical activation process.

Fine porous structures are observed from the SEM images (Figure E.1 and Figure E.2) of the carbonized PMMA-processed lignins. According to the images, nano-sized

pores are observed on both trial 6 and 7 (Figure E.1b and Figure E.2b), which provides the visual confirmation of the high surface area value. The pore size distributions of the lignin and lignin/PMMA carbonized materials are shown in Figure E.3a. Without the incorporation of PMMA, carbonized lignin powder (Trial 1) exhibited pores size mostly between 10 to 20 Å. When carbonized with the presence of PMMA (350 kg/mol), trial 5 exhibited slightly increased pore size ranging from 15 to 30 Å and greatly enhanced incremental pore volume and surface area compared to trial 1. When higher molecular-weight PMMA (996 kg/mol) is used under identical PMMA/lignin solid content, this phenomenon of increasing pore volume is further amplified in trial 7 while the pore size distributions remained unchanged compared to trial 5. This indicates that longer PMMA chain lengths (higher molecular weights) can increase pore volumes of the carbonized products but not the pore size (size of contact sites between PMMA and lignin chains). When the lignin content in the PMMA/lignin film is increased (trial 9), lower surface area (Table C.1) and pore volume of the derived carbon are reported with unchanged pore size compared to trial 7 (Figure E.3b). These observations imply that the pore volume of derived carbons is possible related to the PMMA diffusion and collision frequency between the polymers in solutions. Further investigations of PMMA/lignin content ratio and concentrations in DMF are then required to optimize the surface area values of derived carbons.

Table E.1. Processing conditions and measured surface area of carbonized lignin.

Trial	Lignin type	Lignin content (wt%)	PMMA Mw (g/mol)	BET (m^2/g)	Sample ID
1	APL	100	-	276	AC 5
2	SWL	100	-	234	AC 13
3	APL	67	15 k	478	AC 6
4	SWL	67	15 k	440	AC 7
5	APL	67	350 k	717	AC 3
6	SWL	67	350 k	785	AC 4
7	APL	67	996 K	1031	AC 9
8	SWL	67	996 K	955	AC 10
9	APL	87.5	996 K	564	AC 12

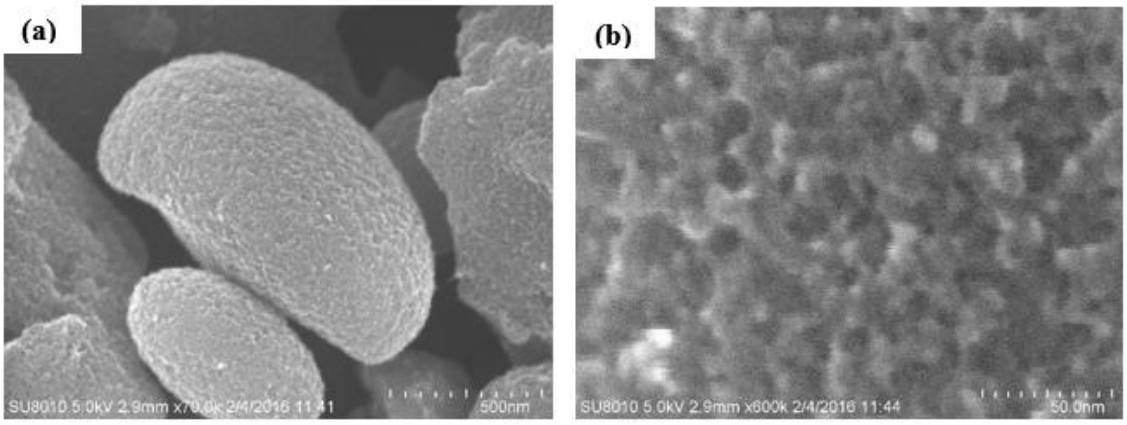

Figure E.1. SEM images of Trial 6 showing the porous carbonized structure.

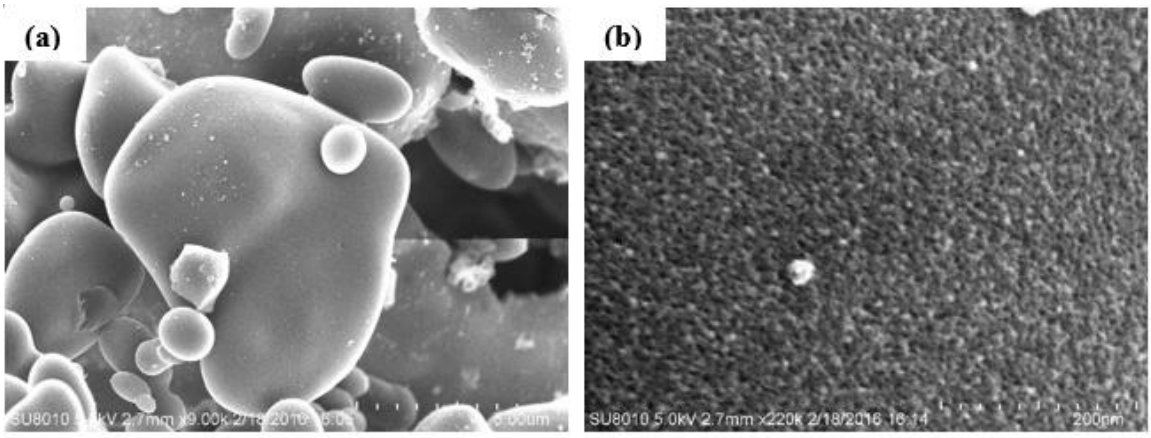

Figure E.2. SEM images of Trial 7 showing the porous carbonized structure.

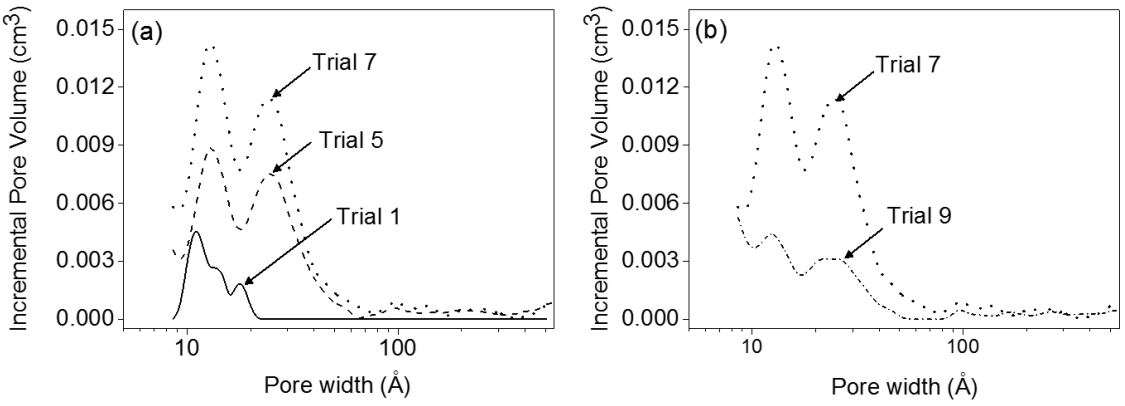

Figure E.3. Pore volume distribution of (a) the carbonized APL without PMMA (trial 1) and various molecular weight of PMMA (Trial 5, Trial 7), and (b) the carbonized APL derived from precursors with various PMMA (996 kg/mol) content.

E.4 CONCLUSIONS

In this work, an eco-friendly manufacturing process of high surface area carbon derived from biorefinery waste is reported. During the fabrication process, used organic solvent (DMF) can be recycled and no chemical activation process is required to avoid environmental hazards. Using PMMA as a sacrificial component, we were able to achieve carbonized lignin with surface area as high as 1030 m^2/g. According to the results, no clear trend between the surface area of derived carbon and the type of lignin precursors (APL or SWL) is observed. While PMMA molecular weight is shown critically related to the surface area values of carbonized products, pore widths of the derived carbon are not affected by PMMA molecular weight. According to the reported technology herein, promising potentials of industrial interest and market penetration can be realized with further optimization and scale-up progress.

E.5 FUTURE WORKS

E.5.1 Optimization

At the current stage, lignin/PMMA with 33 wt% of 996 kg/mol PMMA resulted in the highest surface area, while the carbonized sample with 12.5 wt% PMMA resulted in a lower surface area. Further investigations of various PMMA solid content/ratio in precursor film fabrication are required in order to increase surface area and possibly decrease PMMA consumption. Trials with higher molecular weight PMMA and studies of precursor blended with PMMA of various molecular weights (e.g., combination of different molecular weights) should be conducted.

E.5.2 Short-scheme Manufacturing Process

In current stage of the study, a control stabilization (300 minutes) and carbonization (360 minutes) scheme is implemented for comparison purpose. While a shorter stabilization/carbonization residence time may result in the higher surface area and a higher carbon yield. Studies of short-scheme manufacturing process are recommended to further render advantages of green manufacturing of proposed systems.

E.5.3 Scale-up

Currently, precursor film and carbonization trials are all conducted in small-scale manufacturing process. In order to demonstrate industrial applicability for this work, scale-up trials with comparable carbon properties are required. Currently, precursor films are fabricated at ~720 mg per piece and derived carbons are achieved at 5 to 10 mg per trial. Scale-up fabrications of high surface carbon from higher-mass precursors can be conducted in a box furnace (Lindberg, 51668-HR Box Furnace 1200C, Blue M Electric) as pilot-scale simulation of industrial production.

E.5.4 Carbon Nanotubes-Incorporated Lignin Carbons

While the high surface area carbon in this study serves as a potential in energy storage application, it is difficult to fabricate robust active electrodes with the carbons from current process due to low aspect ratio. (Figure 1 and 2) Carbon nanotubes (CNT) are known for their exceptional aspect ratio and mechanical properties. While previous studies suggest that multi-walled CNT can promote lignin reordering process during carbonization,[2] and increase electrical conductivity of carbonized lignin.[3] It is recommended to investigate the performance of PMMA-lignin derived carbon with minimal loading (0.1-0.5 wt%) of multi-walled CNT along with its feasibility for energy storage applications.

E.5.5 Functionality

To further extend the value propositions of the current system in addition to the green manufacturing process, high surface area carbons herein should be evaluated for carbon capture and adsorption capabilities to compare with commercial activated carbons.

E.6 REFERENCES

[1.] Rabinovich, M. L.; Fedoryak, O.; Dobele, G.; Andersone, A.; Gawdzik, B.; Lindström, M. E.; Sevastyanova, O., Carbon adsorbents from industrial hydrolysis lignin: The USSR/Eastern European experience and its importance for modern biorefineries. *Renewable and Sustainable Energy Reviews* **2016,** *57*, 1008-1024.

[2.] Liu, H. C.; Chien, A. T.; Newcomb, B. A.; Liu, Y.; Kumar, S., Processing, Structure, and Properties of Lignin- and CNT-Incorporated Polyacrylonitrile-Based Carbon Fibers. *ACS Sustainable Chemistry & Engineering* **2015,** *3* (9), 1943-1954.

[3.] Teng, N.; Dallmeyer, I.; Kadla, J. F., Incorporation of Multiwalled Carbon Nanotubes into Electrospun Softwood Kraft Lignin-Based Fibers. *Journal of Wood Chemistry and Technology* **2013,** *33* (4), 299-316.